Metal Nanoparticle and Polymer Composites for Antimicrobial Applications

A Dissertation Submitted in Partial

Fulfillment for the Degree of

DOCTOR OF PHILOSOPHY

By

SADHUCHARAN MALLICK

Roll No. 07612203

Department of Chemistry

Indian Institute of Technology Guwahati

Guwahati -781039, India

March 2013

Dedicated to my Parents

&

Beloved Brother and Sister

INDIAN INSTITUTE OF TECHNOLOGY, GUWAHATI

Department of Chemistry

Declaration

I hereby declare that the matter embodied in this thesis is the result of investigations carried out by me in the Department of Chemistry, Indian Institute of Technology Guwahati, India under the guidance of Dr. Anumita Paul, Associate Professor of Chemistry.

In keeping with the general practice of reporting observations, due acknowledgements have been made wherever the work described is based on the findings of other investigators.

I. I. T. Guwahati **Sadhucharan Mallick**

March, 2013

INDIAN INSTITUTE OF TECHNOLOGY, GUWAHATI

Department of Chemistry

Certificate

It is certified that the work described in this thesis, entitled ***"Metal Nanoparticle and Polymer Composites for Antimicrobial Applications",*** done by **Mr. Sadhucharan Mallick** for the award of degree of Doctor of Philosophy is an authentic record of the results obtained from the research work carried out under my supervision in the Department of Chemistry, Indian Institute of Technology Guwahati, India, and this work has not been submitted elsewhere for a degree.

I. I. T. Guwahati

March, 2013

Dr. Anumita Paul

Associate Professor

(Thesis Supervisor)

Acknowledgements

Writing the acknowledgement now fills my heart with gratitude. It is my immense pleasure to express my sincere gratitude to my guide, Dr Anumita Paul for her constant support, encouragement, precious suggestion and guidance throughout my research work. Her deep knowledge and critical analysis of the experimental results always helped me to figure out through the difficult problems and improve the quality of research work.

I am grateful and indebted to Prof. Arun Chattopadhyay who has been a driving force in shaping my thesis work. He has always been an inspirational figure to the young researcher like me coming into the scientific community. His encouragement and precious suggestions have shown light in my venture into the world of science.

I shall remain indebted to you madam and sir for your kindness, for giving me all the freedom to think and work and giving me your valuable time whenever required and best environment and laboratory to work. I wish to be associated with to my madam and sir throughout my life.

I offer my heartfelt thanks to Prof. Siddhartha Sankar Ghosh of Department of Biotechnology, IIT Guwahati. I am grateful to him for his encouragement and valuable discussions and giving me opportunity to work into the exciting field of nanobiotechnology.

I would like to acknowledge my sincere gratitude to Dr. G. Krishnamoorthy, Chairman of Doctoral Committee, and other Doctoral Committee members Prof. Siddhartha Sankar Ghosh, and Dr. Sandip Paul, who have been constantly guiding me with their valuable suggestions, encouragements which helped to improve my thesis.

Also I also thank all other faculty and staff members Avilasha di, Lipika di, Parikshit, Aniruddha, Diganta, Shyamul, Babulal da and office staffs Nilotpal, Santanu of the department for their cooperation all the time.

Let me also offer my gratitude to Kaustubh da, Pranjoli Di, Indrajit da, of Centre for Nanotechnology, IIT Guwahati and Mr. Sidananda da of Department of Physics, IIT Guwahati for their help with the instruments. I must also thank here to Mr. Chandan Borgohain and Dr. Kula K. Senapati and Madhurjya da, and Kesho da of Central Instruments Facility for helping me with their technical support.

I would like to acknowledge to my lab seniors Dr. Jashmini Deka, Dr. Arumugam Murugadoss, Dr. Sonit K. Gogoi, Dr. Biswa Ranjan Panda, Dr. Krishna Kanti Dey, Dr. Devasish Chowdhury, Dr. Gitanjali Majumdar, and Present labmates Subhojit Das, Raihana Begum, Rumi Khandelia, Md Palashuddin Sheikh, Rama Ghosh, Satyapriya Bhandari, Anushree Dutta, Shilaj Roy, Uday Pan for their helping hands care and support. Our laboratory is one of the best place to work as I had pleasure to share memorable time and knowledge with labmates and seniors.

I would like to give thanks to my research collaborator, Dr. Madhuchanda Banerjee and Dr. Shilpa Sharma with them working in collaboration and learning techniques in biological experiment. I wish to give thanks other Nano center scholars Amaresh Sahoo, Upashi Goswami, for their help during my research work.

It's my great pleasure to thanks all my teachers who have taught and inspired me for higher studies. I express my sincere thanks to my M. Sc teachers for taught me duration of M. Sc Study in IIT Delhi. I am thankful to all my friends at school, college and IITD for their love and support.

I personally thanks my all friends from IITG Atul, Devendra, Faizi, Fulwa, Francis, Mohan Lal, Sayak, Somasekhar, partha protim Boruah, Sandeep, Subhamoy, Ravi Kumar, Himanshu Shekhar Jha and other friends Raju Dey, Subhankar Das, Ramprasad Misra, Somnath Ghosh, Somedatta Pal, Susmita Paul, Shivendra Pandey, Deb K. Das, Niloy Paul, Arvind Gupta, J.P. Anandkumar, Bhargab Deka, Ashim Malakar, Dibyendu da, Subrata Laha, somrita , and family friends Abhijit, sujit, Jagannath, sudip for their help and encouragement.

Stay in IIT Guwahati has been a memorable part of my life both from the personal and the professional point of view. I think it would be appropriate to say 'thank you' to all my friends to start with and mention a few names that flash

in. It has been a great pleasure being able to share my personal and professional life with you people and a great learning experience

I would like to Acknowledge for financial support during my Ph.D. to IIT Guwahati and CSIR New Delhi.

I am grateful to the Department of Physics, Department of Biotechnology, and Centre for Nanotechnology, Centre for the Environment, Central Instruments Facility (CIF), IIT Guwahati, and Department of Physics & Meteorology, IIT Kharagpur for assistance and instrumentation facilities.

Finally, I owe heartfelt gratitude to my grandmother and parents for their blessings and support, and my brother and sister and brother-in-law for constantly inspiring me to carry out my research work to completion. I am thankful to all my relatives and well-wisher for their encouragement.

Sadhucharan Mallick

Table of Contents

ABBREVIATIONS

AAS	Atomic Absorption Spectroscopy
Ag NPs	Silver nanoparticles
B. cereus	Bacillus cereus
CFU	colony-forming unit
CLSM	Confocal laser scanning microscopy
CS	Chitosan
Cu NPs	Copper Nanoparticles
DNA	Deoxyribonucleic acid
E. coli	*Escherichia coli*
EDX	Energy Dispersive X-ray
FACS	Fluorescence Activated Cell Sorting
FESEM	Field Emission Scanning Electron Microscope
FTIR	Fourier Transform Infrared spectroscopy
GFP	Green Fluorescent Protein
I	Iodine
LB	Luria-Bertani
MIC	Minimum inhibitory concentration

MBC	Minimum bactericidal concentration
NBT	Nitro blue tetrazolium chloride
NPs	Nanoparticles
NCs	Nanoclusters
NB	Nutrient Broth
PI	propidium iodide
QDs	Quantum dots
ROS	Reactive oxygen species
SAED	Selected area electron diffraction
SEM	Scanning Electron Microscope
SERS	Surface-Enhanced Raman Scattering
SPR	Surface Plasmon Resonance
TEM	Transmission Electron Microscope
HRTEM	High Resolution Transmission Electron Microscope
IFFT	Inverse Fast Fourier Transform
UV-Vis	Ultraviolet–visible spectroscopy
XPS	X-ray Photoelectron Spectroscopy
XRD	X-ray diffraction

Chapter 1

Introduction and literature review

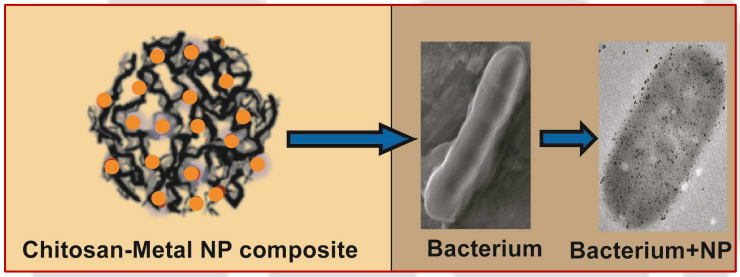

1.1 Nanotechnology

Nanotechnology is technology that deals with the design, fabrication and application of nanostructured materials, which also involves a fundamental understanding of the relationship between the observed properties to the materials' dimensions, which typically ranges from a few nanometers to several hundred nanometers.[1] Presently, nanoscale science and technology, is finding impressive advances on many different sides. The underlying strength of this field lies, generally, on the intrinsic physicochemical and optoelectronic properties of the nanosized particles that are different from their bulk counterparts.[2–7] Inorganic nanoparticles exhibit significant novel and improved physical, chemical, and biological properties, eliciting much interest in the past few decades. Among them, nanoparticles of coinage metals Au, Ag, and Cu exhibit attractive optical properties due to their strong optical absorption in the visible region, as a result of the collective oscillation of conduction band electrons, known as the surface plasmon resonance (SPR) band.[2–5] This is the origin of many interesting physical and related applications such as SPR spectroscopy and surface-enhanced Raman scattering (SERS), which have found wide applications in chemical analysis and biomedical detection.[2,4] Coinage metals NPs also exhibit good catalytic activity when NPs are smaller in size (1-10 nm in diameter) due to large surface to volume ratio.[1,7,8] Dendrimer-encapsulated coinage metals nanoparticles have been employed for several type of reaction particularly hydrogenations and carbon-carbon bond-forming reactions.[8] Recent studies have demonstrated that antimicrobial formulations comprising nanoparticles could be effective bactericidal materials.[9, 10, 11]

1.2: Metal Nanoparticles

In the past two decades, a substantial body of research work in the syntheses of metal nanoparticles (NPs) has been directed towards creating conditions where optical, chemical and biological properties of the NPs could be exploited. In this regard, coinage metals (Cu, Ag and Au) provide special opportunity owing to their biological applications.[12,13] Nanoparticulate research has witnessed tremendous growth due to the unusual chemical and physical properties which have been demonstrated to be an

intermediate state of matter.[14,15] The catalytic activity of the particles generally depends on their size, shape, and stabilizing agents, which are controlled by the preparation conditions.[16] There are diverse approaches to the preparation of the nanoscale materials which have been reported in the literature. Michael Faraday prepared colloidal gold (Au) dispersions by reduction of an aqueous solution of chloroaurate ($AuCl_4^-$) using phosphorus in carbon disulphide in a two-phase system.[17] He described many unusual and wonderful properties of these red color solutions, called activated gold. In 1908, Gustav Mie first explained the origin of the red color of gold NPs. Gustav Mie solved Maxwell's equation for an electromagnetic light wave interacting with small spheres having the same macroscopic frequency dependent material dielectric constant as the bulk metal.[18] Nanostructured materials became more attractive due to applications in optical systems and catalysis. Semiconductor nanocrystals (quantum dots, QDs) exhibit strongly size-dependent optical and electrical properties.[5] QDs are nanometre-sized inorganic structures whose radii are smaller than the bulk exciton Bohr radius. QDs exhibit unique light emission by changing size or composition, and because of this, they have been exploited for a broad-range of applications. [19, 20] QDs have been used as an alternative to organic fluorescent labels for optical imaging and spectroscopy.[20] On the other hand, because of their high surface-to volume ratios, metal NPs (especially Pt and Pd) are important as catalysts.[21, 22]. In 1951 Turkevich and co-workers prepared Au NPs with an average diameter of about 20 nm with a very narrow size distribution and good reproducibility by reduction of an aqueous solution of chloroaurate ($AuCl_4^-$) using sodium citrate.[23,24] The use of Au NPs in catalysis appeared in the 19th century and the real breakthrough came with Haruta's seminal studies on oxide-supported AuNP-catalyzed CO oxidation by O_2 at low temperatures.[25 – 27]Au NPs were found to be remarkably active for low-temperature CO oxidation when it is highly dispersed and deposited on transition metal oxide.

Rapid growth in nanoscience and technology also means that nanomaterials are increasingly coming in contact with humans and the environment on regular basis.[28] Understanding interactions between the NPs with proteins, membranes, cells, DNA, RNA, enzymes and organelles is most important from the perspective of safe use of

nanomaterials.[28] Recent studies have demonstrated that antimicrobial formulations comprising NPs could be effective bactericidal materials. Among inorganic antibacterial agents, Ag and Cu have been employed most extensively because of their effective biocidal ability at low concentrations and relatively less toxicity to mammalian cells.[9, 10, 11, 29 – 34]

1.3: Silver Nanoparticles (Ag NPs)

Coinage metals NPs (Ag, Au and Cu) show plasmon resonance in the visible region; among them Ag exhibit highest efficiency of the plasmonic extinction and its plasmon resonance can be tuned to any wavelength in the visible spectrum.[35, 36] Additionally molecules adsorbed to the surface of Ag NPs and Au NPs, exhibit SERS effects, due to the coupling of the plasmon band of the irradiated metal with the molecular electronic/vibrational states. Ag NPs could be used as a highly active SERS substrates.[35-39] S. Nie et al. have demonstrated that when single rhodamine 6G molecules are adsorbed on Ag NPs, the intrinsic Raman enhancement factors were on the order of 10^{14} to 10^{15}. [37]Ag NPs is also used widely as a catalyst in industrial processes, for example in the oxidation of ethylene to ethylene oxide and methanol to formaldehyde.[40] Ag NPs also have the highest electrical and thermal conductivity among all other metals NPs, making it a popular material for electrical contacts and an additive for conducting adhesives.[41, 42] Lee-Meisel method, which is most common method for the synthesis of Ag NPs, is the reduction of $AgNO_3$ aqueous solution on boiling in presence of 1% sodium citrate .[38]

1.3.1: Mechanism and antibacterial activities of Ag NPs

Infections with multidrug resistant bacteria have become a serious problem in our environment as their growth cannot be controlled by traditional antibiotics. Rather they are able to survive and even multiply in the presence of these traditional antibiotics.[43,44] From earlier studies by Ahearn, D. G. pure silver, silver oxide- and silver chloride surface were found to inhibit bacterial growth through enhanced adherence to an ion-beam-assisted-deposited silver surface followed by loss of viability.[30] That Ag ions and silver-based compounds have bacteriostatic as well as bactericidal properties are known

for centuries.[31] In recent years, due to the development of bacterial strain resistant to the most potent antibiotic formulations, new bactericidal agents based on inorganic nanomaterials have become necessary. Previous studies have established that antimicrobial formulations in the form of NPs could be used as effective bactericidal materials.[9–11] Recently Klabunde and co-workers demonstrated that highly reactive metal oxide NPs and halogen (Cl_2, Br_2) adducts of these metal oxide particles were biocidal.[45] These nanoscale materials are very effective against Gram-positive and Gram-negative bacteria as well as spores. In 2004, Sondi et al. investigated the biocidal action of Ag NPs against *E. coli* using scanning and transmission electron microscopy (SEM and TEM) probes.[9] Their reports showed that treated *E. coli* cells were damaged with pit formation in the cell wall of the bacteria while Ag NPs were found to accumulate in the bacterial membrane. A membrane with such morphology exhibits a significant increase in permeability, resulting in death of the cell. The possible use of Ag NPs as an antibacterial agent has been investigated from our laboratory and several other groups.[9-11,46, 47] In 2007, S. Pal showed that Ag NPs underwent a shape-dependent interaction with the Gram-negative organism *E. coli* with the truncated triangular Ag NPs demonstrating the strongest biocidal action as compared to spherical and rod-shaped NPs and also Ag^+ (from $AgNO_3$).[46] Recent literature reports demonstrate that composites of Ag NPs with polymer results in the improvement of antimicrobial activities of Ag NPs at lower concentrations. Several kinds of Ag-containing antibacterial agents using different carriers, such as zeolite[47] titanium dioxide[48], activated carbon[49], montmorillonite[50], mesoporus silica[51], chitosan,[52,53] polyacrylonitrile[54], siloxane and epoxy resin[55] have been investigated. Zhang, L et al. synthesized Ag nanoclusters and Ag nanoclusters-coated TiO_2 NPs and studied bactericidal activities against *Micrococcuslylae* and found that Ag nanoclusters-coated TiO_2 material with optimal Ag loading showed enhanced photocatalytic and bactericidal activities compared to uncoated TiO_2.[48] Combination of Ag NPs with these polymers increases their efficiency of antimicrobial activity by exploiting the active components of the individual substances.[47-55] These composites have potential applications in various fields, i.e. medical instruments and devices, water treatment and food processing, as food packaging material etc.[56] Ag NPs can be incorporated into numerous materials such as textiles and plastics, making it especially

useful for applications requiring broad spectrum and sustained antimicrobial activity but where traditional antimicrobials agent would be impractical. U.S. Food and Drug Administration (FDA) have approved over a dozen Ag-containing zeolites or other substances for use as food contact materials for the purpose of disinfection, as well as numerous Ag-coated medical devices.

1.4: Copper Nanoparticles (Cu NPs)

Nanoparticles of coinage metals (Cu, Ag and Au) have attractive optical properties, and chemical and biological properties.[36, 57] Coinage metals NPs provides special opportunity owing to their biological applications. Among various metal particles Cu NPs are attractive not only because of their catalytic, optical and electrically conducting properties but also because of their significant antibacterial and antifungal properties.[57-67] Cu NPs serve as low cost heterogeneous catalysts for several chemical reactions. Vukojevic et al. used aluminum-stabilized Cu colloids for methanol synthesis from synthesis gas over industrial $Cu/ZnO/Al_2O_3$ catalysts.[58] Their synthesized Cu NPs (sizes 4.5±1.5 nm) show very high intrinsic activity for methanol synthesis. Ressler used ZnO supported Cu NPs catalysts in methanol synthesis.[59] Another important application of Cu NPs is their potential use as SERS active substrates and enhancement factor is dependent on the strength of the local electric field and the nature of the Cu NPs .[64,65] Cu NPs are also attractive for application in printed circuit boards and flexible electronics. Consequently synthesis of Cu NPs has become more attractive from a scientific as well as an industrial point of view, due to its huge potential for replacing expensive Ag NPs ink used in conductive printing. [66] Cu NP based inkjet inks are used to make various devices such as solar cells, radio frequency identification tags, and electroluminescence devices.[66] Cu nanostructures can play an important role in the development of real world application due to their relatively low cost as compared to Pd, Pd, Ag, and Au.[57−59] A major problem in utilizing Cu NPs is their underlying tendency to get oxidized in the atmosphere. Several methods have been developed to prepare stable Cu NPs by using proper protective layers of an organic polymer, alkene chains, amorphous carbon, graphenes, inorganic materials such as silica and inorganic ions.[66−75]

1.4.1: Antibacterial activities of Cu NPs

Cu is an effective antibacterial agent with low toxicity, known for a long time.[32, 60, 61] Cu has been used for decades as an effective fungicidal agent.[32] Germicidal activity of Cu, both as free and as complex species is well-known and documented for several years.[32] Since the 19th century, Cu or Cu oxide particle dispersions in organic matrixes have been used as antifouling coatings by the paint industry, mainly for maritime applications.[60] In 2006, Kim et al. deposited Cu NPs on SiO_2 surface, which showed excellent inhibitory effect to various microorganisms.[61] Anyaogu, K. C reported Cu NP-polymer composites which exhibited antimicrobial activities similar to that of conventional Cu based biocides.[62] Anyaogu, K. C claimed that Cu ions leaching from chemically bound acrylated Cu NPs is the biocidal species. Y. Wei et al. prepared low-polydispersity CuNPs or Cu nanorods in presence of oleylamine and then functionalized by exchanging oleylamine with alkanethiols.[63] In addition they reported that Cu NPs functionalized with positively charged thiols is stable in water for several months and exhibited very good antifungal properties. Cu NPs and Cu NP-polymer composites are attractive alternatives of common antibiotics as they have significant antibacterial and antifungal properties.[60–63]

1.5: Chitosan

Chitosan is a polycationic polymer composing of randomly distributed (1, 4)-linked 2-amino-2-deoxy- B-D-glucose units (Figure1). It contains more than 5000 glucosamine units and is obtained commercially from shrimp and crab shell chitin (*N*-acetylglucosamine polymer) by alkaline deacetylation (NaOH, 40−50%).[75-80] It is insoluble in water but is soluble in dilute organic acids such as acetic acid, formic acid, succinic acid, lactic acid, and malic acid.[76] As chitosan is insoluble in water many efforts have been made to prepare functional derivatives of chitosan by chemical modifications to increase their solubility in water.[80 – 85] Muzzarelli et al. prepared N-carboxymethyl chitosan, N-carboxybutyl chitosan, 5-methyl pyrrolidinone chitosan which are water soluble.[81– 83,] Heras et al. prepared N-methylene phosphonic chitosan and Jia et al. prepared quaternary ammonium salts of chitosan which are soluble in water.[84, 85] Since

1990 studies on chitin and chitosan have increased because these polysaccharides show excellent biological properties such as biodegradation in the human body, and biocompatibility, broad spectrum of antimicrobial activity, and wound-healing activity.[75 −79,85] In recent studies, chitosan has been found to be a good candidate as a support material for gene delivery, cell culture, and tissue engineering.[86,87] Therefore, chitin and chitosan are receiving greater attention as novel functional materials. The antibacterial, bio-friendly and bio-degradable properties of chitosan makes it useful for various applications such as fibers for textiles materials,[89] photographic paper,[90] novel biodegradable films,[85,91] and biomedical applications in tissue engineering,[86] drug delivery and wound dressing.[76,79,86,89]

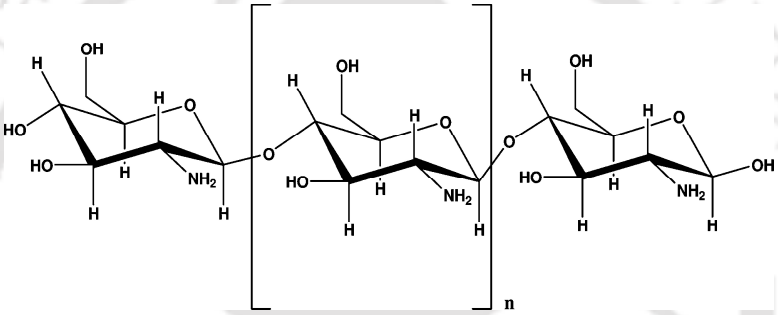

Figure1. Chemical structure of chitosan (β-1, 4-linked poly (d-glucosamine).

1.5.1: Antimicrobial activity of chitosan

Antimicrobial action of chitosan agent against fungi, bacteria, and viruses is well studied.[75-86] There are two proposed modes of action for microbial growth inhibition. Polycationic nature of chitosan strongly interacts with the negatively charged cell envelop and alters cell permeability.[75,76] The other mechanism involves the binding of chitosan with DNA to inhibit mRNA synthesis.[76] Hadwiger et al. proposed that when chitosan is released from the cell wall of fungal pathogens by hydrolytic enzymes of host plant, chitosan penetrates the nuclei of the fungus and interferes with mRNA and protein synthesis.[87] The proposed overall mechanism for its antimicrobial action is binding to the negatively charged bacterial cell wall, consequent destabilization of the cell envelope and altered permeability, followed by attachment to DNA and inhibition of DNA replication.[76]

1.6: Metal Nanoparticle/polymer composites

In recent years, incorporation of metal NPs into polymer found much attention, possibly because of the composites becoming important owing to the small size and large surface area of the NPs, and the composite exhibit better electrical, optical, and mechanical properties not seen in bulk counterpart.[92−98] As a result such NP- polymer composite materials have applications in photovoltaic cells, optical and biological systems, as conductive materials and coating formulations. Our group had synthesized Au NPs-polyaniline composite which has higher electrical conductivity compare to polyaniline NPs alone.[94] In 2005, our group had generated new method preparation of TiO_2 NP-polypyrrole composites which has greater photocatalytic activity compare to bare TiO_2 NPs dispersed in water. [95] Among the polymers, chitosan has been found more useful. Substantial content of primary amines and hydroxyl groups providing it with a strong affinity towards metal ions, which may be incorporated by simple chelation or by ion exchange process, making it an excellent support for synthesis of metal NPs.[96,97] In 2008, our group had also developed a simple method for the preparation of stable chitosan-Ag NP composite with high catalytic activity and antimicrobial activity.[97,98] Chitosan when combined with Ag NPs has higher antimicrobial efficacies reported by us and other groups. [98,99] Recent work in our laboratory has revealed stronger antimicrobial activity of a novel chitosan-Ag NP composite at concentrations lower than that of its individual components i.e. chitosan and Ag NPs. In the composite, the essential function of the positively charged chitosan matrix was to capture negatively charged bacteria on its surface; on the other hand, small - sized Ag NPs created pores on bacterial wall, thereby causing rapid disintegration of the bacteria.[98] Kelechi. et al. reported good antimicrobial activity of acrylated Cu NP composite and Cioffi et al. have reported antifungal and antifouling properties of a Cu NP-polymer composite.[60,62,93] Liu, x. synthesized magnetic chitosan nanocomposites and used them to remove heavy metal ions such as Pb^{2+}, Cd^{2+}, Hg^{2+}, Ni^{2+}, and Cu^{2+} from waste water.

1.7: Core-shell Nanoparticles

Bimetallic NPs, consisting of two different metals, offer greater advantage over their monometallic counterparts, since their optical, catalytic and biological properties can be tuned by changing the composition.[100−109] Two types of bimetallic NPs exist: alloy NPs and layered (core-shell) NPs. NPs with a homogeneous distribution of two metals are called alloys NPs and NPs with heterogeneous arrangement of two metals lead to the formation of core-shell NPs.[101,102,109] The optical properties of bimetallic colloids depend on the composition and the distribution of the two metals.[101− 110] Syntheses and applications of bimetallic colloids containing either Au or Ag in combination with other noble metals have been studied extensively.[101,109−110] Bimetallic NPs are superior to the monometallic NPs because of their synergistic and bifunctional effects.[114−120] Core-shell NPs have been proposed as ideal SERS active substrates.[111] Especially, SERS technique has been useful in biological research because it can detect small number or single molecules. Thus, core-shell NPs can further enhance SERS signal of a molecule by electromagnetic and chemical effects in comparison to pristine NPs. Core-shell NPs have been used for catalytic, optical and magnetic applications. [108-120] In catalytic reactions, the association of two different metals offers superior activity, increased stability and better selectivity.[112−118] In recent years Pt based core-shell NPs of non-noble metals have attracted great interest concerning their application in the field of electrocatalysis. [114-115] Dhavale et al. prepared well dispersed carbon supported core-shell Cu@Pt NPs of Pt possessing remarkable electrocatalytic activities.[114] Pt as a protective thin cell significantly helps Cu core to attain greater electrochemical stability in the operating polymer electrolyte membrane fuel cells.[115] Also, enhanced antibacterial activity of core-shell nanostructures has been noticed recently.[119, 120] Rana, S. et al. synthesized TiO_2-coated $NiFe_2O_4$ NPs which retain the magnetic characteristics of nickel ferrites encouraging their application as removable antimicrobial photocatalyst NPs and can be extracted from the sprayed surface after exposure. [119] In 2010, Chudasama et al. prepared super paramagnetic Fe_3O_4-Ag core-shell NPs that showed bactericidal activity on both Gram-negative and Gram-positive bacterial strains. The magnetic properties of these NPs were utilized to isolate NPs from the medium using external magnetic fields which

helped in preventing contamination of the environment during waste disposal. [120] Currently, core-shell Cu@Ag NPs are used in inkjet printing of conductive patterns. As Cu NPs have tendency to get oxidized at ambient conditions, Grouchko et al. synthesized a non-oxidizable form of Cu NPs by coating them with thin Ag shell and used these Cu@Ag NPs in the dispersions for Inkjet printing on various substrates.[103]

1.8: Mixed Metal Nanoparticles

Mixed Metal NPs can play an appreciable role in many areas of chemistry and physics and biological science. The most common use for mixed NPs has been in the area of catalysis, and researcher has found use both as the catalyst and as catalyst supports.[122–125] This attracted attention toward the preparation of these potentially new mixed metal NPs materials with variable composition having unique optical, catalytic and biological properties.[122–130] Researchers have explored and developed both physical and chemical methods by which such materials can be prepared. Bimetallic NPs with core-shell, heterostructure, or inter metallic and alloyed structures are rising as more important materials than monometallic NPs. [115-120,130–137] Bimetallic NPs (Cu, Ag) with different heterostructure i.e. alloy, core shell, heterodimer has been reported by several group, but in situ synthesis of mixed metal NPs in a polymer matrix and their application is still an unexplored area. [103,104,121,131–136] In 1995, Itakura et al. had synthesized phase-separated Ag-Cu composite colloids containing different molar fractions of Ag and Cu and studied their composition dependent optical spectral properties.[126] In 2003 Suyal et al. observed two plasmon peaks in Ag-Cu mixed colloids irrespective to their molar ratios. [127] Kiran et al. prepared Ag-Cu nanoclusters co-doped in SiO_2 matrix by the sol–gel process, and studied their nonlinear optical properties and the role of the surface-plasmon resonance on optical limiting properties.[128] It is well known that combining a transition metal with Pt gives enhanced catalytic activities for reactions such as oxygen reduction in fuel cells and direct oxidation of methanol. The mixed Pt-Co NPs and mixed Pt-Ru NPs supported on a carbon electrode possess high dispersion and high electrocatalytic activity for methanol oxidation at room temperature.[122,123] Cu NPs and Ag NPs exhibit good electrical conductivity but Cu NPs is susceptible to ambient oxidation. However, mixed Cu-Ag conductive ink is stable and suitable for use.[137,138] Recently Y.-S Li had

developed synthesis of Ag-Cu colloids ink and filled into a felt-tip pen and written on a substrate to make conducting lines using Ag-Cu composite nanoparticles.[138] Recently J, Yan et al. prepared polyvinylpyrrolidone protected Cu-Ag mixed NPs by mixing the highly concentrated Cu NPs and Ag NPs according to different molar ratios for low-temperature bonding application.[139] These mixed Cu NPs and Ag NPs composite could be an alternative option in electronics, catalysis, antimicrobial activity, and bioanalysis.[134–140]

1.9: Objectives of the thesis work

Infections with multidrug-resistant bacteria have become a serious problem in our environment. As the growth of antibiotic resistant bacteria is not controlled or killed by antibiotics, they are able to survive and even multiply in the presence of traditional antibiotics [43–46,143] with time; these serious infection-causing bacteria become resistant to most common antibiotics. Chitosan, derived from chitin found in exoskeleton of arthropods, beaks of cephalopods and it is soluble in weak acid solutions and has mild antibacterial property.[76 – 79] Ag NPs and Cu NPs have broad spectrum antimicrobial activities. [9,10,11,33,34] Microbes are unlikely to developed resistance against Ag NPs and Cu NPs.[45, 60] Moreover copper is inexpensive and non-toxic to mammalian cells.[32] Iodine solution has often been used as an antiseptic and disinfectant for the past more than 100 years.[141, 142]

At the interface between nano composite materials and biological systems, natural compounds and synthetic materials are blended into a new science related with the safe use of nanotechnology and nano materials designed for biological applications.[28] Because metal NPs have unique physical and chemical properties, interactions between NPs and biological systems are expected to depend on a number of NP properties including size, shape, morphology, charge, and surface functionalities. Metal NP-polymer composite materials hold great promise for improvements in human health, quality of life as well as for the environment.[62, 92, 93] The studies undertaken in this thesis illustrate one such effort at the interface between nano materials and biological systems**.** In my thesis, I have described the synthesis of various antibacterial NP composites and

investigated the antibacterial efficacy of these composite on green fluorescent protein (GFP) expressing *E. coli* bacteria and Gram-positive *B. cereus* bacteria and also attempted to understand the molecular mechanism of bactericidal action. Chitosan-Ag NP composite with iodine was found to exert reactive oxygen species generation in the cytoplasm of the bacterial cell leading to cell death. We have developed synthetic protocol of stable Cu NPs under atmospheric conditions in the presence of chitosan and molecular iodine. Studies of antibacterial property show that Cu NPs get attached to the cell walls, resulting in the perforation of the wall, which leads to cell death. Further, stable core-shell Cu@AgNP composites were synthesized using simple transmetallation reaction between Cu NPs in chitosan matrix and Ag^{+} ions. Cs-Cu@Ag NPs composites also exhibited antibacterial activity towards Gram-negative GFP expressing *E. coli* bacteria and Gram-positive *B. cereus* bacteria. We have also prepared CS embedded mix NP composites (Cu NPs and Ag NPs) and studied biocidal activity on GFP expressing *E. coli* bacteria.Use of the above nano materials as bactericidal agents represents a novel paradigm in antibacterial therapeutics owing to the fact that bacterial pathogens have evolved mechanisms to evade the action of most commercially available antibiotics.

1.10: Outline of This Thesis

This dissertation contains five chapters. Apart from **Chapter 1**, which gives a general introduction to the current status of nanotechnology research, our specific goals and a broad outline of this thesis, there are other four chapters which describe the important goals and achievements

Chapter 2 is devoted to our findings regarding the antibacterial activity of iodinated chitosan-Ag NP composite using GFP expressing *Escherichia coli (E. coli*) as a model system for investigating the antibacterial activities of composite.The salient features of this work include synthesis of chitosan-Ag NP composite, doping with molecular iodine and investigating its superior bactericidal potency against GFP-expressing recombinant *E. coli* (DH-5ά) in Lauria-Bertani (LB) bacterial growth medium. Use of GFP expressing *E. coli* simplifies the monitoring of the cell population changes during the action of the iodinated chitosan-Ag NP composite at different time points and provides easy detection

of the bactericidal activity of the composite by just observing the green fluorescence in the bacterial growth medium through fluorescence spectroscopy, fluorescence microscopy and cells viability analysis using a GFP-PI combination by Flow Cytometric Assay. We have used this property to a great benefit in our other studies also. The positively charged chitosan causes the negatively charged bacterial cell wall to get attached to the composite. The Ag NPs embedded in the composite interact with the cell wall of the bacteria to induce formation of pores on the cell wall. Introduction of pores on the cell wall leads bacteria to become unviable. The chitosan-Ag NP composite and iodine combination was found to exert reactive oxygen species generated oxidative stress in the cytoplasm, causes further damage to the cell. Our study reveals the effective bactericidal activity of the three different antibacterial components of the composite at a very low dose and brings us closer to understanding the mechanism of their synergistic action. Understanding the molecular mechanism of the mode of action of iodinated chitosan-Ag NP composite on the bacteria is essential from the scientific point of view for its use in commercial products.

Chapter 3A describes the development a novel method for the synthesis of Cu NPs under atmospheric conditions in the presence of CS as a stabilizer and their detailed characterization.The CS-Cu NP composite was prepared from the reaction of alkaline $CuSO_4$ and hydrazine in the presence of CS, and was separated from the reaction mixture and then redispersed in water in the presence of acetic acid. The spherical Cu NPs were stable in atmospheric conditions when molecular iodine was added to CS-Cu NP composite. Modern Analytical Instruments UV-visible spectroscopy, transmission electron microscopy (TEM) coupled with energy dispersive X-ray spectroscopy (EDX) analyses, field emission scanning electron microscopy (FESEM) and X-ray diffraction (XRD) were used to characterize the iodinated CS-Cu NP composite.

Chapter 3B is devoted to the antibacterial studies of iodinated CS-Cu NP composite on Gram-negative green fluorescent expressing *E. coli* bacteria and Gram-positive *Bacillus cereus (B. cereus)* bacteria. The minimum inhibitory concentration (MIC) of the iodinated composite on *E. coli* was found to be 130.8 µg/mL which contained 21.5µg/mL Cu NPs. This determined value of MIC for Cu NPs was much lower than those reported

in the literature. Effective surface charge (Zeta potential *ζ)* measurements confirmed an attractive interaction between iodinated CS-Cu NP composite and bacteria. Electron microscopic and flow cytometric studies revealed that the composite was attached to the bacterial cell wall which caused irreversible damage to the membrane eventually leading to cell death. Molecular mechanism of bactericidal action of the iodinated composite is discussed in light of our findings.

Chapter 4 describes synthesis, characterization and enhanced antibacterial activity of core-shell Cu@Ag NP composites. We have synthesized CS stabilized core-shell NPs using two-step seed-mediated growth method and studied their antimicrobial activity. Various Analytical techniques i.e. UV-visible spectroscopy, TEM, FESEM coupled with Energy Dispersive X-ray (EDX) and XRD, X-ray photoelectron spectroscopy (XPS) were used to characterize the CS-Cu@Ag NP composite. The Cu@Ag NPs in the CS composite were spherical and relatively uniform in size. Powder X-ray diffraction patterns revealed the presence of crystalline silver and the absence of any copper oxide or other by products. The core-shell structure was confirmed by a combination of UV-Vis, TEM, XRD and XPS probes. XPS analysis confirms metallic Ag, Cu and small amount of CuO species present in the CS-Cu@Ag NPs composite. Gram-negative GFP expressing *E. coli* and Gram-positive bacteria *B. cereus* were used to study the bactericidal activities of the CS-Cu@Ag NPs composite. Electron microscopic investigation, zeta potential measurements and flow cytometric estimates of cell viability revealed that the Cu@Ag NPs in the composite readily attached to the bacterial cell wall through electrostatic interactions causing irreversible damage to the membrane and finally leading to cell death. XPS results on CS-Cu@Ag NP composite treated on bacteria sample revealed comparable shift in Ag $3d_{5/2}$ and Ag $3d_{3/2}$ electrons which supported the existence of Ag-S species or to the expected values for Ag bound to sulfur.

Chapter 5 describes the synthesis, characterization and enhanced bactericidal action iodinated mixed NP composites (Cu NP, Ag NP). I_2-CS-Ag NP-Cu NP composites consisting of 3.4±0.9 nm Ag NPs and 11.4±3 nm Cu NPs were prepared using CS as the stabilizer in various Cu/Ag ratios. Molecular iodine enhances the stability and antimicrobial activity of the composites. The novel I_2-CS-Ag NP-Cu NP composites

were characterized by UV-visible spectroscopy, TEM, FESEM coupled with EDX analysis and XRD. A detailed antibacterial studies were carried out on GFP expressing *E. coli* bacteria. The synergistic bactericidal action of I_2-CS-Ag NP-Cu NP composite on GFP expressing *E. coli* bacteria is found to be more effective, compared to the individual NPs.

References

(1) Cao, G. Nanostructures & nanomaterials: synthesis, properties & applications. World Scientific Publishing Company: **2004.**

(2) Barnes, W. L.; Dereux, A.; Ebbesen, T. W. *Nature* **2003,** *424,* 824-830.

(3) Liz-Marzan, L. M. *Materials Today* **2004,** *7,* 26-31.

(4) Schwartzberg, A. M.; Zhang, J. Z. *J. Phys. Chem. C* **2008,** *112,* 10323-10337.

(5) Link, S.; El-Sayed, M. A., *Int. Reviews in Physical Chemistry* **2000,** *19,* 409-453.

(6) Templeton, A. C.; Pietron, J. J.; Murray, R. W.; Mulvaney, P. *J. Phys. Chem. B* **1999,** *104,* 564-570.

(7) Daniel, M.-C.; Astruc, D. *Chem. Rev.* **2003,** 104, 293-346.

(8) Crooks, R. M.; Zhao, M.; Sun, L.; Chechik, V.; Yeung, L. K. *Acc. Chem. Res.* **2000,** *34,* 181-190.

(9) Sondi, I.; Salopek-Sondi, B. *J. Colloid Interface Sci.* **2004,** *275,* 177-182.

(10) Jose Ruben, M.; Jose Luis, E.; Alejandra, C.; Katherine, H.; Juan, B. K.; Jose Tapia, R. r.; Miguel Jose, Y. *Nanotechnology* **2005,** *16,* 2346.

(11) Gogoi, S. K.; Gopinath, P.; Paul, A.; Ramesh, A.; Ghosh, S. S.; Chattopadhyay, A., *Langmuir* **2006,** *22,* 9322-9328.

(12) Huang, X. H.; Jain, P. K.; El-Sayed, I. H.; El-Sayed, M. A. *Nanomedicine* **2007,** 2, 681.

(13) Jain, P. K.; Huang, X. H.; El-Sayed, I. H.; El-Sayed, M. A. *Acc. Chem. Res.* **2008,** *41,* 1578.

(14) Henglein, A. *Top. Curr. Chem.***1988,** *143,* 113-180.

(15) Henglein, A.*Chem. Rev.***1989,** *89,* 1861-1873.

(16) Roduner, E. *Chem. Soc. Rev.***, 2006,** *35,* 583-592.

(17) Faraday, M. Philos. Trans. **1857,** 147, 145-181.

(18) Mie, G. Ann. Phys. **1908,** *25*, 377-445.

(19) Alivisatos, A. P. The *J. Phys. Chem.* **1996,** *100*, 13226-13239.

(20) Bruchez, M.; Moronne, M.; Gin, P.; Weiss, S.; Alivisatos, A. P. *Science* **1998,** *281*, 2013-2016.

(21) Narayanan, R.; El-Sayed, M. A. *J. Catal.* **2005,** *234*, 348-355.

(22) Kim, S.-W.; Kim, M.; Lee, W. Y.; Hyeon, T. *J. Am. Chem. Soc.* **2002,** *124*, 7642-7643.

(23) Turkevich, J.; Stevenson, P. C.; Hillier, J. *Discuss. Faraday Soc.* **1951,** *11*, 55-75.

(24) Enustun, B. V.; Turkevich, J. *J. Am. Chem. Soc.* **1963,** *85*, 3317-3328.

(25) Haruta, M.; Kobayashi, T.; Sano, H.; Yamada, N. *Chem. Lett.* **1987,** *16*, 405-408.

(26) Haruta, M.; Yamada, N.; Kobayashi, T.; Iijima, S. *J. Catal.***1989,** *115*, 301-309.

(27) Haruta, M.; Tsubota, S.; Kobayashi, T.; Kageyama, H.; Genet, M. J.; Delmon, B. *J. Catal.***1993,** *144*, 175-192.

(28) Nel, A. E.; Madler, L.; Velegol, D.; Xia, T.; Hoek, E. M. V.; Somasundaran, P.; Klaessig, F.; Castranova, V.; Thompson, M. *Nat Mater* **2009,** *8*, 543-557.

(29) Russell, A. D.; Hugo, W. B., *Prog Med Chem.* **1994,** *31*, 351-70.

(30) Ahearn, D. G.; May, L. L.; Gabriel, M. M., *J. Ind. Microbiol.* **1995,** *15*, 372.

(31) Feng, Q. L.; Wu, J.; Chen, G. Q.; Cui, F. Z.; Kim, T. M.; Kim, J. O. *J. Biomed. Mater. Res.* **2000,** *52*, 662–668.

(32) Borkow, G.; Gabbay, J. *Curr. Med. Chem.***2005,** 12, 2163-2175.

(33) Ruparelia, J. P.; Chatterjee, A. K.; Duttagupta, S. P.; Mukherji, S. *Acta Biomaterialia* **2008,** *4*, 707-716.

(34) Yoon, K.-Y.; HoonByeon, J.; Park, J.-H.; Hwang, J. *Sci. Total Environ.* **2007,** *373*, 572-575.

(35) Kreibig, U.; Volmer, M. *Optical properties of metal clusters*. Springer: 1995.

(36) Murphy, C. J.; Sau, T. K.; Gole, A. M.; Orendorff, C. J.; Gao, J.; Gou, L.; Hunyadi, S. E.; Li, T. *J. Phys. Chem. B* **2005,** *109*, 13857-13870

(37) Nie, S.; Emory, S. R. *Science* **1997,** *275*, 1102-1106.

(38) Lee, P. C.; Meisel, D. *J. Phys. Chem.* **1982,** *86*, 3391-3395.

(39) Sherry, L. J.; Chang, S.-H.; Schatz, G. C.; Van Duyne, R. P.; Wiley, B. J.; Xia, Y. *Nano Lett.* **2005,** *5,* 2034-2038.

(40) Nagy, A.; Mestl, G. *Appl. Catal. A: General* **1999,** *188,* 337-353.

(41) Magdassi, S.; Grouchko, M.; Toker, D.; Kamyshny, A.; Balberg, I.; Millo, O. *Langmuir* **2005,** *21,* 10264-10267.

(42) Li, Y.; Wu, Y.; Ong, B. S. *J. Am. Chem. Soc.* **2005,** *127,* 3266-3267.

(43) Julian, J. *J. Environ. Sci. Technol.* **2006,** *40,* 6531-6534.

(44) Tenover, Fred C. *Am. J. Infect. Control* **2006**, *119,* S3-S10

(45) Stoimenov, P. K.; Klinger, R. L.; Marchin, G. L.; Klabunde, K. J. *Langmuir* **2002,** *18,* 6679-6686.

(46) Pal, S.; Tak, Y. K.; Song, J. M. *Appl. Environ. Microbiol.***2007,** *73,* 1712-1720.

(47) McDonnell, A. M. P.; Beving, D.; Wang, A.; Chen, W.; Yan, Y. *Adv. Funct. Mater.* **2005,** 15, 336-340..

(48) Zhang, L.; Yu, J. C.; Yip, H. Y.; Li, Q.; Kwong, K. W.; Xu, A.-W.; Wong, P. K., *Langmuir* **2003,***19,* 10372-10380.

(49) Zhang, S.; Fu, R.; Wu, D.; Xu, W.; Ye, Q.; Chen, Z. *Carbon* **2004,** *42,* 3209-3216.

(50) Oya, A.; Banse, T.; Ohashi, F.; Otani, S., *Appl. Clay Sci.***1991,** *6,* 135.

(51) Kim, Y. H.; Lee, D. K.; Cha, H. G.; Kim, C. W.; Kang, Y. S. *J. Phys. Chem. C***2007,** *111,* 3629-3635.

(52) Rhim, J. W.; Hong, S. I.; Park, H. M.; Ng, P. K., *J. Agric. Food Chem.* **2006,** *54,* 5814-5822.

(53) Sanpui, P.; Murugadoss, A.; Prasad, P. V. D.; Ghosh, S. S.; Chattopadhyay, A. *Int. J. Food Microbiol.***2008,** *124,* 142-146.

(54) Zhang, Z.; Zhang, L.; Wang, S.; Chen, W.; Lei, Y. *Polymer* **2001,** *42,* 8315–8318.

(55) Chauhan, B. P. S.; Rathore, J.; Sardar, R.; Tewari, P.; Latif, U. *J. Organomet. Chem.* **2003,** *686,* 24–31.

(56) Duncan, T. V. *J. Colloid Interface Sci.* **2011,** *363,* 1-24.

(57) Cioffi, N.; Ditaranto, N.; Torsi, L.; Sabbatini, L. In *Nanotechnologies for the Life Sciences*, Wiley-VCH Verlag GmbH & Co. KGaA: 2007.

(58) Vukojevic, S.; Trapp, O.; Grunwaldt, J.-D.; Kiener, C.; Schuth, F. *Angew. Chem., Int. Ed*. **2005,** *44,* 7978–7981.

(59) Ressler, T. B.; Kniep, L.; Kasatkin, I.; Schlogl, R. *Angew. Chem. Int. Ed*. **2005,** *44*, 4704-4707.

(60) Cioffi, N.; Ditaranto, N.; Torsi, L.; Picca, R. A.; De Giglio, E.; Sabbatini, L.; Novello, L.; Tantillo, G.; Bleve-Zacheo, T.; Zambonin, P. G. *Anal Bioanal Chem.* ***2005,*** *382*,1912-1918.

(61) Kim Y. H.; Lee D. K.; Cha H. G.; Kim C. W.; Kang Y. C.; Kang Y. S. *J. Phys. Chem. B* **2006,** *110*, 24923-24928.

(62) Anyaogu, K. C.; Fedorov, A. V.; Neckers, D. C. *Langmuir* **2008,** 24, 4340-4346.

(63) Wei, Y.; Chen, S.; Kowalczyk, B.; Huda, S.; Gray, T. P.; Grzybowski . B. A. *J. Phys. Chem. C* **2010,** *114*, 15612-15616.

(64) Wang, Y.; Asefa, T. *Langmuir* **2010**, *26*, 7469-7474.

(65) Bozzini, B.; D'Urzo, L.; Re, M.; De Riccardis, F. *J. Appl. Electrochem.* **2008,** *38*, 1561.

(66) Magdassi, S.; Grouchko, M.; Kamyshny, A. *Materials* **2010**, *3*, 4626-4638.

(67) Dhas, N. A.; Raj C. P.; Gedanken, A. *Chem. Mater***.1998,***10*, 1446- 1452.

(68) Kumar R.V.; Mastai, Y.; Diamant, Y.; Gedanken , A. *J. Mater. Chem.***2001,*11*,**1209- 1213.

(69) Vitulli, G.; Bernini, M.; Bertozzi, S.; Pitzalis, E.; Salvadori, P.; Coluccia, S.; Martra, G. *Chem. Mater.***2002,*14***,** 1183- 1186.

(70) Casella, I. G.; Cataldi, T. R. I.; Guerrieri , A.; Desimoni, E. *Anal. Chim. Acta* **1996,***335***,** 217-225.

(71) Lisiecki, I.; Pileni, M. P. *J. Am. Chem. Soc.* **1993,** *115***,** 3887-3896.

(72) Yeh, M. S.; Yang, Y. S.; Lee, Y. P.; Lee, H. F.; Yeh, Y. H.; Yeh, C. S. *J. Phys. Chem. B* **1999,***103*, 6851–6857.

(73) Joshi, S. S.; Patil, S. F.; Iyer, V.; Mahumuni, S. *Nanostruct. Mater*.**1998,** *10*, 1135-1144.

(74) Kapoor, S.; Joshi. R.; Mukherjee. T. *Chem. Phys. Lett.* **2002**, *354*, 443-448.\

(75) Rabea, E. I.; Badawy, M. E. -T.; Stevens, C. V.; Smagghe, G.; Steurbaut, W. *Biomacromolecules***2003,** *4*, 1457– 1465.

(76) Sudarshan, N. R.; Hoover, D. G.; Knorr, D., *Food Biotechnol.* **1992,** *6*, 257-272. Antibacterial action of chitosan.

(77) Han, L. K.; Kimura, Y.; Okaauda, H. *Int. J. Obes. Relat. Metab.Disord.* **1999**, *23*, 174-179.

(78) Helander, I. M.; Nurmiaho-Lassila, E. -L.; Ahvenainen, R.; Rhoades, J.; Roller, S. *Int. J. Food Microbiol.***2001,** 71, 235– 244.

(79) Sashiwa, H.; Aiba, S.-i. *Progress in Polymer Science* **2004,** 29, 887-908.

(80) Muzzarelli, R. A. A. *Carbohydr. Polym.* **1992**, *19*, 231-236.

(81) Muzzarelli, R. A. A.; Ilari, P. *Int. J. Biol. Macromol.* **1994**, *16*, 177-180. (Solubility and structure of N-carboxymethylchitosan)

(82) Muzzarelli, R. A. A.; Ilari, P.; Tomasetti, M. *Carbohydr. Polym.* **1993**, *20*, 99-105.

(83) Heras, A.; Rodriguez, N. M.; Ramos, V. M.; Agullo, E. *Carbohydr. Polym.***2001**, *44*, 1-8.

(84) Jia, Z.; Shen, D.; Xu, W. *Carbohydr. Res.* **2001**, *333*, 1-6.

(85) Shigemasa, Y.; Saito, K.; Sashiwa, H.; Saimoto, H. *Int J Biol Macromol.* **1994,** 16, 43-49.

(86) Muzzarelli, R.; Baldassarre, V.; Conti, F.; Ferrara, P.; Biagini, G.; Gazzanelli, G.; Vasi, V. *Biomaterials* **1988,** 9, 247-252.

(87) Fristensky, B.; Riggleman, R. C.; Wagoner, W.; Hadwiger, L. A. *Physiological Plant Pathology* **1985,** 27, 15-28.

(88) Allan, C. R.; Hadwiger, L. A. *Exp. Mycol.* **1979,** 3, 285-287.

(89) Shin, Y.; Yoo, D. I.; Min, K. *J. Appl. Polym. Sci.* **1999,** *74*, 2911-2916.

(90) Hirano, S.; Koishibara, Y.; Kitaura, S.; Taneko, T.; Tsuchida, H.; Murae, K.; Yamamoto, T. *Biochem. Syst. Ecol.* **1991,** 19, 379-384.

(91) Payne, G. F.; Raghavan, S. R. *Soft Matter* **2007,** *3*, 521-527.

(92) Balazs, A. C.; Emrick, T.; Russell, T. P. *Science* **2006,** *314*, 1107-1110.

(93) Cioffi, N.; Torsi, L.; Ditaranto, N.; Tantillo, G.; Ghibelli, L.; Sabbatini, L.; Bleve-Zacheo, T.; D´Alessio, M.; Zambonin, P. G.; Traversa, E. *Chem. Mater.* **2005**, *17*, 5255-5262.

(94) Sarma, T. K.; Chattopadhyay, A. *J. Phys. Chem. A* **2004,** *108*, 7837-7842.

(95) Chowdhury, D.; Paul, A.; Chattopadhyay, A. Langmuir **2005,** *21*, 4123-4128.

(96) Hardy, J. J. E.; Hubert, S.; Macquarrie, D. J.; Wilson, A. J. *Green Chem.* **2004,** 6, 53- 56.

(97) Murugadoss, A.; Chattopadhyay, A. *Nanotechnology* **2008**, 19, 015603(9pp)

(98) Sanpui, P.; Murugadoss, A.; Prasad, P. V. D.; Ghosh, S. S.; Chattopadhyay, A. *Int. J. Food Microbiol.***2008,** 124, 142-146.

(99) Rhim, J. W., Hong, S. I., Park, H. M., and Ng, P. K. *J. Agric. Food Chem.***2006,** *54*, 5814- 5822.

(100) Liu, X.; Hu, Q.; Fang, Z.; Zhang, X.; Zhang, B. *Langmuir* 2008, 25, 3-8.

(101) Morriss, R. H.; Collins L. F. *J. Chem. Phys.* **1964,** *41*, 3357 -3363.

(102) Toshima, N.; Yonezawa, T. New *J. Chem.* **1998,** *22*, 1179-1201.

(103) Grouchko, M.; Kamyshny, A.; Magdassi, S. *J. Mater. Chem.* **2009,** *19*, 3057-3062.

(104) Cazayous, M.; Langlois, C.; Oikawa, T.; Ricolleau, C.; Sacuto, A. *Phys. Rev. B* **2006,** *73*, 113402.

(105) Tsuji, M.; Hikino, S.; Tanabe, R.; Matsunaga, M.; Sano, Y. *CrystEngComm*, **2010,** *12*, 3900-3908.

(106) Zhang, J.; Tang, Y.; Lee, K.; Ouyang, M. *Science* **2010,** *327*, 1634-1638.

(107) Jung, D. S.; Lee, H. M.; Kang Y. C.; Park S. B. *J. Colloid Interface Sci.* **2011,** *364*, 574-581.

(108) Steinbruck, A.; Csaki, A.; Festag, G.; Fritzsche, W. *Plasmonics* **2006,** *1*, 79-85.

(109) Rodriguez-Gonzalez, B.; Burrows, A.; Watanabe, M.; Kiely, C. J.; Liz Marzan, L. M., *J. Mater. Chem.* **2005,** *15*, 1755-1759.

(110) Ma, Y.; Li, W.; Cho, E. C.; Li, Z.; Yu, T.; Zeng, J.; Xie, Z.; Xia, Y. *ACS Nano* 2010, *4*, 6725– 6734 .

(111) Netzer ,N. L.; Qiu, C.; Zhang, Y.; Lin, C.; Zhang, L.; Fong, H.; Jiang, C. *Chem. Commun.* **2011,** *47*, 9606-9608.

(112) Zhou, S.; Varughese, B.; Eichhorn, B.; Jackson, G.; McIlwrath, K. *Angew. Chem. Int. Ed*. **2005,** *44*, 4539-4543.

(113) Sarkar, A.; Manthiram, A. *J. Phys. Chem.C* **2010,** *114*, 4725-4732.

(114) Dhavale, V. M.; Unni, S. M.; Kagalwala, H. N.; Pillai, V. K.; Kurungot, S. *Chem. Commun.* **2011,** *47*, 3951-3953.

(115) Alayoglu, S.; Nilekar, A. U.; Mavrikakis, M.; Eichhorn, B. *Nat Mater* 2008, *7*, 333-338.

(116) Mani, P.; Srivastava, R.; Strasser, P. *J. Phys. Chem.C* 2008, *112*, 2770-2778.

(117) Nilekar, A. U.; Alayoglu, S.; Eichhorn, B.; Mavrikakis, M. *J. Am. Chem. Soc.* 2010, 132, 7418-7428.

(118) Jiang, H.-L.; Xu, Q. *J. Mater. Chem.* **2011,** *21,* 13705-13725.

(119) Rana, S.; Rawat, J.; Misra, R. D. K. *Acta Biomaterialia***.2005,** *1,* 691–703.

(120) Chudasama, B.; Vala, A. K.; Andhariya, N.; Upadhyay, R. V.; Mehta, R. V. *Nano Res* **2009,** *2,* 955-965.

(121) Taner, M.; Sayar, N.; Yulug, I. G.; Suzer S. *J. Mater. Chem.* **2011,** *21,* 13150-13154.

(122) Zhang, X.; Chan, K.-Y. *J. Mater. Chem.* **2002,** *12,* 1203-1206.

(123) Zhang, X.; Chan, K.-Y. Chem. Mater. **2003,** *15,* 451-459.

(124) Liu, Z.; Lee, J. Y.; Han, M.; Chen, W.; Gan, L. M. *J. Mater. Chem.* **2002**, *12,* 2453-2458.

(125) Zeng, J. H.; Lee, J. Y. *Mater. Chem. Phys.* **2007,** *104,* 336-341.

(126) Itakura, T.; Torigoe, K.; Esumi, K. *Langmuir* **1995,** *11,* 4129-4134.

(127) Suyal, G. *Thin Solid Films* **2003,** *426,* 53-61.

(128) Kiran, P. P.; Bhaktha, B. N. S.; Rao, D. N.; De, G. *J. Appl. Phys.* **2004,** *96,* 6717-6723.

(129) Tabrizi, N. S.; Xu, Q.; van der Pers, N. M.; Schmidt-Ott, A. *J. Nanopart. Res.* **2010,** *12,* 247-259.

(130) Li, G. P.; Luo, Y. J. *Inorg. Chem.* **2008,** 47, 360-364.

(131) Xu, Z.; Lai, E.; Shao-Horn, Y.; Hamad-Schifferli, K. *Chem. Commun.* **2012**, *48,* 5626-5628.

(132) Butovsky, E.; Perelshtein, I.; Gedanken, A. *J. Mater. Chem.* **2012**, *22,* 15025-15030.

(133) Huang, X. Q.; Li, Y. J.; Zhou, H. L.; Zhong, X.; Duan, X. F.; Huang, Y., *Chem.-Eur. J.* **2012**, *18,* 9505-9510.

(134) Rapallo, A.; Rossi, G.; Ferrando, R.; Fortunelli, A.; Curley, B. C.; Lloyd, L. D.; Tarbuck, G. M.; Johnston, R. L . *J. Chem. Phys.* **2005,** *122,* 194308 (9 pp).

(135) Chowdhury, S.; Bhethanabotla, V. R.; Sen, R. *Appl. Phys. Lett.* **2009,** *95,*131115 (3 pp).

(136) Valodkar, M.; Modi, S.; Pal, A.; Thakore, S. *Mater Res Bull* **2011,** *46,* 384–389.

(137) Woo K.; Kim, D.; Kim, J. S.; Lim, S.; Moon, J. *Langmuir* **2009,** *25*, 429-433.

(138) Li, Y.-S.; Lu, Y.-C.; Chou, K.-S.; Liu, F.-J. *Mater Res Bull* **2010,** 45, 1837-1843.

(139) Yan, J.; Zou, G.; Wu, A.; Ren, J.; Hu, A.; Zhou, Y. N. *J. Electron. Mater.* **2012,** *41*, 1886-1892.

(140) McLean, R. J. C.; Hussain, A. A.; Sayer, M.; Vincent, P. J.; Hughes, D. J.; Smith, T. J. N. *Can. J. Microbiol.* **1993,** 39, 895-899.

(141) Gottardi W, Iodine and Iodine compounds. in "*Disinfection, sterilization, and Preservation*" 4th ed., ed. Bloc, S. S., Lea and Febiger, Philadelphia, PA, **1991**, pp. 152-166.

(142) Gottardi, W. *Arch. Pharm. Med. Chem*. **1999**, *332*, 151-157.

(143) Russell, A. D. *J Hosp Infect* **1999,** *43*, S57-S68.

Chapter 2

Antimicrobial iodine-doped silver nanoparticle-chitosan composite: synthesis, characterization and applications

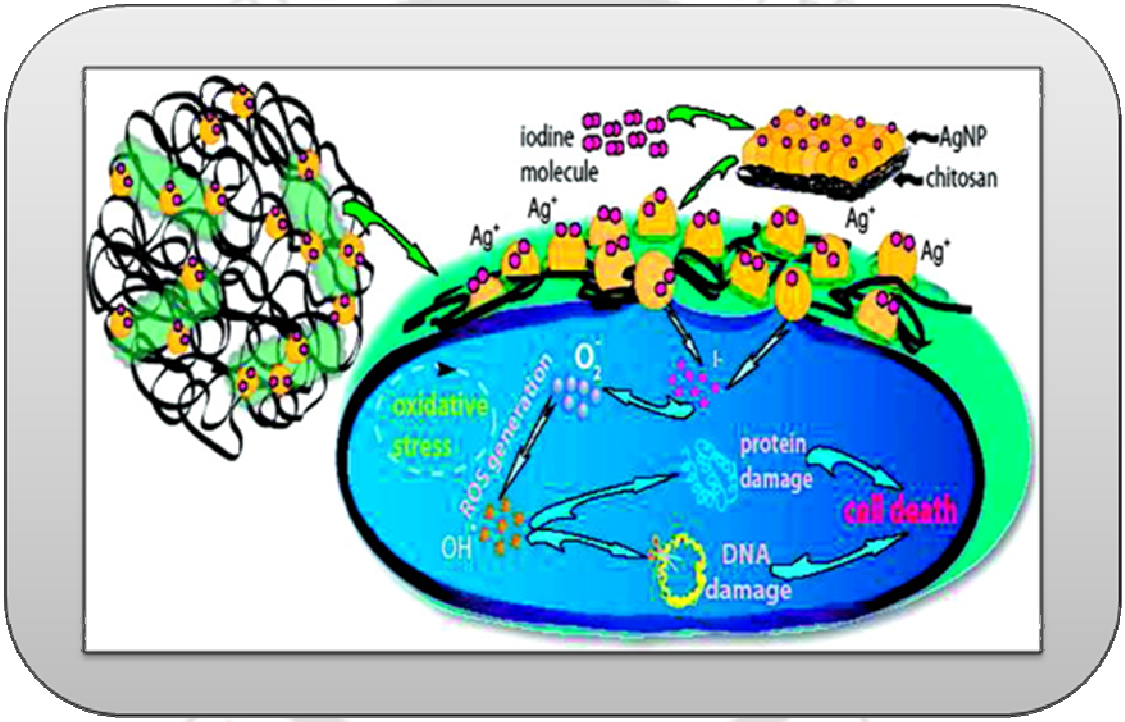

The work embodied herein has been published as an article as described below.

"Heightened reactive oxygen species generation in the antimicrobial activity of a three component iodinated chitosan-Ag nanoparticle composite. Madhuchanda Banerjee , **Sadhucharan Mallick ,** Anumita Paul, Arun Chattopadhyay, and Siddhartha Sankar Ghosh composite *Langmuir* **2010,** *26(8),* 5901–5908."

2.1: Introduction

The advent of nanoscale science and technology has recently propelled the introduction of inorganic nanoparticles (NPs) as antimicrobial agents.[1-6] interestingly, among the extensively studied inorganic antibacterial agents; silver has been the most prominent owing to effective biocidal abilities of both silver ions and Ag NPs at low concentrations.[5-20] The advantage over conventional and narrow-target antibiotics is that microbes are less likely to develop resistance against silver, as they do against antibiotics. The general understanding of the mode of action of Ag NPs is that the NPs get attached to the sulfur-containing proteins on the bacterial cell wall, leading to increased permeability of the membrane, finally causing cell death. In addition, Ag^+ ions have been reported to induce generation of intracellular reactive oxygen species in bacterial cells.[3] A few reports have suggested Ag^+ ions as the actual biocidal species, which are provided by active surfaces of silver nanoparticles and silver oxide present on the surfaces of these nanoparticles. The silver ions enter the bacterial cells, where they are reduced as the cell attempts to remove them from the cell interior, eventually leading to cell destruction.[13] The possible use of silver nanoparticles (Ag NPs) as antibacterial agent has been investigated from our laboratory and other several groups. [9, 14] In 2006 our group have established that Ag NPs of less than 10 nm diameter create pores on the bacterial cell walls, thereby releasing the cytoplasmic content to the medium, which leads to cell death without affecting the intracellular and extracellular proteins and nucleic acids of the bacterium.[9]

It has been demonstrated that composites of Ag NP with polymer results in the enhancement of antimicrobial activities of Ag NPs at lower concentrations.[22, 23, 26] Among the polymers that have been found useful in this regard chitosan a cationic polysaccharide composing of randomly distributed (1,4)-linked 2-amino-2-deoxy-β-d-glucose units has been reported to be used as such[33] or in the form of composite with Ag NPs with high antimicrobial efficacies.[21, 25, 26] It is generally accepted that polycationic chitosan can bind with negatively charged cell membranes, which will then lead to decrease in the osmotic stability of the cell, followed by subsequent leakage of

intracellular constituents.[27, 28] In 2008 our group [9] has shown higher bactericidal efficiency of a novel chitosan Ag NP composite at concentrations lower than that of its individual components i.e. chitosan and Ag NPs. In the composite, the essential use of the positively charged chitosan getting attached to the negatively charged bacterial cell surface; while the Ag NPs in the composite created pores on bacterial wall, thereby causing rapid disintegration of the bacteria. The antibacterial activity of the composite has further enhanced by doping chitosan-Ag NP composite with other inorganic compound with heightened killing capacity. In this regard, iodine is an easily available antiseptic and disinfectant, the powerful disinfecting activity of which has been highly documented. It has the broadest range of action, fewest side effects and bacterial resistance against it is not known. Molecular iodine (I_2) and hypoiodous acid (HIO) are believed to be mainly responsible for bactericidal activity.[29, 30] Both of these substances can penetrate the cell wall of microorganisms rapidly. The toxicity mechanism of iodine on bacterial cells has generally been attributed to its ability to generate reactive oxygen species (ROS). The ROS subsequently trigger various types of cell damage, such as lipid peroxidation, DNA damage, and protein oxidation.[30] The toxicity of iodine is assumed to involve four different reactions. First, iodine can oxidize the sulfhydryl group (SH) of the amino acid cysteine, thereby interfering with the formation of disulfide (−S−S−) bridges, which are important in protein folding. Second, N-iododerivatives block a hydrogen bond in certain amino acids or nucleotides (e.g., lysine, histidine, arginine, adenine, cytosine, and guanine). As a result, a lethal disorder due to impaired functioning of proteins and other biomolecules may occur. Third, iodine can react with phenolic group of tyrosine, forming monoiododerivatives or diiododerivatives. In this case, the bulky iodine atoms in the ortho-position can cause steric hindrance during hydrogen bonding of the phenolic OH group, thus preventing its normal biological activity. Lastly, iodine can react with carbon-carbon double bond of the unsaturated fatty acids, leading to changes in membrane functions.

After a continuous and evolving effort we have been able to develop newer composites of Ag NP with polymers and other antibacterial agents in order to minimize the use of relatively toxic Ag, while taking advantage of its antimicrobial and anticancer properties. Understanding the mechanism of action is central to the development of

newer materials and compositions, especially when the synergy of action of components need to be utilized. In the present study, we have investigated the synergy in the bactericidal potency of a chitosan-Ag NP composite in the presence of molecular iodine. Briefly, the iodine-doped chitosan-silver nanoparticle composite was synthesized using an established method.[36] UV-Vis spectroscopy was used to establish the formation of Ag NPs, incorporation of iodine in the composite and to study the bacterial growth in the presence of various agents. Scanning electron microscopy (SEM) and transmission electron microscopy (TEM) were used to establish the formation of the composite with the presence of Ag NPs. In addition, TEM indicated the interaction of the composite with the bacteria. Fluorescence spectroscopic and microscopic methods were used to follow the growth of bacteria. Flow cytometric analyses indicated possible enhanced cell wall damage in the presence of the composite. Assay of oxidative stress in bacterial cells was pursued using nitroblue tetrazolium reduction (NBT) method. GFP-expressing recombinant *Escherichia coli* (*E. coli*) bacteria have been used to study the efficacy as well as investigate the mechanism of action of the combination. The results suggest that production of iodine radical (atom) on the surface of Ag NPs triggers the generation of reactive oxygen species (ROS). Essentially, the negatively charged bacterial cell wall gets attached to the positively charged chitosan polymer, while the Ag NPs present in the composite make the cell wall porous and the iodine radials created on the surface of the NP induce the production of ROS, thereby providing the synergy of action of the three components. Thus, the combination exhibits superior antimicrobial activity in comparison to either of the component species. The generation of free radical species in the medium is a new way of achieving antimicrobial activity involving a three-component agent, with concentration of Ag NP far below than that required in its composite with chitosan or the NP alone. The present study indicates that a novel material with three antimicrobial components has been used where the component plays their roles in tandem, in order to achieve superior activity.

2.2: Outline of the research work

I. Use of nanoscale materials as bactericidal agents represents a novel paradigm in antibacterial therapeutics owing to the fact that bacterial pathogens have evolved mechanisms to evade the action of most commercially available antibiotics.

II. Ag NPs have been variously portrayed as antimicrobial agent owing to their biocidal activity at low concentrations and comparatively less toxicity to mammalian cells.

III. Combining Ag NPs with antimicrobial polymers increases their efficiency by exploiting the active components of the individual substances.

IV. In the present work, the superior antimicrobial activity of a chitosan-Ag NP composite in the presence of molecular iodine was investigated using GFP expressing *E. coli* bacteria.

V. A plausible mechanism of antibacterial activity has been proposed with the chitosan polymer getting attached to the bacterial cell wall, while the Ag NPs in the composite turn the cell wall porous. The iodine radicals produced on Ag NP surface induced oxidative stress by producing reactive oxygen species.

VI. Overall, an increase in antibacterial activity of chitosan-Ag NP composite was achieved by synergy with the antibacterial properties of chitosan, Ag NP and iodine.

2.3: Experimental section

2.3.1: Materials and methods

Silver nitrate ($AgNO_3$, 99.5%; Merck), chitosan of high molecular weight (75% deacetylated; Sigma-Aldrich Chemical Co.), sodium hydroxide (NaOH, 98%; Merck, India), acetic acid (glacial, 99–100%; Merck, India) were used as received without further purification. Milli-Q grade (resistivity 18.2 $M\Omega cm^{-1}$) water was used in all experiments. Luria-Bertani (LB) broth was purchased from HiMedia, Mumbai, India.

Agarose for gel electrophoresis was obtained from Sigma-Aldrich Chemical Pvt. Ltd., Kolkata, India. GFP-expressing recombinant *E. coli* were grown in LB broth at 37°C and at 220 rpm for 12 h.

2.3.2: Iodine doped silver nanoparticle-chitosan composite preparation

Chitosan-Ag NP composite was synthesized, by adding 2 mL of freshly prepared 10mM $AgNO_3$ solution and 100 µL of 0.3M NaOH solution to 50 mL of 0.2%(w/v) chitosan solution in water, with constant stirring and being kept at 95^0 C. The appearance of a yellow color in 1min after addition of the NaOH solution indicated formation of Ag NPs. The reaction was stopped after 10 min and the precipitate was filtered and washed with sterile distilled water. The filtrate was dried, and then a 0.2% (w/v) solution of composite in 0.1%(v/v) acetic acid solution was prepared . To the chitosan-Ag NP composite solution, 0.2 M iodine solution in ethanol (50µL/mL) was added and mixed thoroughly. Different concentrations of this solution obtained by systematic dilution were then used for antibacterial activity studies. The corresponding solution pH was adjusted to 6.3 by the addition of dilute NaOH solution prior to antibacterial activity study.

2.3.3: Characterization of the iodine doped silver nanoparticle-chitosan composite

2.3.3.1: UV-Vis spectroscopic measurements

UV-visible spectra of the iodinated chitosan-Ag NP composite were obtained using a spectrophotometer (Lambda 45; Perkin-Elmer156 Fremont, CA). GFP recombinant *E. coli* (DH5α) cells were grown 12 h in 5 mL of LB ampicillin medium aerobically at 37 °C. Samples were withdrawn periodically to measure the optical density (O.D) at 595 nm using a UV-Vis spectrophotometer and the GFP-associated fluorescence using a fluorescence spectrophotometer (Varian Cary Eclipse).

2.3.3.2: Fluorescence spectroscopy

To monitor bacterial cell population fluorescence spectroscopic studies were carried out using Fluorescence spectrophotometer (Varian Cary Eclipse). The excitation wavelength for fluorescence studies was set at 400 nm. Fluorescence spectra of the GFP expressing *E. coli* were recorded for untreated bacteria and bacteria treated with chitosan-Ag NP composite, iodine and iodinated chitosan-Ag NP composite respectively, at different time intervals (2, 4, 8 and 12 h). Samples for fluorescence spectroscopic measurement were prepared by following a similar procedure as mentioned before for the O. D measurements. Also the fluorescence spectra of the supernatant were recorded upon centrifugation, in order to monitor the leakage of GFP on to the bacterial growth medium due to the action of chitosan-Ag NP composite, iodine and iodinated chitosan-Ag NP composite respectively.

2.3.3.3: Fluorescence microscopy

Fluorescence microscopic techniques have been utilized to evaluate the antibacterial efficiency of the composite. Fluorescence from the GFP-expressing E. coli cells was well utilized to monitor the population growth of the bacteria by observing the chitosan-Ag NP composite and iodinated chitosan-Ag NP composite treated samples under an epifluorescence microscope (Axioskop2MAT, Carl Zeiss) at different time points. Samples for fluorescence microscopic studies were prepared by taking out 50 µL aliquots from the GFP-expressing E. coli incubated with chitosan-Ag NP composite, iodinated chitosan-Ag NP composite and without composite in LB medium and then spreading the aliquots on microscopic slides. The excitation wavelength used was controlled by a band pass filter of 445-495 nm, and the observation filter had a long-pass filter wavelength above 515 nm. The effects of iodinated chitosan-Ag NP composite on DNA studied using a confocal laser scanning microscope (CLSM; Axiovert 200 M, LSM 510 META, Carl Zeiss, Jena, Germany).

2.3.3.4: Transmission electron microscopy analysis

For TEM investigations, 5 μL of each sample was drop coated onto a carbon coated copper TEM grid followed by air drying. The drop coated grid was then analyzed under TEM (JEM 2100, Jeol, Peabody, MA, USA). The interactions of the composite with bacterial cells were also examined using a high resolution transmission electron microscope operating at a maximum accelerating voltage of 80 KeV. The sample for iodinated chitosan-Ag NP composite treated bacteria was kept in the LB medium (with the concentration of the composite being at MIC i.e. 87.2μg/mL) for 3 h. For this, the composite treated on E. coli samples were drop coated onto the TEM grid followed by air drying.

2.3.3.5: Scanning electron microscopy

The iodinated chitosan-Ag NP composite was also characterized using scanning electron microscopy (SEM; LEO 1430VP,Carl Zeiss),10 μL drop of each sample was deposited on a glass slide, dried and sputter-coated with gold film using a sputter coater (SC7620“Mini”, Polaron Sputter Coater, Quorum Technologies, Newhaven, England).

2.3.3.6: pH measurements

All the pH measurements were performed using a pH meter (Inolab pH720, WTW, Germany) after proper calibration with WTW technical buffer solutions at room temperature.

2.3.3.7: GFP Construct

The recombinant GFP-expressing *E. coli* (DH5α) was generated by cloning the GFP gene into an ampicillin-resistant pUC-derived plasmid vector (GeNei ™ GFP cloning kit) in our lab.

2.3.3.8: Determination of bactericidal activity of the iodinated chitosan–Ag NP composite

To determine the minimum inhibitory concentration (MIC) and the minimum bactericidal concentration (MBC) of the iodinated composite, the GFP-expressing *E. coli* (10^8 cfu/mL) were inoculated into LB medium supplemented with various concentrations of the composite and grown overnight at 37°C. The minimum concentration of the composite at which microbial growth was measurably inhibited (with the appearance of no turbidity) was taken to be the MIC. The cultures that were not turbid were reinoculated into fresh LB containing ampicillin at 100μg/mL. The MBC of the iodinated composite was taken to be the minimum concentration of composite that prevented growth of the bacterial cells following reinoculation, as observed by the lack of visual turbidity. Control experiments were performed with acetic acid only. It may be mentioned here that the optimum concentration of iodine was chosen such that the UV-Vis peak due to iodinated chitosan was more intense than that due to Ag NP in the composite. The bactericidal activity of the composite was determined by growing GFP-expressing *E. coli* overnight in 150 mL LB ampicillin medium at pH 6.3. The cells were harvested by centrifugation and resuspended in 300μl LB. Three 100μl portions of the cell suspension were inoculated into 50ml volumes of fresh LB ampicillin media, without the composite or with composite at different concentrations.

2.3.3.9: Flow cytometric assay for bacterial cell viability using GFP-Propidium iodide combination

GFP-expressing recombinant bacterial cell viability was assessed using propidium iodide (PI) a dye which enters permeabilzes cells, binds DNA, and fluoresces at 620 nm when stimulated by a laser at 488 nm; during flow cytometry. In intact cells, PI remains in the medium and does not fluoresce; in compromised cells, PI enters the cell and binds DNA which makes it fluoresce. Briefly, several tubes containing 500 μL (10^8 cells/mL) of the recombinant *E. coli* cells and 500 μL of the iodinated composite at various concentrations (treatment I containing 38.4 μg of CS-Ag NP and 48.8 μg of iodine;

treatment II containing 51.7 µg of CS-Ag NP and 67.3 µg of iodine; treatment III containing 74.1 µg of CS-Ag NP and 94.0 µg of iodine, respectively) were incubated at 25^0C. After 2 h of incubation, 1.5µL of 0.2 mM PI was added to each of the tubes; the contents were mixed and diluted with 150 mM NaCl. Samples were analyzed by a Flow Cytometer (BD FACS calibur System, BD Biosciences, San Jose, CA). Samples were illuminated with a 15 mW argon ion laser (488 nm), and the fluorescence was detected via 525±10 nm (green) and 620±10 nm (red) band pass filters. Signals were amplified with the logarithmic mode for side scattering, forward scattering, and fluorescence. In dot plots of fluorescence, different bacterial populations were gated according to the viability stage. This method also detects disruption of membrane integrity.

2.3.3.10: Assay of oxidative stress in bacterial cells using the nitroblue tetrazolium reduction (NBT) method

Bacterial suspensions (10^8cfu/mL) in 0.1 mL of Hanks' balanced salt solution (HBSS) were incubated with the iodinated composite at 37 ^{0}C for 5, 10, 15, 20, and 30 min time intervals, respectively. Then 0.5 mL of 1 mg/mL nitroblue tetrazolium was added to each of the solutions and incubated for 30 min at37 ^{0}C. The reaction was stopped with 0.1 mL of 0.1 M HCl, and the tubes were centrifuged at 5000 rpm for 10 min to separate cells from supernatants. The bacteria pellets were treated with 0.4 mL of dimethyl sulfoxide (DMSO) to extract the followed by addition of 0.8mL of HBSS for dilution. Absorption of Formazan blue obtained from cells was measured at 575 nm using a spectrophotometer.

2.4: Results and discussion

2.4.1: Synthesis and characterization of iodinated chitosan-Ag NP composite

Addition of diluted NaOH to the solution containing chitosan and $AgNO_3$ at 95°C turned the solution color to yellow within a minute. The yellow precipitate obtained from the solution was dissolved in aqueous acetic acid to record UV-Vis spectrum. The UV-Vis spectrum consisted of a single sharp peak at 417 nm (Figure 2.1a), indicative of the

formation of Ag NP. Further, addition of iodine to the chitosan-Ag NP solution did not lead to appearance of new peaks at 290, 355, and 500 nm discounting the presence of iodine, silver iodide, and chitosan-iodine composite independently in the medium. A ternary brown-colored complex was formed with the appearance of a prominent peak at 462 nm, when iodine was added to the solution containing chitosan-Ag NP composite and mixed thoroughly. In addition, the spectrum consisted of a shoulder at 420 nm indicating that Ag NP was present in the composite when treated with iodine (Figure 2.1b).

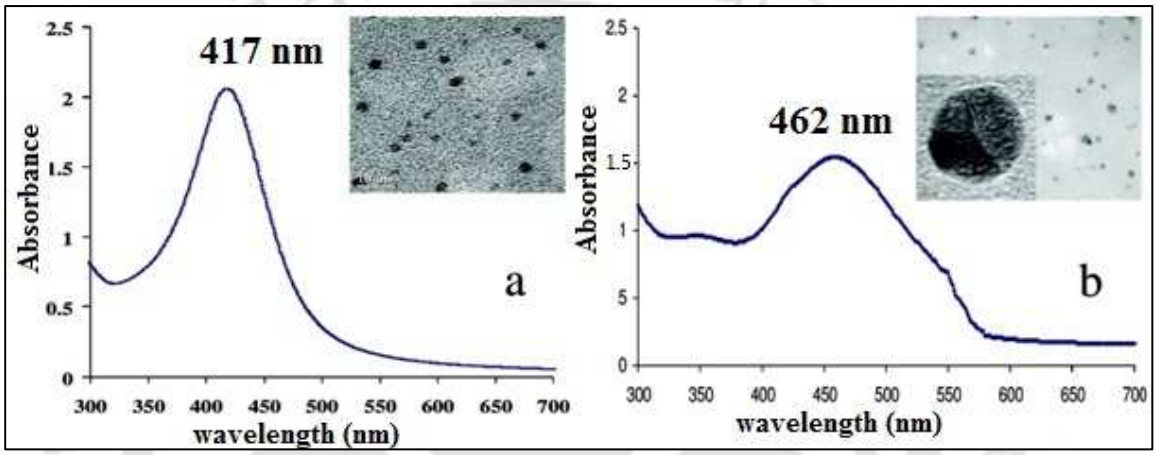

Figure 2.1: (a) UV-visible spectra of CS-Ag NP composite (b) Iodinated CS-Ag NP composite Insets show the TEM images of corresponding particles.

The SEM image of the iodinated CS-Ag NP composite (Figure 2.2 a) showed typical petal like structure of the chitosan matrix, where the presence of silver and iodine was confirmed by energy dispersive X-ray (EDX) spectrum (Figure 2.2 d). TEM image (Figure 2b) clearly indicated the presence of spherical Ag NP in the polymer suggesting the formation of a stable Ag NP-chitosan composite. The average diameter of the NPs was less than 10 nm. In addition, the high-resolution TEM image of a single Ag NP showed clear lattice planes (Figure 2c), which indicated that Ag NPs were intact in the composite and were not affected by the presence of iodine in the medium.

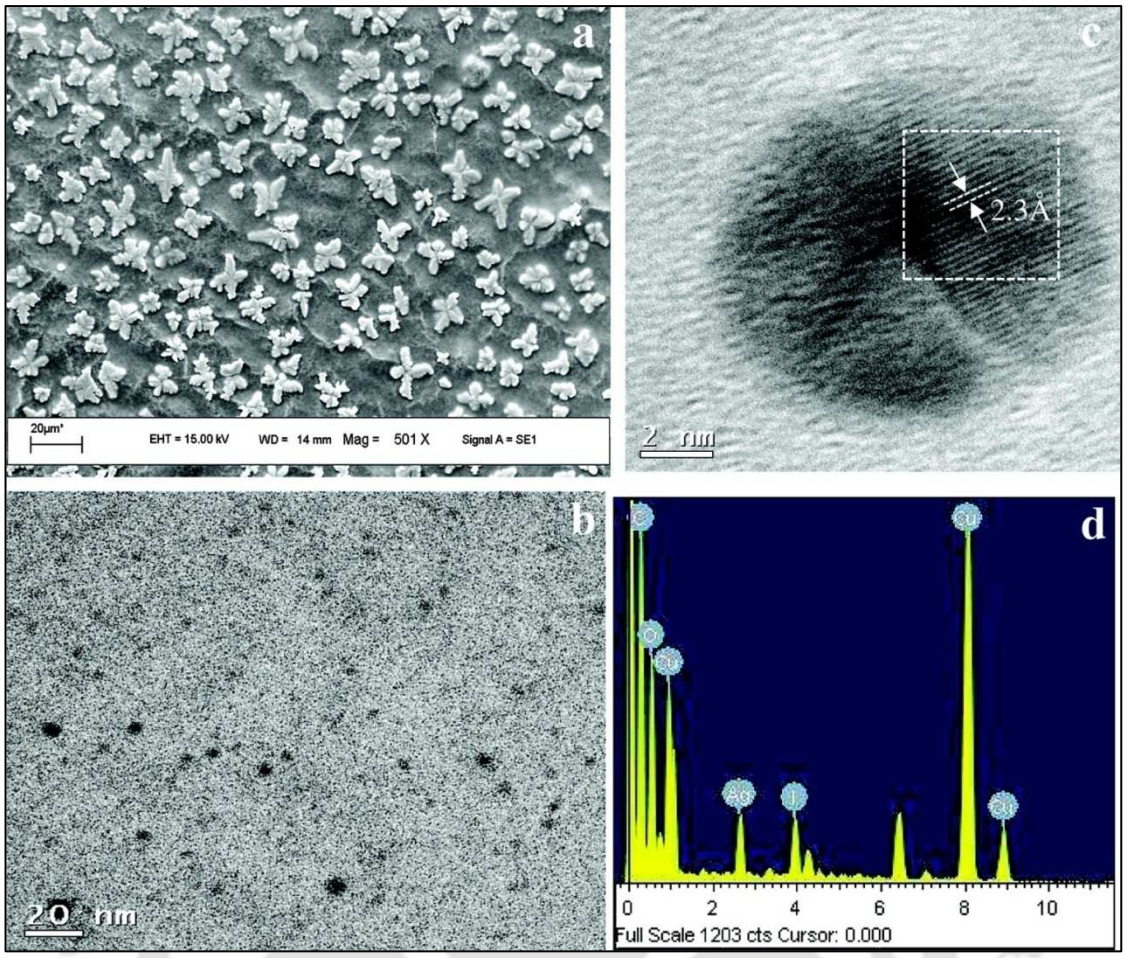

Figure 2.2: (a) SEM micrograph (b) TEM micrograph of iodinated chitosan-Ag NP composite. (c) High resolution TEM micrograph showed the presence of lattice fringes corresponding to (111) planes of pure silver and (d) EDX spectrum of iodinated chitosan-Ag NP composite. The copper peaks are due to the carbon-coated copper TEM grid used as a support for the sample.

TEM images indicate the presence of spherical silver nanoparticles embedded inside the polymer suggesting interaction of silver nanoparticles with chitosan. The images showed that diameter of the nanoparticles were less than 10 nm (Figure 2b).

2.4.2: Antibacterial effect of iodine doped silver nanoparticle-chitosan composite

The antibacterial properties of the iodinated composite were tested against recombinant GFP-expressing *E. coli* The relative antibacterial activities of the iodinated chitosan-Ag NP composite, chitosan-Ag NP composite, chitosan, iodine, and Ag NP only, toward recombinant GFP-expressing *E. coli* were detected in aqueous LB broth.

The minimum inhibitory concentration (MIC) and minimum bactericidal concentration (MBC) were also determined. The bacterial growth was monitored by measuring optical density (OD) at 595 nm at different points of time (Figure 2.3). The MIC of the iodinated composite (87.2 μg/mL) consisted of 38.4 and 48.8 μg/mL of chitosan-Ag NP and iodine, whereas the corresponding MBC (119 μg/mL) contained 51.7 and 67.3 μg/mL, respectively. In these above concentrations, the quantity of Ag NP was 0.82 μg/mL for MIC and 1.1μg/mL for MBC respectively, which was significantly lower than those reported previously with either Ag NP or chitosan Ag NP composite.[13] Control samples with 0.02 M acetic acid and15μL ethanol only in LB media showed no growth inhibition (Figure 2.3). The experiments were performed three times to ensure reproducibility. The doses at which Ag NPs and iodine can independently show antibacterial activity are 28.3μg/mL and 200-2500ppm, respectively. Clearly, iodinated CS-Ag NP composite exhibited higher antibacterial activity at much lower dose in comparison to the bactericidal dose of the individual components.

In order to probe the contribution of Ag^+ ions to the bactericidal activity of the composite, an excess of NaCl was added to remove Ag^+ from the solution containing the composite, and it was found that there was no difference in bacterial growth (Appendix, Figure A. 2.1). This indicates that Ag^+ if present in the composite-did not contribute greatly to the biocidal activity of the composite, probably because of low concentration. The bactericidal activity of the iodinated composite in the presence of excess NaCl is included in the Appendix, Chapter 2. However, Ag^+ ions present in the composite, even at very low concentrations, would contribute to the overall efficacy of the antimicrobial composite. Further, although it is known that ligated Ag NPs could enter the bacterial cell without killing them,[26] the Ag NPs used here have surfaces exposed without ligation. A part of the NP is attached to the stabilizing chitosan matrix thus making a large part of the reactive NP available for interaction with the cell wall of bacteria.

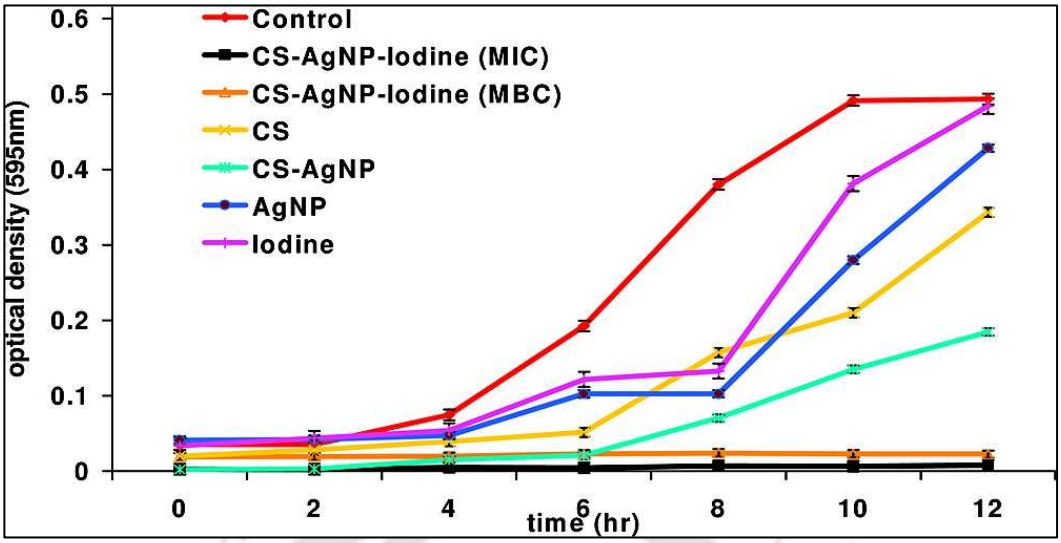

Figure 2.3: Effect of different concentrations of iodinated chitosan-Ag NP composite (at MIC and MBC) and individual components of the composite on the growth of GFP recombinant E. coli.

2.4.3: Fluorescence spectroscopy measurement

The results of fluorescent spectroscopic studies of the recombinant GFP expressing bacteria treated with iodinated chitosan-Ag NP composite, chitosan-Ag NP composite and iodine separately were distinctly different. For example, a time-dependent significant enhancement of fluorescence intensity in control sample (untreated) over increasing period of time (Figure 2.4) was observed. Bacteria treated with chitosan-Ag NP and iodine independently also showed increase in fluorescence over a period of 12 h (Figure 2.4, parts b and c), where as samples treated with iodinated chitosan-Ag NP did not exhibit any increase in fluorescence with time (Figure 2.4 d). The possible explanation could be as follows. The fluorescence in the sample was obtained from excitation of the bacterial GFP protein present inside the bacterial cells. Thus, it correlated directly with the bacterial cell population. The emission intensities of all the samples were almost identical at 2 h, since at the beginning all samples had the same concentration of the bacterial cells. However, with progress of time, as the bacterial cells started getting attached to chitosan embedded with Ag NPs and interacted with iodine present in the composite, the bacterial growth got arrested, thus no detectable fluorescence increase in treated samples was observed. On the other hand, control samples without composite

showed increase in optical density over increasing time period due to increase in bacterial count and thus higher detectable fluorescence. Further, since the concentrations of chitosan-Ag NP composite or iodine were much less than MIC, the cell population grew with time and hence the increase in fluorescence

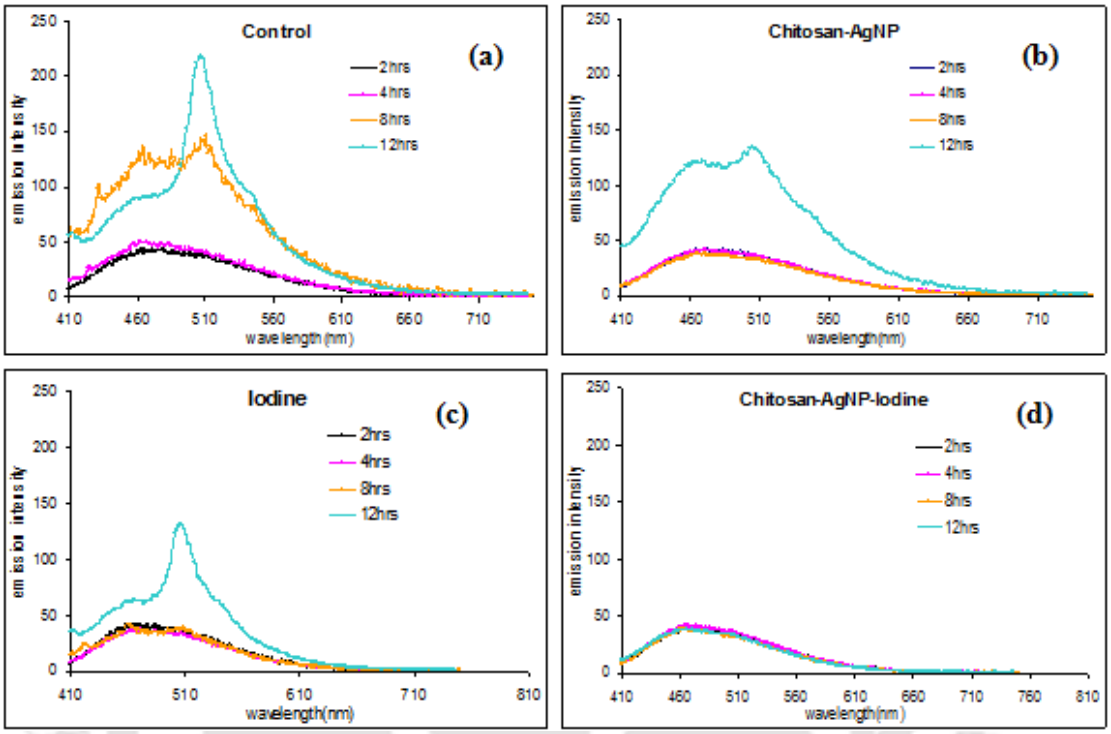

Figure 2.4: Time-dependent fluorescence spectra of GFP recombinant *E. coli* Excitation wavelength was set at 400 nm. Emission spectra were obtained for samples which were (a) in the absence of composite (b) in the presence of chitosan-Ag NP composite (c) in the presence of iodine and (d) in the presence of the iodinated chitosan-Ag NP composite.

The cellular media, in contrast, when separated from the cells showed a completely different picture. The fluorescence was marginal in the cell-free media obtained from control samples whereas the media of the treated samples showed detectable increase in fluorescence, the highest being in case of iodinated chitosan-Ag NP composite. This indicated that the composite killed effectively the bacterial cells over progression of time resulting in possible maximum leakage of GFP protein from the cell to the medium, in comparison to all other treatment with all other reagents at their specific concentrations.

2.4.4: Fluorescence microscopy measurement

The results obtained from fluorescence spectroscopic studies were further substantiated by observing the treated cells via time-dependent fluorescence microscopic studies, where a clear difference in bacterial cell population was observed between the control and treated samples because of progressive cell death for the later cases (Figure 2.5). In Figure 2.5 shows images of cell population among untreated bacteria (control, A-1, 2, 3) and bacteria treated with chitosan-Ag NP (B-1, 2, 3) and iodinated chitosan-Ag NP (C-1, 2, 3) respectively at different time intervals (3, 6 and 12 h).

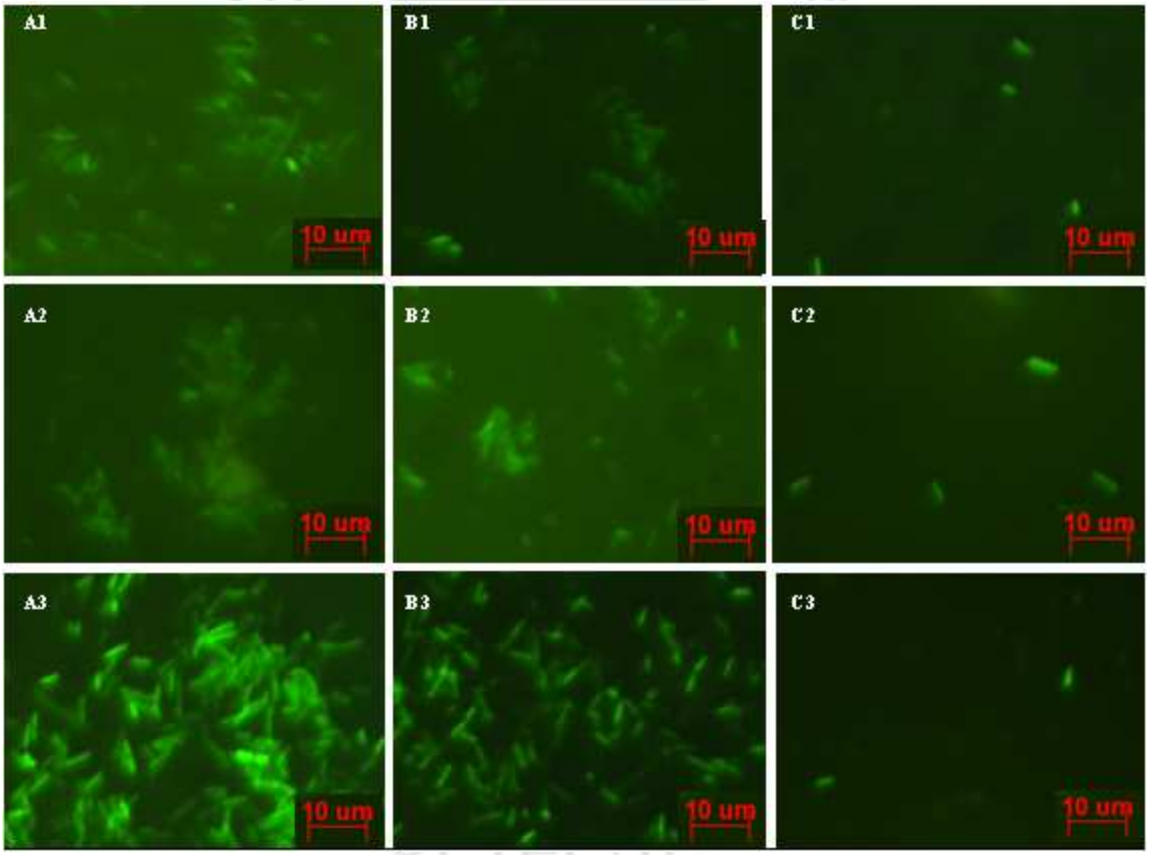

Figure 2.5: Time-dependent fluorescence micrographs of GFP recombinant *E. coli* (x 40X). Series A, B, C refer to control, CS-Ag NP composite and iodinated chitosan-Ag NP composite treated samples, respectively, while series 1, 2, 3 refer to the samples at 3, 6 and 12 hrs time points, respectively

As is apparent in the images, even at 3 h there is considerable difference in (higher) bacterial cell population in control in comparison to the other two. At 6 h and 12 h, the

bacterial population shows continuous growth in control whereas in chitosan-Ag NP treated sample considerable loss of population had occurred. On the other hand, the iodinated composite treated sample had the maximum bacterial population loss among all the groups. It may be mentioned here that the amounts of chitosan and Ag NPs were the same for both the composite and iodinated composite, thus demonstrating the synergy of using iodine with the composite for superior bactericidal activities.

2.4.5: TEM analysis of *E. coli* bacteria treated with iodinated chitosan-Ag NP composite

In order to study the interaction of the iodinated chitosan-Ag NP composite with the bacterial cells was further studied by performing TEM analysis of bacterial cells treated with the composite. TEM images clearly confirmed that Ag NPs attached on the *E. coli* cell surface (Figure 2.6). The positively charged chitosan (with the formation NH_3^+ group at pH 6.3) is known to interact with the negatively charged bacterial cell wall [26] and thus, the Ag NPs and iodine present in the composite could also interact with the bacteria. That the bacteria adhered to the iodinated composite and came in contact with the Ag NPs was evident from TEM images of the bacteria treated iodinated composite. As is evident from Figure 2.6 bacteria were present on the composite and Ag NPs present in the composite could be viewed through the bacteria adhered to the surface. It may be mentioned here that results from the laboratory of ours and others have indicated that while bacteria are adhered to the composite, the Ag NPs that are present in the composite are known to create pores on the bacterial cell surface thereby increasing the potency of killing the bacteria more than either the chitosan or Ag NPs independently. On the other hand, the presence of iodine in the present system increased the effectiveness of the antimicrobial activity of the composite, the details of effects of which are mentioned below.

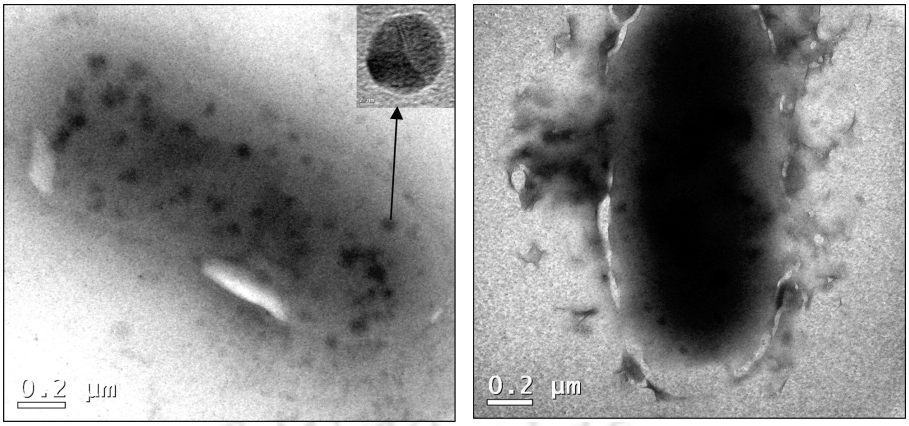

Figure 2.6: TEM micrograph showing interactions between Ag NPs (in the iodinated chitosan-Ag NP composite) and bacteria; large deposits of Ag NPs can be seen on connected to the cell surface. Inset shows an expanded view of Ag NP.

2.4.6: Flow cytometric analysis of bacterial cell viability

Bacterial viability analysis of the iodinated composite treated cells revealed four different cell populations, specifically, living, compromised, dead, and lysed cells. It is usually assumed that bacterial permeability to nucleic acid dye such as propidium iodide (PI) is associated with the presence of substantial, irreparable breaches in the membrane, in the presence of which the organisms cannot maintain their membrane potential and are therefore nonviable. The intact cell only show green fluorescence (from GFP of the recombinant bacteria) as PI remains in the medium and does not fluoresce; in compromised cells, PI enters the cell and binds to DNA showing red fluorescence in addition to green fluorescence; in dead cells the GFP leaks out of the cell and thus only red fluorescence is visible and lysed cells do not show any kind of fluorescence. It was observed that the intensity of green fluorescence and red fluorescence (PI) of the analyzed cells changed as a function of increasing iodinated composite concentration and incubation time. For example, the intensity of green fluorescence decreased at high iodinated composite concentrations, indicating rapid loss of membrane integrity. The changes in fluorescence intensity are associated with different viability stages of *E. coli* cells at various composite concentrations (treatment I corresponding to 38.4 µg of CS-Ag NP and 48.8 µg of iodine,

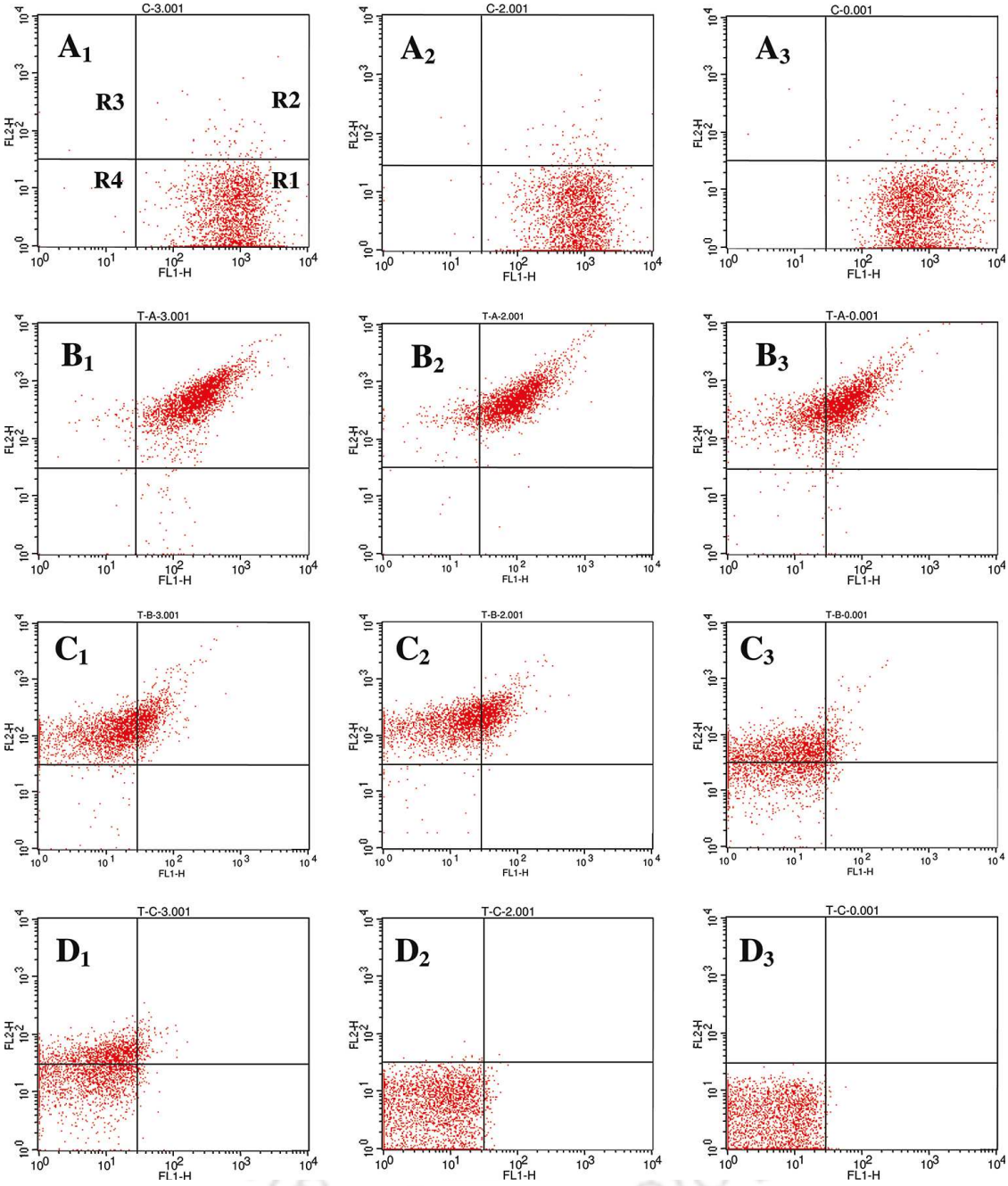

Figure 2.7: Dot plots showing populations of *E. coli* cells (PI stained containing GFP) at different viability stages, measured by flow cytometry at different time points and with varying concentration of the iodinated composite. Series A refers to control and series B, C, and D refer to increasing concentration of iodinated chitosan-Ag NP in the treated samples and 1, 2, and 3 refers to samples at 1, 2, and 3 h respectively. Different viability stages are denoted as R1 (live), R2 (compromised), R3 (dead) and R4 (lysed).

Table2.1. Percentage of *E. coli* cells at various concentration of the iodinated composite and at different time points as measured by flow cytometry.

		Control (%)	Treated-I(%)	Treated-II(%)	Treated-III(%)
Amount of Component/Time	CS-Ag NP(µg) Iodine (µg)	0.0 0.0	38.4 48.8	51.7 67.3	74.1 94.0
1hour	Live	97.70	1.82	0.16	2.74
	Compromised	2.02	96.0	38.63	7.33
	Dead	0.08	1.81	59.40	38.09
	lysed	0.20	0.27	1..81	51.84
2hour	Live	96.53	0.14	0.14	2.29
	Compromised	3.09	93.56	31.79	0.11
	Dead	0.12	6.05	66.23	0.55
	Lysed	0.26	0.25	1.84	97.05
3hour	Live	96.88	0.36	1.28	2.32
	Compromised	3.06	70.58	7.61	0.00
	Dead	0.04	28.30	56.32	0.00
	lysed	0.03	0.76	34.39	97.68

treatment II corresponding to 51.7 µg of CS-Ag NP and 67.3 µg of iodine, and treatment III corresponding to 74.1µg of CS-Ag NP and 94.0µg of iodine respectively) observed as distinct cell population (Figure 2.7 and Table 2.1). The results further confirm that the iodinated composite affects the membrane integrity and also facilitates lysis of cells. It may be mentioned here that cell lysis was more prevalent over longer periods of incubation and at very high concentrations.

2.4.7: Iodinated chitosan-Ag NP composite in oxidative stress

To understand the complete mechanism of enhanced bactericidal activity of iodinated chitosan-Ag NP composite, the possible involvement of the ROS pathway was studied. ROS occur naturally in aerobic cells arising from various intracellular and extracellular sources and cells maintain a strong defence against oxidative stress. Under certain

circumstances, the concentration of active oxygen rises to a level that overwhelms the basal level of the scavenging capacity of the cell, giving rise to oxidative stress. Previous reports have emphasized on the role played by NPs in inducing oxidative stress. [31, 32] Oxidative stress can have specific effects to the cells including oxidative damage to proteins and DNA. To establish the role of oxidative stress in the present systems, NBT assay was performed. Untreated cells showed negligible increase in reactive oxygen species production. In contrast, significant increase (more than 2-fold) in ROS production was found in iodinated composite treated cells (Figure 2.8). On the other hand, bacterial cells, when treated with chitosan, Ag NPs, iodine or chitosan-Ag NP independently, at concentrations that constitute the iodinated composite, did not show any significant increase in ROS concentration. It has been demonstrated that Ag NPs present in the composite when attached to the bacterial cell creates pore on the cell wall. Our previous report has established that Ag NPs could catalytically convert iodine to iodine atom on their surfaces.[36] In case of iodinated composite treatment, pores that were made by the Ag NPs, possibly allowed iodine atoms (produced on the surfaces of Ag NPs) to penetrate the compromised cell. This in turn could result into the ROS production cascade. This may well be the case here and excessive ROS productions might lead to cell death.

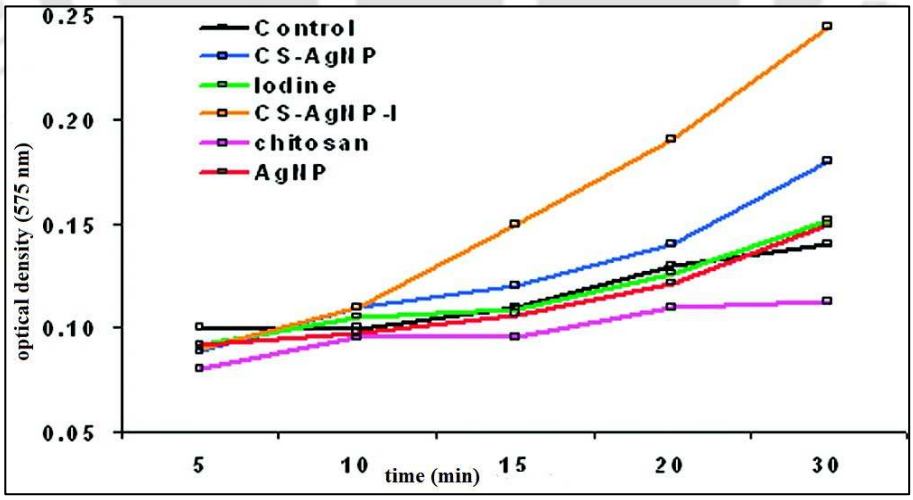

Figure 2.8: Effect of iodinated chitosan-Ag NP and individual components of the composite on the intracellular ROS concentration of the bacteria.

Furthermore, in order to understand the interaction between DNA and iodinated composite isolated plasmid DNA[34] of the bacterium, upon staining with EtBr, was treated with iodinated composite in the medium (refer to Appendix, for further details). Confocal laser scanning microscopy (CLSM) of the evaporated medium on a glass slide indicated presence of DNA on the composite (Figure 2.9a). In addition, gel retardation assay of the mixture clearly indicated the attachment of iodinated composite with DNA (Figure 2.9b). Thus, it is possibly correct to conclude that DNA of the compromised bacterial cell might well have been attached to the composite after perforation of the cell wall by Ag NPs present in the composite.

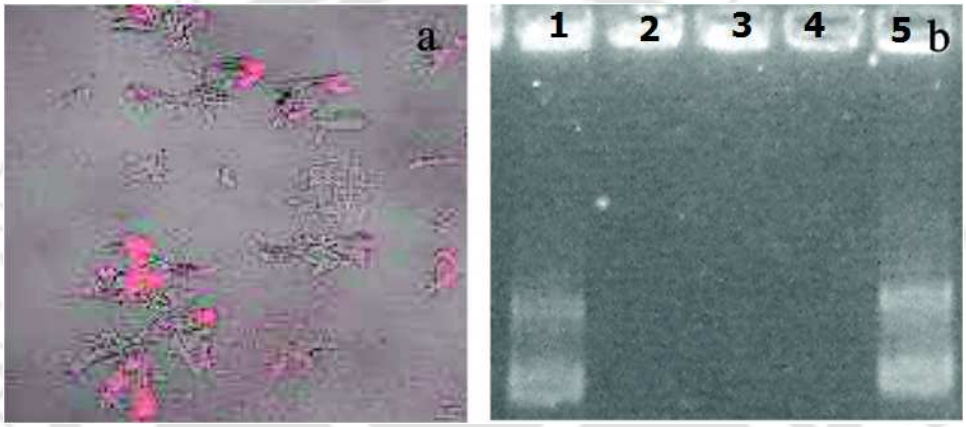

Figure 2.9: CLSM micrograph showing attachment of DNA (tagged with EtBr) with iodinated chitosan-Ag NP composite (b) Gel retardation assay showing complex of iodinated chitosan Ag NP with DNA at different time points of incubation. Key: lanes 1 and 5, control DNA; lanes 2, 3, and 4 complex of DNA with the composite at various time points of 30 min, 1 h, and 2 h.

Finally, the essence of the antimicrobial activity of the iodinated composite is presented schematically in Figure 2.10. The positively charged chitosan polymer causes the negatively charged bacterial cell wall to get attached to the composite. The Ag NPs embedded in the composite interact with the cell wall of the bacteria to induce formation of pores on the cell wall. Introduction of pores on the cell wall leads bacteria to become unviable. It is also important to note that Ag NPs are known to induce increased ROS productions in bacteria. On the other hand, the Ag NPs in the composite also produce iodine atom from iodine molecule deposited on its surface. The iodine atoms thus induced enhanced production of ROS which cause further damage to the cell. The damage in the cells could lead to the damage in DNA and proteins, and thus cells

become further unviable. Overall, chitosan, Ag NP, and iodine (which in turn forms an iodine atom) work in tandem for superior antibacterial activity in comparison to either of the components and at lower concentrations of each of the species in the composite than their potency individually, which works at much higher concentrations.

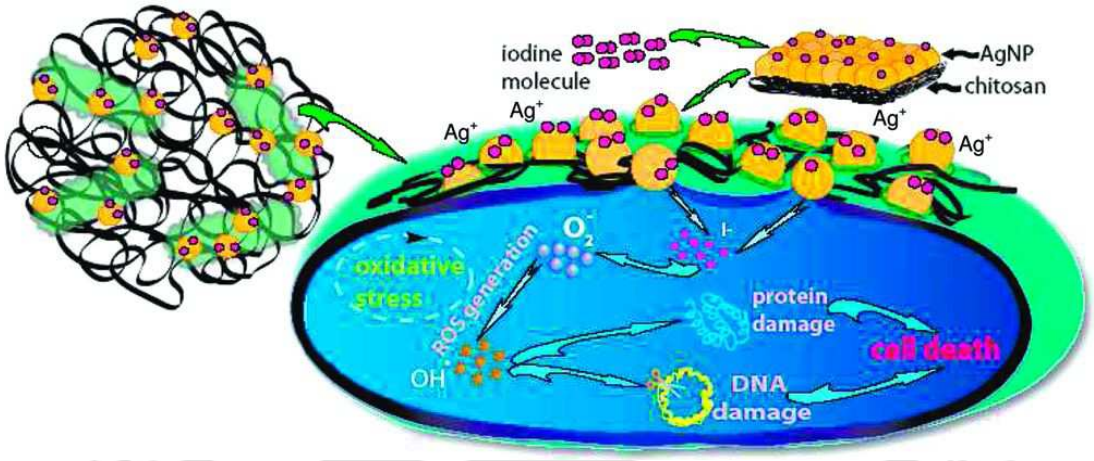

Figure 2.10: Schematic representation of the proposed mechanism of antibacterial activity of the iodinated chitosan-Ag NP composite.

2.5: Conclusion

It is known that chitosan, Ag NPs and iodine all have antimicrobial properties individually. It has also been established that a chitosan-Ag NP composite has higher antibacterial properties at a concentration lower than that of its components i.e. chitosan and Ag NPs. In the present set of experiments, we have demonstrated that in the presence of iodine the concentrations of both but especially of Ag NPs could further be lowered so that the use of Ag NPs with known toxicity to mammalian cells could be minimized. GFP expressing *E. coli* bacteria have been used to establish the superior bactericidal activity of the iodinated composite vis-à-vis its components. UV-Vis and fluorescence spectroscopy and fluorescence microscopy have been used to establish the enhanced efficacy of the iodinated composite in comparison to composite, Ag NP or iodine independently. TEM has been used to establish the attachment of the bacteria to the composite especially to Ag NPs. Fluorescence microscopy and gel retardation assay also supported the idea of attachment of DNA to the composite. Flow cytometry revealed

different levels of cell perforation in the presence of iodinated composite in addition to that in the presence of composite only. On the other hand, the enhanced production of ROS in the iodinated composite was established by UV-Vis spectroscopy. In brief, the catalytic production of iodine atoms by the composite, as reported recently from the laboratory[36] led to enhanced antimicrobial activity of the composite via increased ROS productions, in comparison to the composite only. There, the formation of iodine atoms on the surfaces of catalytic Ag NPs was evidenced by the selective coupling of phenols and its derivatives in the presence of iodinated chitosan-Ag NP. The details of reaction studied had revealed that the iodine atoms formed on the surface of Ag NP led to the selective coupling reaction via *p*-iodophenol intermediate formation. This could be possible only when iodine atoms are generated on the surface of Ag NP. On the other hand, although, Ag^+ ions are known to exhibit high cytotoxicity at the concentration of 10^{-4} M but very little, if any, biocidal effect was observed at much lower concentrations, which could be the case herein.[14] In other words, most of the original Ag^+ ions had been reduced to form Ag NPs and little was left for antimicrobial activity. The residual Ag^+ ions, though, could contribute to the overall efficacy of the composite. The experiments established the importance of synergy of a three-component antimicrobial material when working in tandem in comparison to individual components, taking advantage of the mechanism of action of each.

References

(1) Kim, Y. H.; Lee, D. K.; Cha, H. G.; Kim, C. W.; Kang, Y. C.; Kang, Y. S. *J. Phys. Chem. B.* **2006**, *110*, 24923–24928.

(2) Feng, Q. L.; Wu, J.; Chen, G. Q.; Cui, F. Z.; Kim, T. M.; Kim, J. O. *J. Biomed. Mater. Res.* **2000**, *52*, 662–668.

(3) Morones, J. R.; Elechiguerra, J. L.; Camacho, A.; Holt, K.; Kouri, J. B.; Ramı´rez, J. T.; Yacaman, M. J. *Nanotechnology* **2005**, *16*, 2346–2353.

(4) Brigger, I.; Dubernet, C.; Couvreur, P. *Adv. Drug Delivery Rev.* **2002,** *54*, 631–651.

(5) Sondi, I.; Salopek-Sondi, B. *J. Colloid Interface Sci.* **2004,** *275*, 177–182.

(6) Stoimenov, P. K.; Klinger, R. L.; Marchin, G. L.; Klabunde, K. J. *Langmuir* **2002,** *18,* 6679–6686.

(7) Volker, A.; Thorsten, B.; Peter, S.; Michael, W.; Peter, S.; Elvira, D.; Eugen, D.; Reinhard, S. *Biomaterials* **2004,** *25,* 4383–4391.

(8) Ahearn, D. G.; May, L. L.; Gabriel, M. M. *J. Ind. Microbiol.* **1995,** *15,* 372–376.

(9) Gogoi, S. K.; Gopinath, P.; Paul,A.; Ramesh, A.; Ghosh, S. S.; Chattopadhyay, A. *Langmuir* **2006**, 22, 9322–9328.

(10) Aymonier, C.; Schlotterbeck, U.; Antonietti, L.; Zacharias, P.; Thomann, R.; Tiller, J. C.; Mecking, S. *Chem. Commun.* **2002,** 3018–3019.

(11) Alt, V.; Bechert, T.; Steinrucke, P.; Wagener, M.; Seidel, P.; Dingeldein, E.; Domann, E.; Schnettler, R. *Biomaterials* **2004,** *25,* 4383–4391.

(12) Li, P.; Li, J.; Wu, C.; Wu, Q.; Li, J. *Nanotechnology* **2005,** *16,* 1912–1917.

(13) Smetana, A B.; Klabunde, K J.; Marchin, G R.; Sorensen, C M. *Langmuir* **2008,** *24*, 7457–7464.

(14) Gopinath, P.; Gogoi, S K.; Chattopadhyay, A.; Ghosh, S S.; *Nanotechnology*, **2008,** *19*, 075104.

(15) McDonnell, M. P.; Beving, D.; Wang, A.; Chen, W.; Yan, Y. *Adv. Funct. Mater.* **2005,** *15,* 336–340.

(16) Zhang, L.; Yu, J. C.; Yip, H. Y.; Li, Q.; Kwong, K. W.; Xu, A. W.; Wong, P. K. *Langmuir* **2003,** *19,* 10372–10380.

(17) Zhang, S.; Fu, R.; Wu, D.; Xu, W.; Ye, Q.; Chen, Z. *Carbon* **2004,** *42,* 3209–3216.

(18) Oya, A.; Banse, T.; Ohashi, F.; Otani, S. *Appl. Clay Sci.* **1991,** *6,* 135–142.

(19) Verne, E.; Nunzio, S. D.; Bosetti, M.; Appendino, P.; Brovarone, C. V.; Maina, G.; Cannas, M. Biomaterials 2005, 25, 5111–5119.

(20) Hornebecq, V.; Antonietti, M.; Cardinal, T.; Treguer-Delapierre, M. *Chem. Mater.* **2003,** *15,* 1993–1999.

(21) Huang, H.; Yuan, Q.; Yang, X. *Colloids Surf. B* **2004,** *39,* 31–37.

(22) Zhang, Z.; Zhang, L.; Wang, S.; Chen, W.; Lei, Y. *Polymer* **2001,** 42, 8315–8318.

(23) Chauhan, B. P. S.; Rathore, J.; Sardar, R.; Tewari, P.; Latif, U. *J. Organomet. Chem.* **2003,** *686,* 24–31.

(24) Rong, M.; Zhang, M.; Liu, H.; Zeng, H. *Polymer* **1999,** *40*, 6169–6178.

(25) Rhim, J. W.; Hong, S. I.; Park, H. M.; Ng, P. K. *J. Agric. Food Chem.* **2006,** *54*, 5814–5822.

(26) Sanpui, P.; Murugadoss, A.; Durgaprasad, P. V.; Ghosh, S. S.; Chattopadhyay, A. *Int. J. Food Microbiol.* **2008,** *124*, 142–146.

(27) Rabea, E. I.; Badawy, M.E-T.; Stevens, C. V.; Smagghe, G.; Steurbaut, W. *Biomacromolecules* **2003,** *4*, 1457–1465.

(28) Devlieghere, F.; Vermeulen, A.; Debevere, *J. Food Microbial.* **2004,** *21*, 703–714.

(29) Gottardi, W., Iodine and Iodine compounds. *In Disinfection, sterilization, and Preservation*, 4th ed.; Bloc, S. S., Ed.; Lea and Febiger: Philadelphia, PA, **1991;** pp 152-166.

(30) Kitagawa, E.; Akama, K.; Iwahashi, H. *Biosci. Biotechnol. Biochem* **2005,** *69*, 2285–2293.

(31) Hussain, S. M.; Hess, K. L.; Gearhart, J. M.; Geiss, K. T.; Schlager, *J. Toxocol. In Vitro* **2005,** *19*, 975–983.

(32) Hussain, S. M.; Javorina, A. K.; Schrand, A. M.; Duhart, H. M.; Ali, S. F.; Schlager, J. *J. Toxicol. Sci.* **2006,** *92*, 456–463.

(33) Sudarshan, N. R.; Hoover, D. G.; Knorr, D. *Food Biotechnol.* **1992,** *6*, 257–272.

(34) Sambrook, J.; Russell, D. W. *Molecular Cloning; A Laboratory Manual*, 3rd ed.; Cold Spring Harbor Press: New York, **2001,** Vol. 1, pp 1.31-1.34.

(35) Lehtinen, J.; Nuutila, J.; Lilius, E.-M. *Cytometry Part A* **2004,** 60A, 165–172.

(36) Murugadoss, A.; Goswami, P.; Paul, A.; Chattopadhyay, A. *J. Mol. Catal. A: Chem.* **2009,** *304*, 153–158.

(37) Hwang, E. T.; Lee, J. H.; Chae, Y. J.; Kim, Y. S.; Kim, B. C.; Sang, B. I.; Gu, M. B. *Small* **2008**, *4*, 746-750.

Chapter 3A

Stable three component iodinated chitosan-Cu nanoparticle composite: Synthesis and characterization

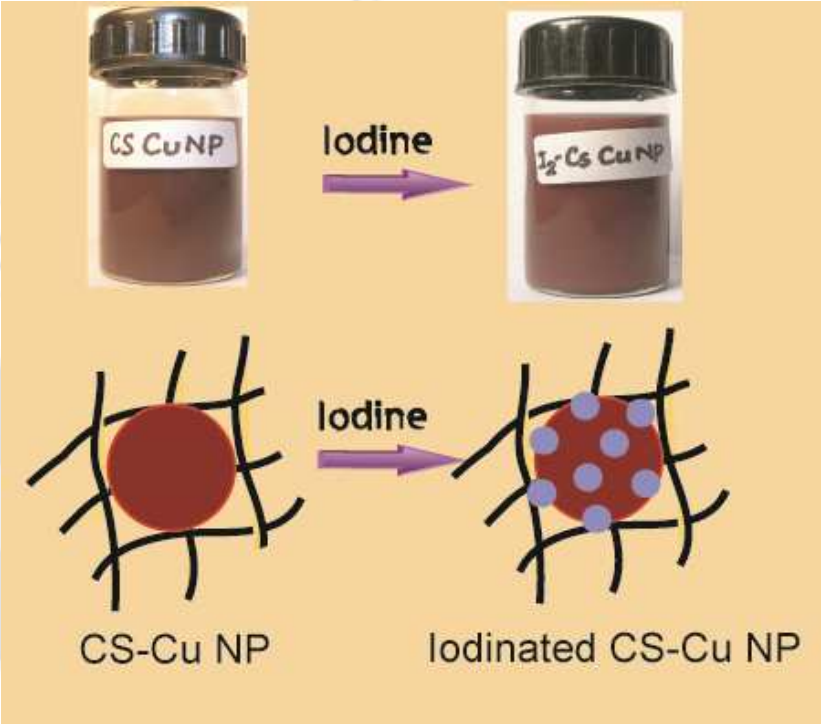

The work embodied herein has been published as an article as described below

"Iodine-Stabilized Cu Nanoparticle Chitosan Composite for Antibacterial applications. **Sadhucharan Mallick,** Shilpa Sharma, Madhuchanda Banerjee, Siddhartha Sankar Ghosh, Arun Chattopadhyay, and Anumita Paul *ACS Appl. Mater. Interfaces,* **2012,** *4(3),* 1313–1323."

3A.1: Introduction

In the past two decades a substantial body of research work in the syntheses of metal nanoparticles (NPs) has been directed towards creating conditions where optical, chemical and biological properties of the NPs could be exploited. In this regard, coinage metals (Cu, Ag and Au) provide special opportunity owing to their biological applications. For example, it has been established that optical and optothermal properties of Au NPs or nanorods could be utilized in healthcare diagnostics and therapeutics such as in hyperthermia treatment of cancer cells.[1,2] On the other hand, colloidal silver has been used and in recent times Ag NPs have been proposed for antimicrobial and anticancer therapy in the form of either NPs or the NPs present in the composite. However, the use of Ag NPs has been a cause of concern-albeit they are being addressed systematically-especially because of their persistent presence in living systems and lack of any suitable sequestering agent. For example, implications of Ag NPs being present in the environment need to be understood before their widespread use in antibacterial treatments such as in water filter systems and Ag NP lined clothing.[3] In this regard, Cu NPs are attractive alternatives because in addition to their catalytic, optical and electrically conducting properties they are known to have significant antibacterial and antifungal properties.[4−15] Ag is known to accumulate in the humans body over time can lead to toxicity such as argyria.[17] Importantly, there are known sequestering agents for Cu[18, 19] in order for their release out of the human body following their use. However, use of Cu NPs still poses a fundamental challenge owing to their ease of oxidation especially in an aqueous environment of living systems and in open atmosphere. This is where an opportunity lies in terms of developing a reaction condition where Cu NPs would not only be synthesized but also remain stable for sufficiently long time in order for them to be useful.

As a natural response to the demand, several methods have recently been developed for the syntheses of Cu NPs which include thermal reduction,[20] sono-chemical reduction,[21] metal vapor synthesis,[22] chemical reduction,[7] vacuum vapor deposition,[8] radiation methods,[23] microemulsion techniques[24− 26] and laser ablation.[27] Interestingly,

most of these methods utilize oxygen-free environment for the synthesis as the incipient Cu NPs get readily oxidized in the atmosphere.[7,9,11,21,24,28] For example, Lisiecki et al.[24] reported the synthesis of Cu NPs in aqueous solution using sodium dodecyl sulfate as the capping agent where they used the inert environment of a glove box with nitrogen flow to prevent the oxidation of the generated Cu NPs. Further, Joshi et al.[28] reported the synthesis of Cu NPs by gamma radiolysis, in an aqueous system under nitrogen atmosphere. Thus there is still a need for the development of a method for the atmospheric synthesis of Cu NPs where the NPs would remain stable for sufficiently long time for their use especially in antimicrobial and antifungal applications.

Herein we report the development of a new method for the preparation of Cu NPs under atmospheric conditions in the presence of chitosan (CS) as the stabilizing agent and in the form of a composite with CS. Chitosan (CS) is a naturally occurring, cationic polysaccharide composed of (1,4)-linked 2-amino-2-deoxy-β-d-glucose and 2-acetamido-2-deoxy-β-d-glucose units. The polymer has significant content of primary amines and hydroxyl groups thus providing it with a strong affinity towards metal ions, which can be incorporated by simple chelation or by ion exchange, making it an excellent support for synthesis of metal NPs.[30,31] The synthesis was carried out by reducing Cu^{2+} using hydrazine as the reducing agent and in the presence of CS as the stabilizer. The methods produced Cu NPs with average size 8±4 nm. It was further observed that the as-prepared NPs were oxidized rather rapidly (within hours of preparation) in the medium while they were reasonably stable in the presence of hydrazine in the medium or in vacuum dried sample. On the other hand, addition of molecular iodine to the prepared NPs in the medium provided stability to the NPs in the medium which could then be used for antimicrobial studies.

3A.2: Outline of the research work

I. Molecular iodine has been used in conjunction with a biopolymer CS to stabilize Cu NPs in a composite in aqueous medium.

II. UV-Visible spectroscopy, transmission electron microscopy (TEM), field emission scanning electron microscopy (FESEM) and X-ray diffraction (XRD) were used to characterize the nanocomposites.

III. Iodine prevent copper oxide formation, possible dissociation of molecular iodine on the surface of Cu NPs into iodine atoms which chemisorbs to form CuI films on the surface of Cu NPs , inhibits agglomeration and stable towards oxidation.

IV. Enhancement in antibacterial activity as well as Stability of CS-Cu NPs composite in the presence of molecular iodine.

3A.3: Experimental section

3A.3.1: Materials and methods

Copper (ll) sulphate pentahydrate ($CuSO_4.5H_2O$; Merck, India), Chitosan of high molecular weight (75% deacetylated; Sigma-Aldrich Chemical Co.), sodium hydroxide (NaOH, 98%; Merck, India), Hydrazine hydrates solution (80%; Merck, India), acetic acid (glacial, 99–100%; Merck, India) and ethanol were used as received without further purification. Milli-Q grade (resistivity 18.2 $M\Omega cm^{-1}$) water was used in all experiments.

3A.3.2: Synthesis and characterization of iodinated CS-Cu NP Composite

Chitosan stabilized Cu NPs were synthesized under normal atmospheric conditions, as shown in Scheme 1. For this, 50 mg of chitosan and 40 mg of copper (II) sulphate pentahydrate were added to 50 mL Milli-Q grade water in a 100 mL round bottom flask placed in an oil bath with vigorous stirring and refluxed for 20 min at ~ 100^0C resulting in a light blue colored solution. To this 0.6 mL of 0.6 M NaOH was added upon which the color of the solution turned brown. After about 15 min 0.4 mL of hydrazine hydrate solution was added to the above solution with constant stirring. Within 10 min a yellow solution was formed. The reaction was allowed to continue for an additional 30 min till a reddish colored solid appeared at the bottom of the round bottom flask. The flask was then taken out from the oil bath and cooled to room temperature.

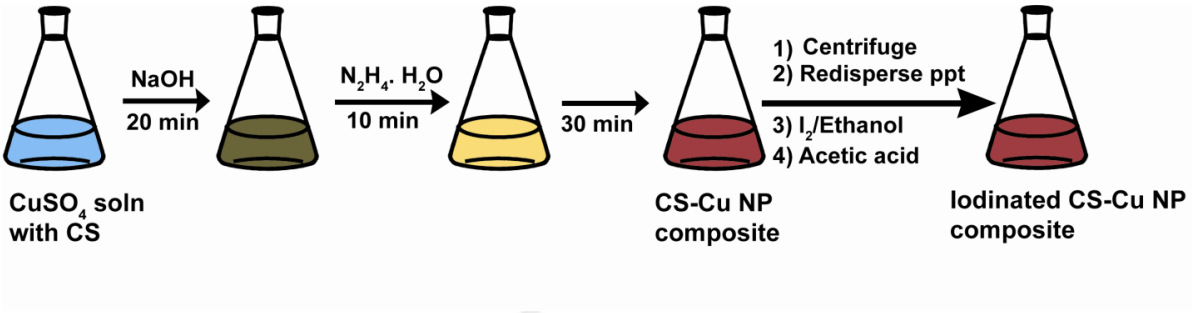

Scheme3A. 1. Schematic representation of the procedure used for the synthesis of iodinated CS- Cu NP composite.

The solution along with the precipitate was centrifuged at 5300 rpm and the precipitate was washed with milli-Q grade water and the precipitate is made into a pellet. The pellet was then redispersed in 20 mL of 0.25% aqueous acetic acid solution. To that CS- Cu NP redisperse solution 300 μL of 0.2 M iodine solution in ethanol was added and mixed thoroughly. The resulting reddish colored solution was characterized and used for antibacterial studies. The pH of the solution was adjusted to 6.3 prior to bactericidal activity studies. The supernatant solution was treated with excess $NH_2NH_2.H_2O$ to check for any excess of Cu^{2+} present in the medium, which was negative. In other words, all of Cu^{2+} ions present in the medium had reacted. For characterization of the product, the reddish solution was centrifuged, vacuum dried and stored under vacuum before analysis. Further, control experiment in absence of hydrazine hydrate yielded CuO NPs from $CuSO_4$, showing that CS did not reduce $CuSO_4$ to Cu NPs (refer to Appendix Figures A. 3A.1 a, b and c)

3A.3.3: UV-Vis spectroscopic measurements

UV-visible spectra of the the reddish dispersion was measured using a Hitachi U 2900 spectrophotometer. The bacterial growth was monitored by measuring optical density (OD) at 595 nm using a UV-visible spectrophotometer (Lambda 45; Perkin-Elmer, Fremont, CA, USA) of the sample at different times

3A.3.4: Transmission electron microscopy (TEM) analysis

For TEM investigations, 5 μL of each sample was drop coated onto a carbon coated copper TEM grid (300 mesh) followed by air drying. The drop coated grid was then analyzed under TEM at a maximum acceleration voltage of 200 kV. The interactions of the composite with bacterial cells were also examined using a high resolution transmission electron microscope operating at a maximum accelerating voltage of 80 KeV.

3A.3.5: X-ray diffraction measurements

We performed X-ray diffraction measurements to characterize the CS-Cu NP composite and iodinated CS-Cu NP composite. We also studied and fate of the composite during antibacterial studies using XRD measurement. Firstly, vacuum dried composites were spread on glass microslides and XRD was recorded using Bruker AXS D8 Advance X-ray diffractometer with Cu Kα1 radiation (λ= 1.54060 Å), operating at 40 kV and 40 mA.

3A.3.6: Atomic absorption spectrometry (AAS)

Quantitative analysis of the concentration of copper ion release from the iodinated CS-Cu NP composite was performed by using atomic absorption spectrophotometer (Model: AA240 Varian Inc). For this the supernatant solution obtained after centrifugation of the composites was investigated by AAS**.**

3A.3.7: Zeta potential *(ζ)* measurements

Zeta potential *(ζ)* measurements were performed to determine the charge of iodinated CS-Cu NP composite, chitosan, iodine in aqueous solution at pH 6.3. Zeta potential *(ζ)* values were measured using Delsa™ Nano Submicron Particle Size and Zeta Potential Particle Analyzer (PN A54412AA, Beckman Coulter).

3A.3.8: Fourier Transform Infrared (FTIR) spectroscopy

FT-IR spectra were recorded on a Perkin-Elmer-Spectrum One spectrometer with KBr disks in the range 4000-450 cm^{-1} for structural analysis of CS, CS-Cu NPs composite and iodinated CS-Cu NP composite. CS, CS-Cu NPs composite and iodinated CS-Cu NPs composite powders were mixed with KBr in order to make pellets for FTIR studies.

3A.4: Results and discussion

3A.4.1: Synthesis and characterization of the CS-Cu NP composite: The role of chitosan and iodine

As mentioned earlier the synthesis of Cu NPs in the presence of CS was carried out under normal atmospheric conditions. The reddish solid produced from the reaction of alkaline $CuSO_4$ and hydrazine (in the presence of CS) was separated from the reaction mixture and then redispersed in water in the presence of acetic acid. UV visible spectrum of this reddish solution showed a prominent peak at 591 nm (Figure 3A.1a), which broadened rapidly in about 2 days (refer to Appendix Figure A. 3A.2a). The peak is attributed to the surface Plasmon resonance (SPR) of Cu NPs. The peak disappeared in about 3 days. The peak at 591 is characteristic of formation of Cu NPs in the medium and the dissolution of the solid in acetic acid solution indicated that the NPs were associated with CS (which itself dissolves in acidic condition) and thus a polymer-NP composite might have formed.[6] It is also important to mention here that the Cu NPs present in the composite were rather unstable as the peak due to NPs was observed to have disappeared within a matter of days. The presence of CS in the composite was confirmed by FTIR studies wherein the peaks corresponding to CS were present (Appendix, Figure A. 3A.4). Interestingly, powder XRD pattern of the composite recorded after 1 day of synthesis indicated the presence of Cu. The XRD pattern, shown in Figure 3A.1b, indicated the occurrence of diffraction at 2θ values of 43.34°, 50.46°, 74.14^0 which were indexed as due to diffraction from (111), (200), and (220) planes respectively of face-centered-cubic (fcc) crystal planes of Cu(0).

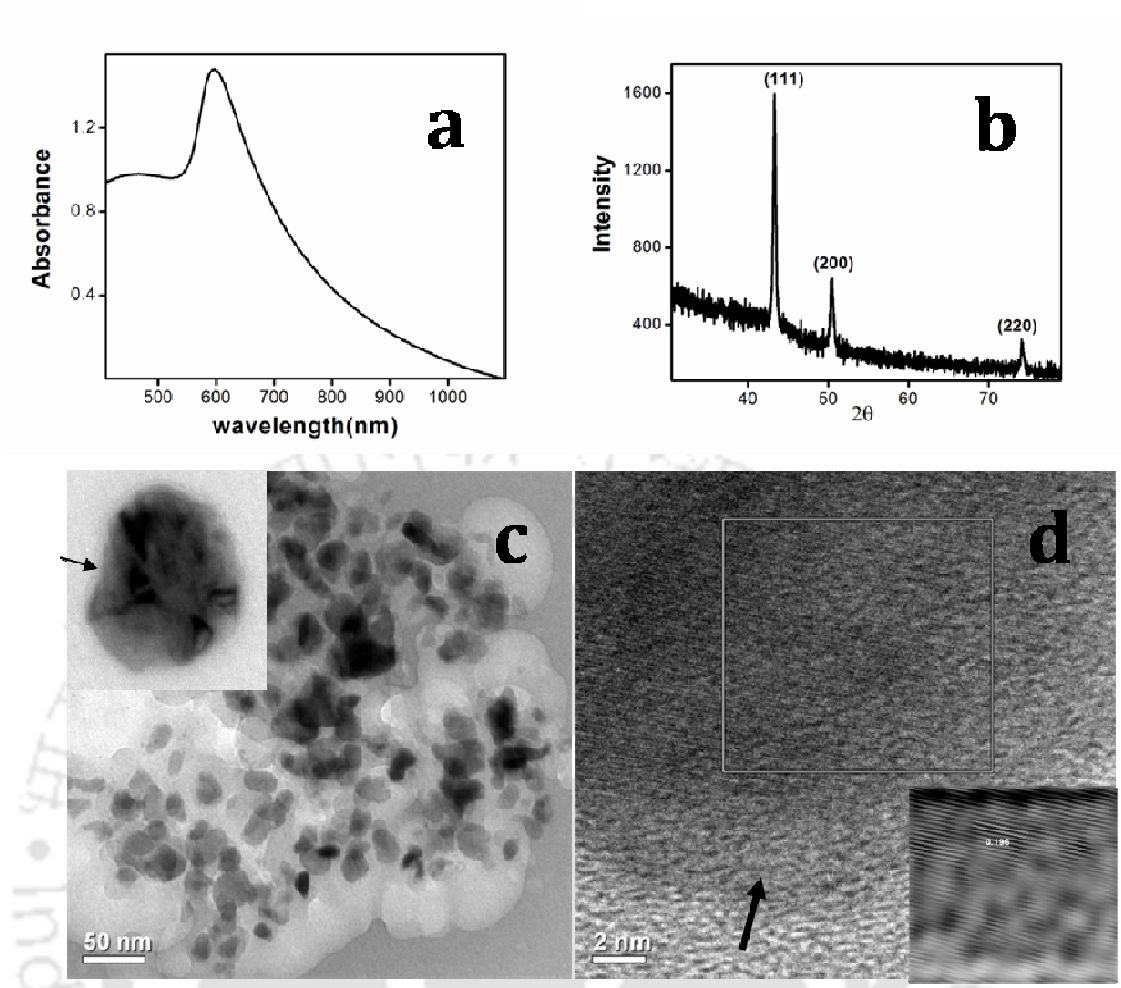

Figure 3A.1: (a) UV-Visible spectrum of freshly prepared CS-Cu NP composite. (b) Powder XRD pattern of freshly prepared CS-Cu NP composite. (c) TEM image of freshly prepared CS-Cu NP composite. Inset is TEM image of a single Cu NP. Arrow indicates amorphous layer. (d) High-resolution TEM (HRTEM) image of a particle. Arrow indicates amorphous layer. Inverse Fourier transform of the region indicated in d showing the lattice fringes due to reflection from (111) planes of Cu(0), a better view of which is shown in the inset. The lattice fringe spacing corresponding to (111) plane is 0.196 nm.

The XRD pattern of the composite was matched with the standard powder diffraction data file for copper (face-centered cubic, JCPDS file No. 04–0836). Further, the presence of cupric oxide (CuO) or cuprous oxide (Cu_2O) was not detected in the diffraction. It may be mentioned here that 10 day old samples also showed similar XRD patterns (Appendix, Figure A. 3A.3b**).** This possibly indicates that the surface of Cu NPs present in the composite was possibly oxidized in the atmosphere gradually, which changed the optical extinction spectrum but was not reflected in the XRD pattern. In

other words, a thin film (shell) of copper oxide grown from the Cu NP might have affected the optical properties of the Cu NPs inside, but the metal was still present there. It has been established that modification of the surface of metal NPs by deposition of another metal or even polymer may lead to disappearance of the characteristic SPR of the original metal.

That the Cu NPs were synthesized and present in the composite was further confirmed by TEM measurements. As shown in Figure 3A.1c, particulates were formed in the medium with average particle size of 17±4 nm. HRTEM image of a particle, shown in Figure 3A.1d clearly indicated crystalline nature of the same. Additionally, the lattice space of 0.196 nm measured from the image (Figure 3A.1d, inset) indicated the presence of crystalline Cu. This matched well with the reported literature value for the lattice fringe of (111) planes of copper.[10,29] On careful examination of the edges of Cu NP, (Figure 3A.1 d) show that the lattice fringes do not extend to the periphery, but rather give way to a thin region of amorphous growth, probably due to oxide formation. TEM image in Figure 3A.1 d also shows such an amorphous layer covering the surface of Cu NP. Further, TEM image of 10 day old samples (Appendix, Figure A. 3A.3b) show extensive agglomeration of the Cu NPs into larger particles of ~ 50−200 nm in sizes. The broadening of the SPR band in aged samples is probably due to a combination of oxidation and agglomeration of the Cu NPs in the composite. This fact is consistent with the XRD results of the aged sample, which still show the presence of peaks due to copper. Thus the present method provided a composite of Cu NP and CS, where the Cu NP surface might have been oxidized slightly in atmosphere, which was sufficiently thin not to alter the NP but might have contributed to the loss of extinction spectrum.

It is understandable that the utility of the NPs in the composite gets reduced when the NPs themselves are prone to oxidation and agglomeration under atmospheric condition. This is especially true when application such as in antimicrobial activity, which is an important aim of the present study, is involved. This problem was alleviated by using molecular iodine in order to stabilize the NPs over a longer period of time. When the composite was redispersed into dilute acetic acid solution followed by treatment with molecular iodine, the color of the composite still retained its original reddish nature.

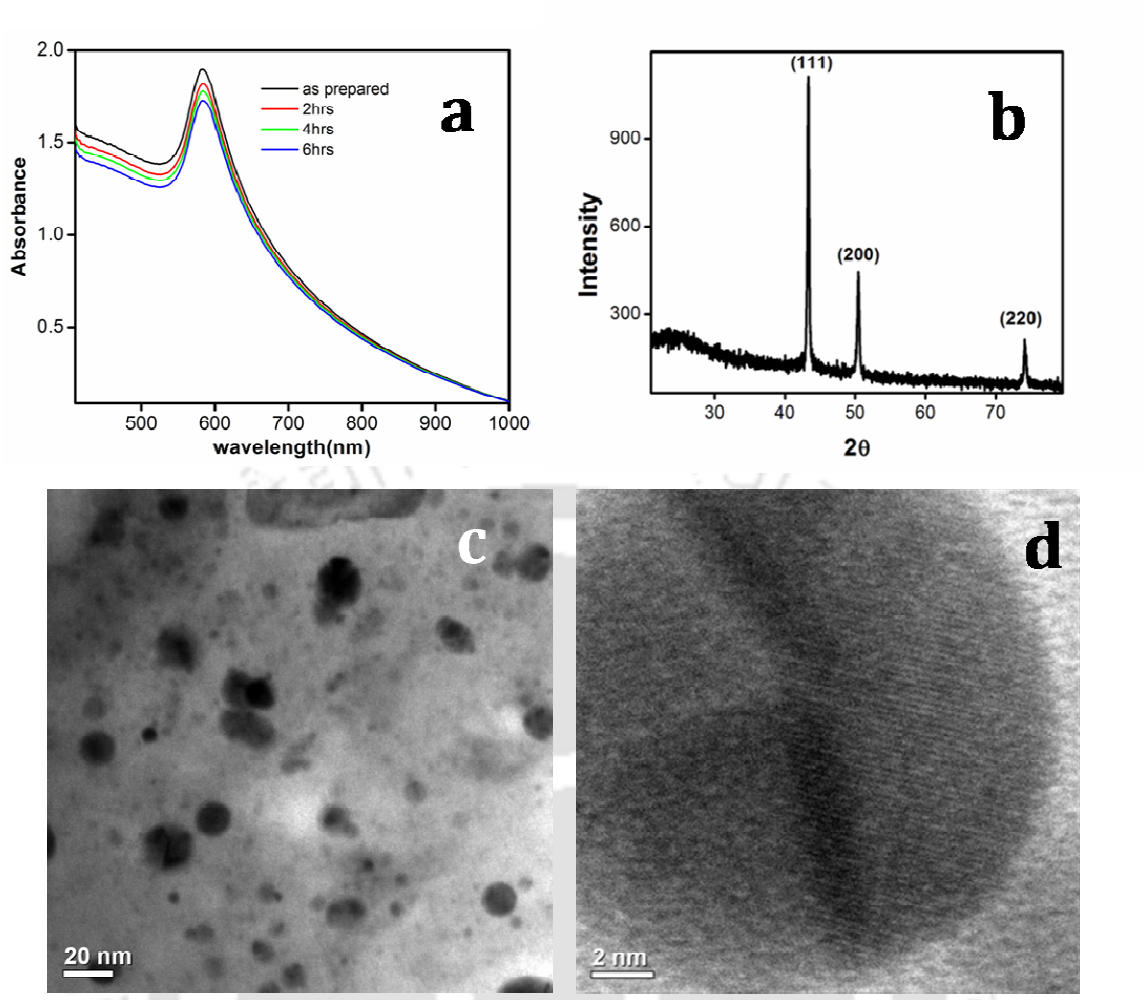

Figure 3A.2: (a) Time-dependent UV-Visible spectra of iodinated CS - Cu NP composite as recorded under atmospheric conditions. (b) Powder XRD pattern of freshly prepared iodinated CS-Cu NP composite. (c) TEM image of freshly prepared iodinated CS-Cu NP composite. (d) HRTEM image of a particle showing the lattice fringes corresponding to the (111) planes of copper.

The UV-visible spectrum consisted of a sharp peak at 583 nm (Figure3A. 2a). The shift in the peak may be due to the presence of iodine on the surface of the NPs thereby changing the dielectric constant of the medium in the immediate vicinity of the NPs i.e. surrounding the NPs. Interestingly in the presence of the iodine the peak corresponding to Cu NPs was rather stable. [32] As is clear from Figure 3A.2a, for the first 6 h the change in the peak intensity was minimal, although there was a systematic decrease in the background scattering thereby reducing the overall intensity. Further, the peak due to Cu NPs was clearly present for the first 3 days although the background scattering was

continuously decreasing (refer to Appendix, Figure A.3A.2b). In addition, the broadening of the peak with time was also slower in the presence of iodine than in its absence. Essentially, UV-Visible spectroscopic studies indicated that the Cu NPs in the composite were relatively more stable in presence of iodine than in its absence. The stability could be provided by the formation of trace amounts of I atoms on the Cu NP surface. Molecular iodine is known to dissociate to iodine atoms on clean copper surfaces[33, 34]. On the other hand, under normal atmospheric conditions and in absence of iodine, the NPs become unstable possibly due to surface oxidation and agglomeration. Powder XRD patterns of the iodinated CS-Cu NP composite-when the sample was prepared within 1 h of addition of iodine-indicated that they were rather stable (Figure3A. 2b). This was evidenced by the presence of all three peaks corresponding to (111), (200) and (220) occurring at 2θ values 43.34°, 50.46° and 74.14^{o} respectively. Further, TEM images of the sample corroborated the stability of the NPs in the presence of iodine as there was hardly, if any, agglomeration and oxidation (Figure 3A.2c). Also the Cu NPs were spherical, much smaller in size in presence of iodine (Figure3A.2c) with measured average size of 8±4 nm. HRTEM image in Figure 3A. 2d lattice spacing which matched with that of Cu metal and the fringes were found to extend all the way to the edge of the NP, indicating the absence of amorphous oxide formation on the surface of the NP. Thus the composite in the presence of iodine would be a good candidate for antimicrobial studies due to its enhanced stability. It is also important to mention here that the stability of Cu NPs in the presence of iodide has been reported recently.[32]

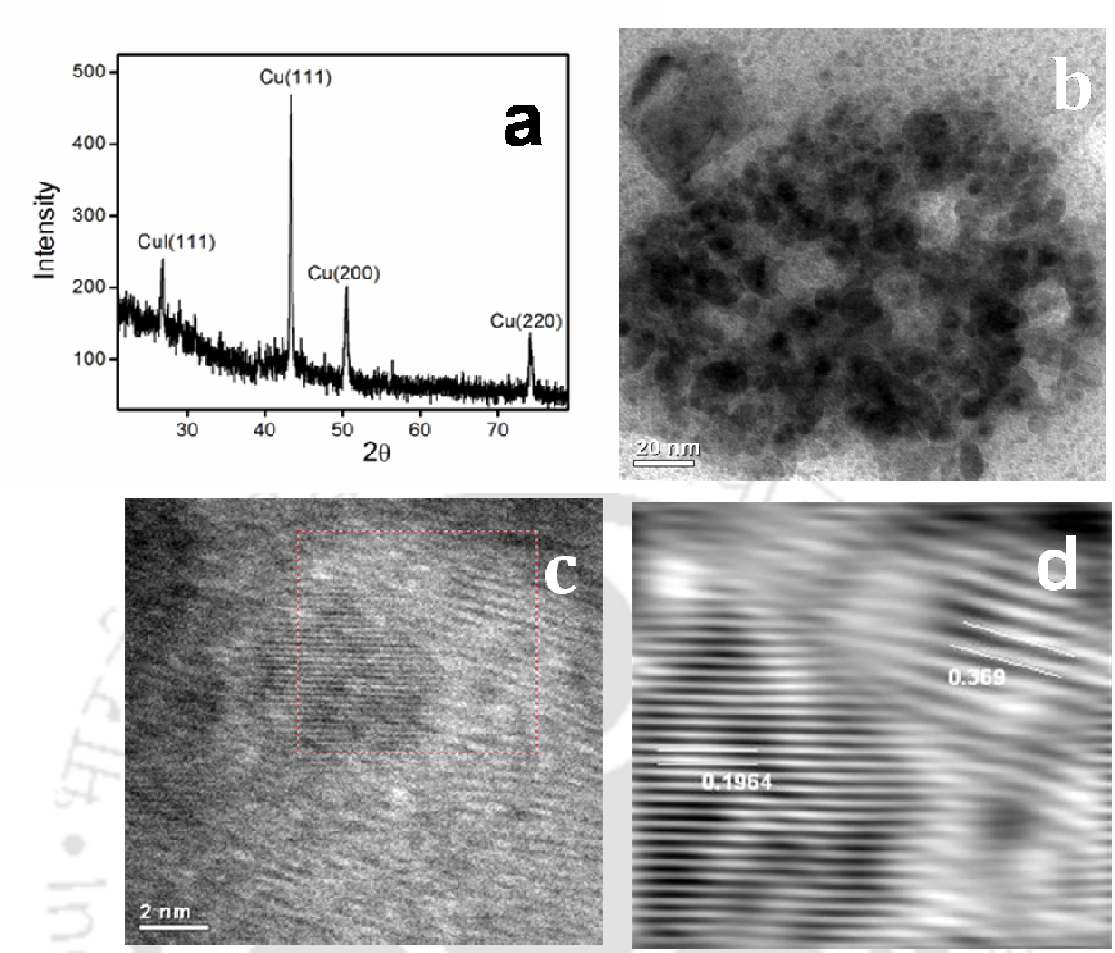

Figure 3A. 3: (a) Powder XRD pattern of 10 day old iodinated CS-Cu NP composite. 2θ= 26.84^0 is the diffraction angle of CuI (111) plane. (b) TEM image of iodinated CS-Cu NP composite of 10 days old sample. (c) HRTEM of the 10 day old iodinated CS-Cu NP composite showing the presence of lattice fringes corresponding to the (111) planes of copper and CuI. (d) Inverse Fourier transform of selected region in c showing the lattice fringes corresponding to the (111) planes of copper and copper iodide. The lattice fringe spacing corresponding to (111) plane of copper and copper iodide are 0.196 nm and 0.369 nm respectively.

That the stability of Cu NPs in the composite was enhanced in the presence of molecular iodine is clear from the results of the experiments mentioned above. However, we were further interested in finding the mechanism of stability and thus probed the NPs in the composite treated with iodine. This was pursued by recording the powder XRD and TEM of the composite treated with molecular iodine for 10 days. Figure 3A.3a shows the powder XRD patterns of the sample. As is clear from the figure, the pattern consisted of peaks due to Cu (111), (200) and (220) occurring at 2θ values 43.34°, 50.46^0 and 74.14^0 respectively. On the other hand, there was an additional peak occurring at 26.73^0

which is ascribed to the presence of CuI and the diffraction is due to (111) plane of the salt. This means that the composite even after 10 days retained Cu NPs, although formation of CuI took place in the presence of iodine. Further, TEM measurements indicated that (Figure3A. 3b) that although there was some degree of agglomeration with time, the particle largely retained their size and thus were stable. On the other hand, HRTEM image of a particle indicated the presence of Cu and CuI as the lattice spacing of 0.196 nm and 0.369 nm were both observed in the same image. That the lattice of CuI was present indicated conversion of nanocrystals of Cu into CuI nanocrystals, possibly in the form of a core-shell structures.

To sum up, we find that both CS and iodine have different roles in stabilization of Cu NPs. CS is a naturally occurring, cationic polysaccharide composed of (1,4)-linked 2-amino-2-deoxy-β-d-glucose and 2- acetamido-2-deoxy-β-d-glucose units, and is able to physisorb on Cu surface due to its significant content of primary amines and hydroxyl groups. In CS-Cu NP composite we observed that CS stabilized the Cu NPs and slowed down their aerial oxidation. However CS was unable to prevent the agglomeration of the Cu NPs and after 4 hours the sample started showing agglomeration of Cu NPs (i.e. Appendix, figure A. 3A.2a). The interaction of molecular iodide on copper surfaces has been studied extensively and reported in the literature.[35–37] On copper surfaces molecular iodine dissociatively chemisorbs to form CuI films. [35,36] In our I-CS-Cu NP composite, where we used molecular iodine, we also observed the formation of CuI on the surface of Cu NPs, which inhibited its agglomeration (Figure 3A.3b). This is consistent with the fact that in the iodine-CS-Cu NP composite the ratio of Cu:I_2 used during synthesis was 26.7:1, i.e. there was excess of Cu in comparison with I. Thus in our I-CS-Cu NP sample, in which both CS and molecular iodine were present, Cu NPs are stable towards oxidation and agglomeration for about 4 days in ambient conditions.

3A.5: Conclusion

We have prepared a new CS-Cu NP composite using biocompatible and biodegradable environmentally friendly polyelectrolyte CS. The CS-Cu NP composite as such in the atmosphere was not stable and was prone to oxidation. However, in the

presence of molecular iodine the composite was rather stable. The added stability of the iodinated CS-Cu NP composite permitted its efficacy as a potent antimicrobial agent. Iodine prevent copper oxide formation, possible dissociation of molecular iodine on the surface of Cu NPs into iodine atoms which chemisorbs to form CuI films on the surface of Cu NPs, inhibits agglomeration and stable towards oxidation. Studies on Gram-negative GFP expressing *E. coli* and Gram-positive *B. cereus* bacteria and revealed the effectiveness of the composite Antibacterial activity studies of iodinated CS-Cu NP composite are discussed in next chapter of the thesis.

References

(1) Huang, X. H.; Jain, P. K.; El-Sayed, I. H.; El-Sayed, M. A. *Nanomedicine* **2007,** *2*, 681-693.

(2) Jain, P. K.; Huang, X. H.; El-Sayed, I. H.; El-Sayed, M. A. *Accounts Chem. Res.* **2008,** *41*, 1578-1586.

(3) Jain, P.; Pradeep, T. *Biotechnology and Bioengineering* **2005,** *90*, 59–63.

(4) Vukojevic, S.; Trapp, O.; Grunwaldt, J.-D.; Kiener, C.; Schuth, F. *Angew. Chem., Int. Ed*. **2005,** *44*, 7978–7981.

(5) Ressler, T. B.; Kniep, L.; Kasatkin, I.; Schlogl, R. *Angew. Chem. Int. Ed*. **2005,** *44*, 4704-4707.

(6) Creighton, J. A.; Eadon, D. G. *J. Chem. Soc., Faraday Trans.* **1991,** *87*, 3881-3891.

(7) Huang, H. H.; Yan, F. Q.; Kek, Y. M.; Chew, C. H.; Xu, G. Q.; Ji, W.; Oh , P. S.; Tang, S. H. *Langmuir* **1997,** ***13***, 172- 175.

(8) Liu, Z.; Bando, Y. *Adv. Mater*. **2003,** *15*, 303- 305.

(9) Cioffi, N.; Torsi, L.; Ditaranto, N.; Tantillo, G.; Ghibelli, L.; Sabbatini, L.; Bleve Zacheo, T.; D'Alessio, M.; Zambonin, P. G.; Traversa, E. *Chem. Mater*. **2005,** *17*, 5255-5262.

(10) Anyaogu, K. C.; Fedorov, A. V.; Neckers, D. C. *Langmuir* **2008,** *24*, 4340-4346.

(11) Wei, Y.; Chen, S.; Kowalczyk, B.; Huda, S.; Gray, T. P.; Grzybowski . B. A. *J. Phys. Chem. C* **2010,** *114*, 15612-15616.

(12) Kim Y. H.; Lee D. K.; Cha H. G.; Kim C. W.; Kang Y. C.; Kang Y. S. *J. Phys. Chem. B* **2006,** *110,* 24923-24928.

(13) Yoon, K. -Y.; Byeon, J. H.; Park, J. -H.; Hwang, J. *Sci. Total Environ.* **2007,** *373,* 572–575.

(14) Ruparelia, J. P.; Chatterjee, A. K.; Duttagupta, S. P.; Mukherji, S. *Acta Biomaterialia* **2008,** *4,*707-716.

(15) Raffi, M.; Mehrwan, S.; Bhatti, T. M.; Akhter, J. I.; Hameed, A.; Yawar, W.; Hasan, M. M. ul. *Annals of Microbiology* **2010,** *60,* 75-80.

(16) Esteban-Cubillo, A.; Pecharroman, C.; Aguilar, E.; Santaren, J.; Moya, J .S. *J. Mater. Sci.* **2006,** *41,* 5208-5212.

(17) Fung, M. C.; Bowen, D. L. *Clin. Toxicol.* **1996,** *34,* 119-126.

(18) Gaggelli, E.; Kozlowski, H.; Valensin, D.; Valensin , G .*Chem. Rev.* **2006,** *106* , 1995-2044.

(19) Cater, M. A.; Fontaine S. L.; Shield, K.; Deal, Y.; Mercer, Julian F. B. *Gastroenterology* **2006,** *130,*493-506.

(20) Dhas, N. A.; Raj C. P.; Gedanken, A. *Chem. Mater.* **1998,** *10,* 1446- 1452.

(21) Kumar R.V.; Mastai, Y.; Diamant, Y.; Gedanken , A. *J. Mater. Chem.* **2001, *11,*** 1209- 1213.

(22) Vitulli, G.; Bernini, M.; Bertozzi, S.; Pitzalis, E.; Salvadori, P.; Coluccia, S.; Martra, G. *Chem. Mater.* **2002, *14*,** 1183- 1186.

(23) Casella, I. G.; Cataldi, T. R. I.; Guerrieri , A.; Desimoni, E. *Anal. Chim. Acta* **1996, *335*,** 217-225.

(24) Lisiecki, I.; Pileni, M. P. *J. Am. Chem. Soc.* **1993, *115*,** 3887-3896.

(25) Qi, L.; Ma J.; Shen, J. *J. Colloid Interface Sci.* **1997, *186,*** 498-500.

(26) Lisiecki, I.; Billoudet, F.; Pileni, M. P. *J. Phys. Chem.* **1996, *100,*** 4160-4166.

(27) Yeh, M. S.; Yang, Y. S.; Lee, Y. P.; Lee, H. F.; Yeh, Y. H.; Yeh, C. S. *J. Phys. Chem. B* **1999,** *103,* 6851–6857.

(28) Joshi, S. S.; Patil, S. F.; Iyer, V.; Mahumuni, S. *Nanostructured Materials* **1998,** *10,* 1135-1144.

(29) Hansen, P. L.; Wagner, J. B.; Helveg, S.; Rostrup-Nielsen, J. R.; Clausen, B. S.; Topsoe, H. *Science* **2002,** *295,* 2053-2058.

(30) Hardy, J. J. E.; Hubert, S.; Macquarrie, D. J.; Wilson, A. *J. Green Chem.* **2004,** *6*, 53-56.

(31) Murugadoss, A.; Chattopadhyay, A. *Nanotechnology* **2008,** *19*, 015603 (9pp)

(32) Kapoor, S.; Joshi, R.; Mukherjee, T. *Chem. Phys. Lett.* **2002,** *354*, 443-448.

(33) Lin, J. -L.; Bent, B. E. *J. Phys. Chem.***1992,** *96*, 8529-8538.

(34) Jenks, C. J.; Paul, A.; Smoliar, L. A.; Bent B. E. *J. Phys. Chem.***1994,** *98*, 572-578.

(35) Andryushechkin, B. V.; Baranovsky, R. E.; Eltsov, K. N.; Yurov, V. Y. *Surf. Sci.* **2001,** *488*, L541-L546.

(36) Andryushechkin, B. V.; Eltsov, K. N.; Shevlyuga, V. M. *Surf. Sci.* **2004,** *566-568*, 203-209.

(37) Andryushechkin, B. V.; Eltsov, K. N.; Cherkez, V. V. *JETP Letters* **2006,** *83*, 162-166.

Chapter 3B

Stable three component iodinated chitosan-Cu nanoparticle composite: Antibacterial activity studies

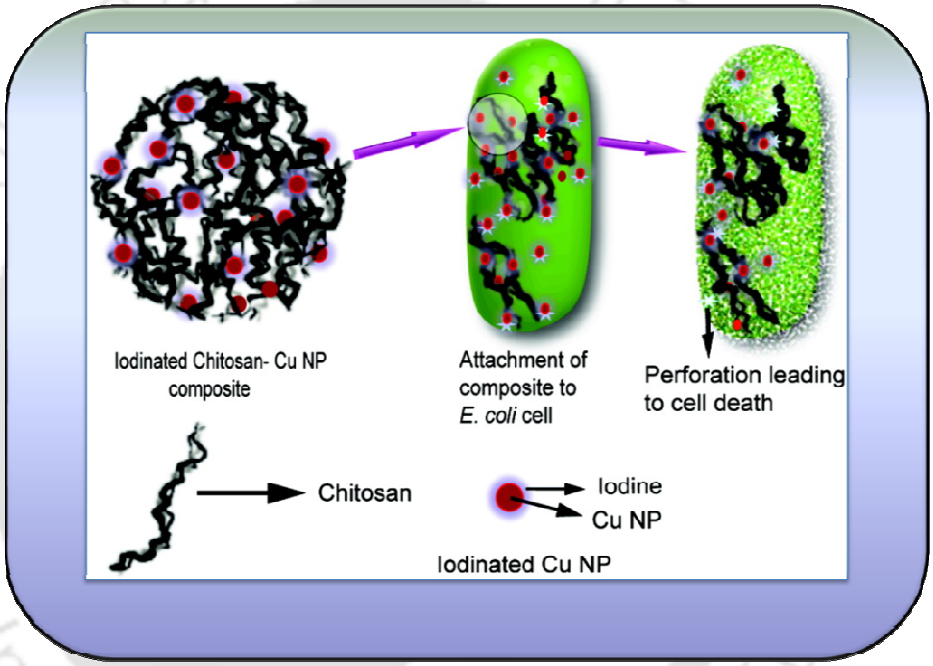

The work embodied herein has been published as an article as described below.

"Iodine-Stabilized Cu Nanoparticle Chitosan Composite for Antibacterial applications. **Sadhucharan Mallick,** Shilpa Sharma, Madhuchanda Banerjee, Siddhartha Sankar Ghosh, Arun Chattopadhyay, and Anumita Paul *ACS Appl. Mater. Interfaces*, **2012,** *4(3),* 1313–1323"

3B.1: Introduction

Colloidal silver has been known to possess excellent antibacterial properties; their use was very limited in the past.[1,2] However, very recently Ag NPs have found wide applications such as in water purification systems and in air purification systems.[3,4,5] Further, Ag NPs have also been proposed in anticancer therapy.[6,7,8] Hence in the last decade, while on one hand Ag NPs are being used more widely it has also been a cause of concern to the environment especially due to lack of any suitable sequestering agent and their persistent presence in the environment.[9] In this respect Cu NPs find use not only as catalysts and as optical and electrical conducting materials but also as antibacterial and antifungal agent.[10−25] Further, there are known sequestering agents for Cu for their release out of the human body following their use. [26,27] Thus Cu NPs are an attractive alternative to Ag NPs in bactericidal applications.

Esteban-Cubillo and coworkers have demonstrated bactericidal properties of Cu NPs prepared in the matrix of sepiolite.[23] On the other hand, Kelechi C. et al. reported that the antimicrobial activity of acrylated Cu NPs is similar to that of conventional copper based biocides.[17] Additionally, Cioffi, et al.[16] have reported antifungal and antifouling properties of a Cu NP-polymer composite. In 2006, Y.H. Kim deposited Cu NPs on the surface of SiO_2 NPs which showed excellent inhibitory effects to various microorganisms.[19] M. Taner et al. recently reported Ag-Cu nanoalloys synthesis and their bactericidal behaviour against *E. coli*.[24] Recently Valodkar et al. prepared starch-stabilized Cu, Ag and Cu-Ag alloy NPs and found interesting antibacterial activity against both Gram-positive and Gram-negative bacteria.[25] In this regard, it is also important to address the issue of the species involved in antimicrobial or antifungal activities and the mechanism of action. For example, whether the NPs remain as such or get oxidized to Cu^{2+} species is still largely an open question. In addition, the details of the mechanism of action of the NPs still remain to be fully understood. Further, the presence of iodine in the composite is likely to enhance the antimicrobial activity of Cu NPs. The antimicrobial studies were carried out using GFP expressing recombinant *E. coli* bacteria[28] and Gram-positive *Bacillus cereus (B. cereus)* bacteria. Considering that CS itself is antimicrobial, the three-component (Cu NPs, CS and iodine) system provided

a new way of antimicrobial action where the minimum inhibitory concentration (MIC) and minimum bactericidal concentration (MBC) of iodinated CS-Cu NP composite against *E coli* were found to be 130.8 μg/mL and 239.4 μg/mL respectively. Quite a few studies attribute the antimicrobial property of copper and their oxides to the released Cu ions in aqueous medium. [16, 17] On the other hand, our findings from electron microscopic, optical and biochemical studies indicated that iodinated CS-Cu NP composite was attached to the bacterial cell surface, causing irreparable membrane damage followed by membrane disintegration and finally leading to cell death. Importantly, while the Cu NPs contributed to the overall bactericidal activity, atomic absorption spectroscopic measurements indicated that the copper ions, being released - if any, played a minor role in the bactericidal activity of the composite.

3B.2: Outline of the research work

I. Enhancement in antibacterial activity as well as stability of CS-Cu NPs composite in the presence of molecular iodine.

II. Positively charged CS helped in the attachment of the bacterium (negatively charged cell wall) to the composite, Cu NP present in the composite led to creation of pores on the cell wall, leading to cell death.

III. Zeta potential *(ζ)* measurements supported an attractive interaction between iodinated CS-Cu NP composite and bacteria. Electron microscopic and flow cytometric studies revealed that the iodinated CS-Cu NP composite was attached to the bacterial cell wall, which caused irreversible damage to the membrane eventually leading to cell death.

IV. CS, Cu NPs, and iodine work in tandem for superior antimicrobial activity.

3B. 3: Experimental section

3B.3.1: Growth media and Bacterial strains

Luria-Bertani (LB) broth and nutrient broth (NB) were purchased from HiMedia, Mumbai, India. Iodine and other high-purity molecular biology grade chemicals and reagents used for agarose gel electrophoresis were obtained from Sigma-Aldrich Chemical Pvt. Ltd., Kolkata, India. GFP-expressing recombinant *E. coli* were grown in LB broth at 37^0C and at 220 rpm for 12 h; whereas *B. cereus* were grown in NB at 37^0C and at 220 rpm for 12 h.

3B.3.2: Zeta potential (ζ)

Zeta potential (ζ) measurements were performed to determine the charge of iodinated CS-Cu NP composite, chitosan, iodine in aqueous solution at pH 6.3. Zeta potential (ζ) values were measured using Delsa™ Nano Submicron Particle Size and Zeta Potential Particle Analyzer (PN A54412AA, Beckman Coulter).

3B.3.3: Atomic absorption spectrometry (AAS)

In order to directly probe the contribution of Cu ions to the bactericidal activity of the iodinated CS-Cu NP composite, we have measured the released Cu^{2+} ions from the surface, over time, due to diffusion. Quantitative analysis of Cu^{2+} ions was measured by using atomic absorption spectrophotometer (Model: AA240 Varian Inc).

3B.3.4: Transmission electron microscopy (TEM) analysis

The interactions of the Iodinated CS-Cu NP composite with bacterial cells were also examined using a high resolution transmission electron microscope operating at a maximum accelerating voltage of 80 KeV. The sample for iodinated CS-Cu NP composite (at MIC i.e. 130.84 μg/mL) treated *E. coli* was kept in the LB medium for 3 h. For this, the iodinated CS-Cu NP composite treated on *E. coli* samples were drop coated

onto the TEM grid followed by air drying and the resulting grid was then analyzed under TEM.

3B.3.5: Field emission scanning electron microscopy (FESEM)

Interaction of the iodinated CS-Cu NP composite with bacterial cells was further studied by using Field emission scanning electron microscopy (Carl Zeiss, SIGMA VP) instrument. Typically, 10 µL drop of each sample was deposited on a glass slide, dried and sputter-coated with gold film using a sputter coater and imaged under the FESEM.

3B.3.6: X-ray diffraction studies

In order to confirm the role of Cu NP of the iodinated CS-Cu NP composite in inhibiting the growth of *E. coli*, we have centrifuged a bacterial growth culture treated with MIC of iodinated CS-Cu NP after 4 hours and vacuum dried and stored under vacuum before analysis. The dried cell pellet spread on a glass slide and XRD was recorded using Bruker AXS D8 Advance X-ray diffractometer.

3B.3.7: Antibacterial activity assessment

For bactericidal activity, *B. cereus* was chosen as the Gram positive bacteria and GFP-expressing *E. coli* as the Gram negative bacteria. GFP-expressing *E. coli* was cultured in LB ampicillin media and *B. cereus* in NB media. Different concentrations of iodinated CS-Cu NP composite were used to determine the minimum inhibitory concentration (MIC) and minimum bactericidal concentration (MBC) at pH 6.3. Bacteria (10^8cfu/ml) were grown in media in the presence of different concentrations of iodinated CS-Cu NP composite for 12 h at 37^0C. The lowest concentration of composite at which there was no visual turbidity was taken as the MIC value of the composite. Further, the cultures which lacked visual turbidity were reinoculated in fresh media. The lowest concentration of the composite that killed at least 99.9% of original inoculums was taken as MBC. The experiments were performed at least in triplicate to ensure reproducibility. The bacterial growth was monitored by measuring optical density (OD) at 595 nm using a UV-Visible

spectrophotometer (Lambda-45; Perkin-Elmer, Fremont, CA, USA) of the sample at different times.

3B.3.8: Flow cytometric assay for viability analysis of bacterial cells using GFP-Propidium iodide combination

Viability of GFP-expressing recombinant bacterial cells and disruption of membrane integrity was assessed using propidium iodide (PI), which enters only permeable cells, binds DNA, and fluoresces at 620 nm when stimulated by a laser at 488 nm. In viable cells, PI remains in the medium and does not fluoresce; in compromised cells, PI enters the cell through damaged membrane and binds DNA exhibiting fluorescence signals. [29] Briefly, several tubes containing 500 µL (10^8 cells/mL) of the recombinant *E. coli* cells and 350 µL of the iodinated composite (at MIC of 130.84 µg/mL iodinated CS-Cu NP consisting of 127.62 µg/mL of CS -Cu NP and 3.22 µg/mL iodine) were incubated at 25°C for various time periods (1 h, 2 h, 4 h and 6 h). After incubation, 1.5µL of 0.2 mM PI was mixed into each tube and diluted with 150 mM NaCl. Samples were analyzed by a Flow Cytometer (BD FACS calibur System, BD Biosciences, San Jose, CA). Samples were illuminated with a 15 mW argon ion laser (488 nm), and the fluorescence was detected via 525±10 nm (green) and 620±10 nm (red) band pass filters. Signals were amplified with the logarithmic mode for side scattering, forward scattering, and fluorescence. In dot plots of fluorescence, different bacterial populations were gated according to the viability stages.

3B.3.9: Agarose gel electrophoresis of GFP recombinant plasmid DNA

Effect of iodinated CS-Cu NP composite on plasmid DNA was performed by incubating the iodinated CS-Cu NP composite with plasmid DNA at 37^0C. DNA-composite complex formation was checked by 0.8% agarose gel electrophoresis followed by visualization of EtBr stained DNA under UV- transilluminator (refer to Appendix, Figure A. 3B.6).

3B.4: Results and discussion

3B.4:1 Antibacterial studies of the iodinated CS-Cu NP composite

The bactericidal activity of the iodinated CS-Cu NP composite was determined on Gram-negative GFP-expressing *E.coli* and Gram-positive *B. cereus* bacteria. Turbidity tests indicated that freshly prepared iodinated CS-Cu NP composite exhibited superior bactericidal activity as opposed to aged samples. Hence for antibacterial studies only freshly prepared samples (within 6 h of preparation) of iodinated CS-Cu NPs were used. From the results reported above, it is clear that such samples used underwent minimum changes thus ensuring reproducibility of the results with maximum effectiveness of the composite. In order to determine the MIC and MBC, 10^8 cfu/mL of GFP-expressing *E. coli* were inoculated into Luria-Bertani (LB) medium supplemented with various concentrations of the composite (i.e. in the presence of iodine) and grown overnight at 37°C. The minimum concentration of the iodinated CS-Cu NP composite at which microbial growth was measurably inhibited was taken to be the MIC. Thus MIC was the concentration of the iodinated composite where no visual turbidity of the culture was observed. The cultures that were not turbid were reinoculated into fresh LB containing ampicillin at 100μg/mL. The MBC of the iodinated Cs-Cu NP composite was considered to be the minimum concentration of the composite that prevented growth of the bacterial cells following reinoculation, as observed visually by the lack of turbidity. Control experiments were performed with acetic acid and ethanol only. For comparison, the antibacterial activities of the CS-Cu NP composite, chitosan, and iodine towards the recombinant GFP-expressing *E. coli* were also measured.

The results of the antimicrobial activity of the iodinated composite are shown in Figure3B.1. The MIC of the iodinated composite was found to be 130.84 μg/mL, which consisted of 127.62 μg/mL of CS-Cu NP composite and 3.22 μg/mL of iodine. The corresponding MBC (239.4 μg/mL) contained 233.50 μg/mL of CS-Cu NP and 5.9 μg/mL of iodine. In the above concentrations of the iodinated CS-Cu NPs composites, the quantity of Cu NP was 21.55 μg/mL for MIC and 39.43 μg/mL for MBC

respectively. These determined values of MIC for Cu NPs are much lower than those reported for Cu NPs in the literature[20, 21, 22] Control samples with 0.02 M acetic acid and 6 µL ethanol only in LB media showed no growth inhibition (Figure 3B.1). The doses at which Cu NPs can independently show antibacterial activity (MIC) has been reported to be 60-150 µg/mL.[20,21,22] In our case, separate experiments showed that freshly prepared Cu NPs (without CS and iodine) above 468.2 µg/mL inhibited growth of the bacteria in LB medium. Clearly, iodinated CS-Cu NP composite exhibited higher antibacterial activity at much lower dose of Cu NPs in comparison to the bactericidal dose of the individual components, i.e. MIC of chitosan is known to be 468 µg/mL towards *E. coli* [30,31] and MIC of iodine towards *E. coli* is 155.6 µg/mL[32,33] and, of course, of Cu as mentioned before. This is also corroborated by our results shown in Figure 3B.1, where we observe that individual components at their individual concentrations (in the composite) either did not exhibit antibacterial properties (i.e. 21.55 µg/mL of Cu NP and 3.22 µg/mL of iodine) or exhibited limited bactericidal properties (i.e.106.07 µg/mL of CS) when present as CS-Cu NP composite. However, when present as iodinated composite as in I-CS-Cu NPs (MIC) they inhibited the growth of *E. coli* Furthermore, growth of GFP expressing *E. coli* was monitored up to 24h under various treated conditions with no apparent changes in profile (refer to Appendix, Figure A.3B.1). The MIC value of our turbidity experiments was also substantiated by plate counts of GFP expressing recombinant *E. coli* treated with I-CS-Cu NPs composites (239.4 µg/mL at MBC dose) in a dilution experiment (refer to Appendix, Table A.3B.1).

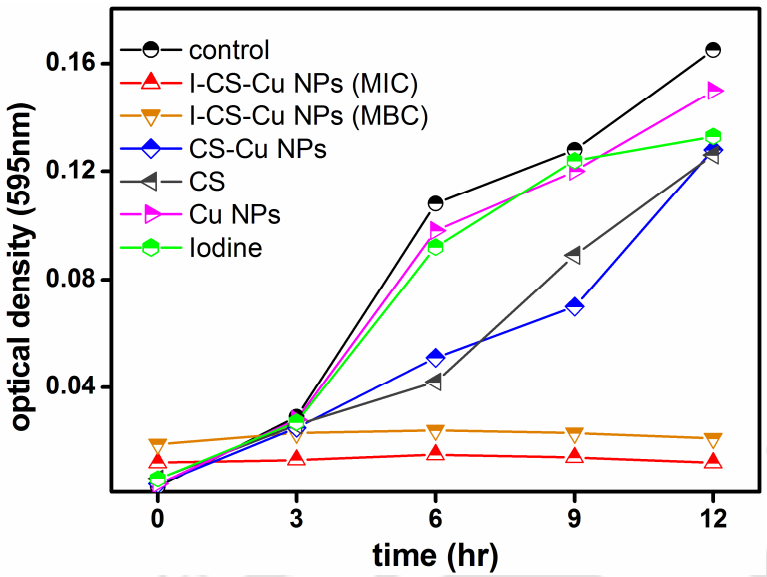

Optical density	cfu/ml
0.003	0.067×10^7
0.029	0.650×10^7
0.108	2.42×10^7
0.128	2.86×10^7

Figure 3B.1: Growth curve of GFP recombinant *E. coli* in the presence of the following (as also indicated in the legends). **Control**: 0.02 M acetic acid and 6 µl ethanol only in LB media; **I-CS - Cu NPs (MIC)**: iodinated CS-Cu NP composite at 130.84 µg/mL; **I-CS - Cu NPs (MBC)**: iodinated CS-Cu NP composite at 239.4 µg/mL; **CS - Cu NPs** : CS - Cu NPs composite at 127.62 µg/mL; **CS**: Chitosan at 106.07 µg/mL, **Iodine**: Iodine at 3.22 µg/mL. and **Cu NPs**: Cu NPs at 21.55 µg/mL.

In addition, the MIC of I-CS-Cu NP composite on Gram positive *B. cereus* was found to be 165.13 µg/mL, which contains of 27.19 µg/mL of Cu NPs, and the corresponding MBC was 275.86 µg/mL, which contains of 45.42 µg/mL of Cu NPs. The values were slightly higher than Gram negative *E. coli* bacteria.

Fluorescence microscopic investigation (refer to Appendix , Figure A. 3B. 3) with the GFP-expressing *E. coli* bacteria indicated that at the MIC of the iodinated composite the bacterial population did not grow appreciably after 3 h. On the other hand, at MBC bacterial population was obliterated and hardly any bacterium could be observed to be present 3 h after treatment. However, in the control sample the bacteria grew within the time period of measurement.

The effect of the composite on the bacteria especially the development of porosity on their cell was further investigated using cytometry. In general, flow cytometric assessment of bacterial cell viability in response to a bactericidal agent typically reveals the existence of four different cell populations corresponding to living, compromised,

dead and lysed. Also, it is known that bacterial permeability to nucleic acid staining dye such as propidium iodide (PI) is associated with the occurrence of substantial damage to the membrane, indicating alternation of cell membrane potential, which finally causes cell death. Thus when the cell is not affected by the agent then green fluorescence (from GFP of the recombinant bacteria) is observed as PI does not fluoresce as it remains in the medium. On the other hand, when the cells are compromised and membrane porosity is developed, PI could enter the cell and binds to DNA showing red fluorescence in addition to green fluorescence. However, when the cells are dead cells, the GFP leaks out and thus only red fluorescence is observed. Finally, lysed cells are devoid of fluorescence. Thus measurements of fluorescence could reveal the population of different cells (as above) leading one to better understanding of the working of the antimicrobial agent.

In the present study, bacterial cells, when treated with MIC of iodinated CS -Cu NP composite and incubated for different time periods- say1 h, 2 h, 4 h and 6 h - showed gradual shift of population from viable to compromised cells (Figure 3B.2). Results showed negligible amount of dead or lysed cells in the above time periods. Interestingly, after 1 h of treatment almost all the cells were found to be living and healthy. However, with the progression of time the population of compromised cells gradually increased and reached its maximum at 6 h where almost 50% of the total cell population appeared to have been compromised. Incidentally, parallel to this, the untreated group of bacteria (control) exhibited less number of compromised cells. The results are further detailed in Table 3B.1. The results suggested that the iodinated CS-Cu NP composite caused irreparable damage to the bacterial cell membrane, which began as early as 2 h following treatment.

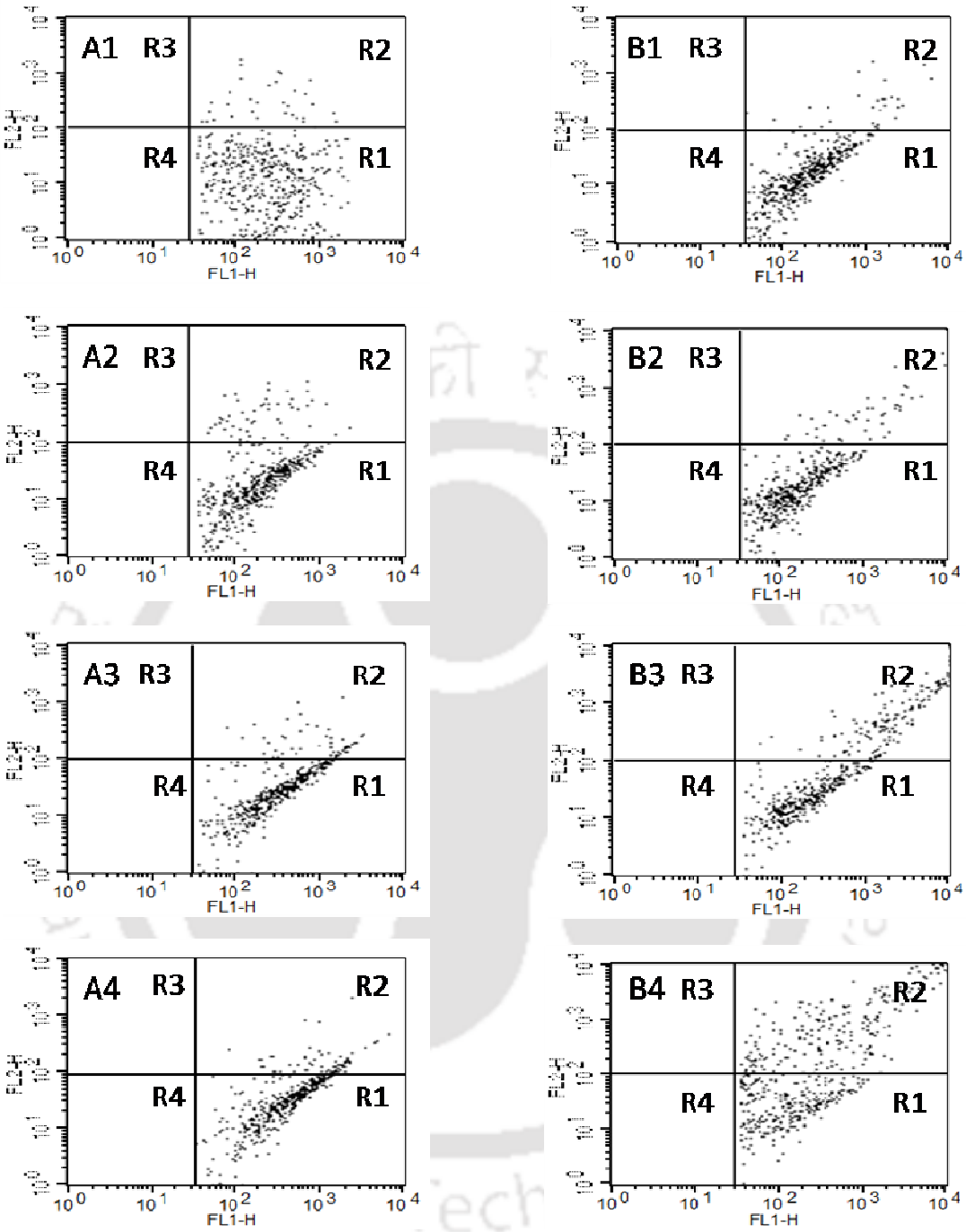

Figure 3B.2: Dot plots showing populations of *E. coli* cells (GFP expressing stained with PI) at different viability stages, measured by flow cytometry at different time points treated with iodinated CS-Cu NP composite. Series A refers to untreated cells and series B refers to cells treated with MIC (130.84 µg/mL) of the composite. Different viability stages are denoted as R1 (live), R2 (compromised), R3 (dead) and R4 (lysed) cells.

Table 3B.1 Percentage of total *E. coli* cells untreated and treated with iodinated CS-Cu NP composite (130.84 µg/mL) at different viability stages during different time points measured by flow cytometry. Percentages of Dead and lysed cells were negligible.

	Untreated (% of total cells)				Treated (% of total cells)			
Time (hours)	**1**	**2**	**4**	**6**	**1**	**2**	**4**	**6**
Live	91.95	90.26	86.24	85.50	92.31	87.88	66.89	51.09
Compromise	8.05	9.73	13.74	14.39	7.12	12.11	33.11	48.91

Interaction of the composite with bacterial cells was further studied by TEM and FESEM. FESEM images of both the untreated and the composite treated GFP recombinant *E. coli* are shown in Figure 3B.(3a, 3b). The sample for composite treated bacteria was kept in the medium (with the concentration of the composite being at MIC i.e. 130.84 µg/mL) for 3 h prior to evaporation for sample preparation. It is interesting to observe from Figures 3B.3a and 3B.3b that while untreated bacterium was healthy and of usual surface morphology the one being treated with the composite clearly was different and the cell was covered with particles. The diameter of the particles (~ 5-15 nm) indicated that the particles were made of Cu NPs as they were the same as in the composite (the particle sizes as measured from TEM, Figure 3A. 2c. TEM investigations of the composite treated bacteria further supported the attachment of the composite to the cells. For example, as shown in Figure 3B.3c, darker spots of particle were observed to have been superimposed on the image of a bacterium. This is also evidenced from TEM image (Figure A. 3B.4a, Appendix,) and SAED (Appendix, Figure A. 3B.4b) which further confirmed that the NPs attached to the cell wall were Cu. Thus the composite was indeed interacting with the bacterium. Also, the image of a bacterium being damaged owing possibility to development of porosity on its cell wall (Figure 3B.3d) further support the interaction leading to cell death via cell wall damage. It is important to mention here that the NPs (in the composite) being present on the cell surface retained their individual character as the particle sizes when attached to the bacterium and as-prepared were comparable. In other words, no agglomeration of NP was observable when the composite was attached to the bacterial cell surface. Further, it is important to note here that XRD pattern of the composite-treated bacteria, where the sample was prepared 4 h after treatment, indicated that Cu NPs were still present in the medium as

the diffraction pattern due to (111), (200) and (220) planes could still be observed, although peaks due to CuI were also present (Appendix, Figure A. 3B.5). It may also be noted that aged samples of the composite, when formation of CuI was observed extensively, did not show antibacterial activity at a concentration of 130.84 µg/mL (MIC) as was probed using turbidity test.

Polycationic chitosan is well known to interact with negatively charged cell envelop which permeabilzes the cell membrane leading to leakage of intracellular components.[34,35,36,37] Zeta potential *(ζ)* measurements were performed to determine the charge of iodinated CS-Cu NP composite, chitosan , iodine in aqueous solution at pH 6.3. Zeta potential *(ζ)* values were measured using Delsa™ Nano Submicron Particle Size and Zeta Potential Particle Analyzer. Zeta potential values at pH 6.3 were as follows: iodine: -75.37 mV; chitosan: +59.57 mV; and iodinated CS-Cu NP composite: +36.49 mV. Further, zeta potential measurements on various strains of *E. coli* in pH ranges 2 to 9 have shown that the surface charge of bacterial cells is negative.[38,39] Hence, presumably, *E coli* cells negative surface charge adheres to the positively-charged iodinated CS-Cu NP composite through electrostatic interactions. Once the composite gets attached to the bacterial cell wall, Cu NPs possibly get attached to sulfur-containing proteins [40] of bacterial cell membrane leading to greater permeability of the membrane, causing leakage of proteins and other intracellular constituents and death of bacteria.

Gel retardation assay indicated the possibility of attachment of iodinated CS-Cu NP composite with plasmid DNA (Appendix, Figure A.3B. 6). Thus, it is probable that DNA of the compromised bacterial cell might well have been attached to the composite after perforation of the cell wall by Cu NPs present in the composite, ultimately killing it. This observation is similar to our previous study. [29]

It is important to understand the antimicrobial activity of the composite vis-à-vis the presence of Cu NPs. In this regard, several studies attribute the antibacterial property of copper to the Cu^{2+} ions released in aqueous medium .[16,17] We have investigated whether in our composite too, the antibacterial properties of Cu NP is due to released Cu^{2+} ions, using atomic absorption spectroscopic (AAS) studies. AAS data in Appendix, Figure A.

3B.2a shows that the freshly prepared iodinated CS-Cu NP composite at MIC (130.84 µg/mL of composite containing 21.55 µg/mL of Cu NPs) slowly released Cu^{2+} ions into the aqueous medium such that at ~ 1½ h the concentration of Cu^{2+} in solution was 17.8 ppm which increased up to 32.2 ppm in ~ 4 h. Note that this time was greater that the time taken to inhibit the growth at MIC, which is 3 h as is clear from Figure 3B.1. Moreover, 5 day old aged samples where the concentration of Cu^{2+} ions was 46 ppm, did not show antibacterial property at MIC of the composite.

In order to directly probe the contribution of Cu ions to the bactericidal activity of the composite, growth analysis studies were carried out in presence of different strengths of $CuSO_4$ solutions and that of a control experiment without Cu ions (Appendix, A. 3B.2b).

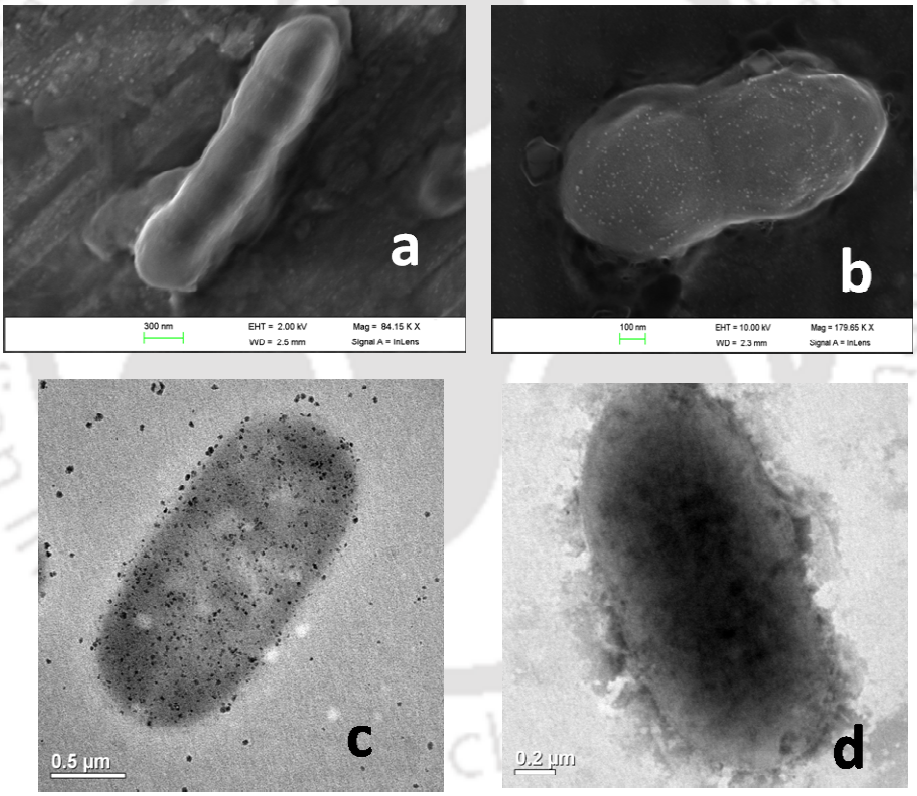

Figure 3B.3: (a) Field emission scanning electron micrograph of GFP expressing recombinant *E. coli* cells and (b) *E. coli* cells treated with 130.84 µg/mL (MIC) iodinated CS-Cu NP composite in liquid LB medium for 3 h. (c) TEM image of a GFP expressing recombinant *E. coli* cell treated with 130.84 µg/mL (MIC) iodinated CS-Cu NP composite in liquid LB medium for 3h. (d) TEM of a cell treated with MIC of iodinated CS-Cu NP composite showing damage.

In these solutions, the concentrations of Cu ion was similar to those which leached from the iodinated CS-Cu NP composite between ~1 ½ h to 5 days. It was found that there was no retardation of bacterial growth due to Cu ions. This indicated that Cu ions that release from the iodinated CS-Cu NP have little or no effect on the bactericidal potency of the composite

We thus conclude that released Cu^{2+} ions did not play an important role in killing the bacteria in our studies. Rather it's the attachment to the cell wall of the Cu NPs from the iodinated CS- Cu NP composite which perforated–the cell wall causing leakage of proteins and other intracellular constituents and ultimately caused cell death.

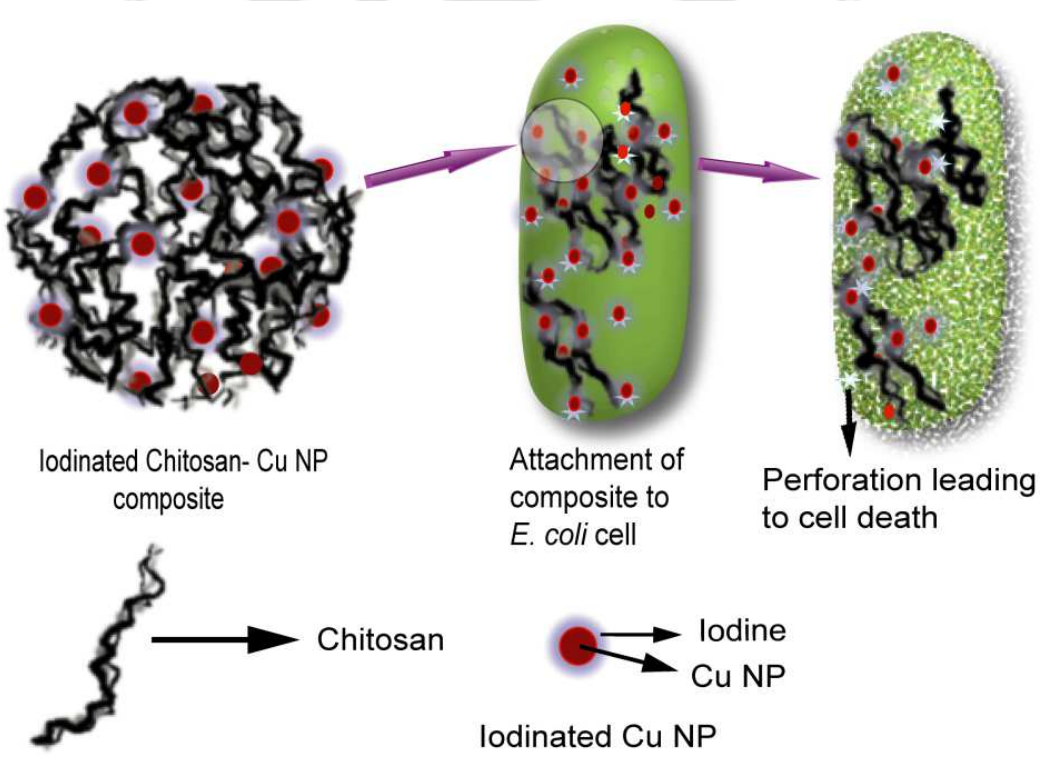

Scheme 3B.1: A schematic representation of the proposed mechanism of antibacterial action of the iodinated CS-Cu NP composite.

Essentially, various studies indicated that the bacterial cells were attached to the composite, possibly due to their opposite charges. Once attached, while the polymer helped keep the bacterium attached, the Cu NPs present in there possibly led to perforation of the cell wall causing irreparable damage to the membrane. The iodine

present on the surface of the NP not only stabilized them but also may have contributed to the overall activity as it is a known antimicrobial agent. The three components working in coordination led the bacteria to become unviable and finally causing cell death. A schematic representation of the process is shown in Scheme 3B.1.

Finally, a question may arise about the feasibility of the use of the present composite in real antimicrobial applications. First of all the CS-Cu-NP composite could be isolated as solid powder following synthesis and weighed amount could then be stored in evacuated ampoules. This would add not only to long term stability but also to ease in transportability. Similarly, molecular iodine could be made available in another container. A dispersion of the composite and iodine in acetic acid could then be prepared on site for appropriate use. This concoction could then be used for external and internal applications. Further, one could conceive of making a paste out of the components and then apply especially externally. In addition, our observations of enhanced stability of the dried powder form of iodinated CS-Cu-NP composite indicated its possible use in the form of powder also.

3B.5: Conclusion

We have synthesized of a new CS-Cu NP composite under ambient conditions, which was less stable and was prone to surface oxidation. This problem was alleviated by using molecular iodine to stabilize the CS-Cu NP composite over a longer period of time. The composite was rather stable when redispersed in dilute acetic acid solution followed by molecular iodine treatment. The added stability of the iodinated CS-Cu NP composite permitted its efficacy as a potent antimicrobial agent. Studies on Gram-negative GFP-expressing *E. coli* and Gram-positive *B. cereus* bacteria revealed the effectiveness of the composite. Polycationic chitosan interacted with the negatively charged cell envelope. In addition, Cu NPs possibly got attached to sulfur-containing proteins of bacterial cell membrane. This caused permeability of the membrane leading to leakage of proteins and other intracellular constituents and death of bacteria. Interestingly, the MIC and MBC of Cu NPs (when present in the iodinated composite) against *E. coli* bacteria were found to be 21.5 μg/mL and 39.4 μg/mL respectively, which are much lower than the

values reported for Cu NPs only. AAS studies and growth analysis in presence of Cu ions also indicated the role of Cu NPs rather than leached out Cu^{2+} ions for the killing activity against bacteria. That there are known sequestering agents for Cu from human body adds value to a new composite which might be much less of health and environmental hazards compared to Ag NP based materials. That the iodinated composite has been found to have antagonistic activity against both Gram-positive and Gram-negative bacteria augur well for possible use as a general antimicrobial agent.

References

(1) Liau, S. Y.; Read, D. C.; Pugh, W. J.; Furr, J. R.; Russell, A. D. *Lett. Appl. Microbiol.* **1997,** 25, 279-283.

(2) Kim, J. S.; Kuk, E.; Yu, K. N.; Kim, J.-H.; Park, S. J.; Lee, H. J.; Kim, S. H.; Park, Y. K.; Park, Y. H.; Hwang, C.-Y.; Kim, Y.-K.; Lee, Y.-S.; Jeong, D. H.; Cho, M.-H. *Nanomedicine: Nanotechnology, Biology and Medicine* **2007,** *3,* 95-101.

(3) Liu, H. L.; Dai, S. A.; Fu, K. Y.; Hsu, S. H. *Int J Nanomedicine* **2010,** *5,* 1017-1028.

(4) Kaegi, R.; Voegelin, A.; Sinnet, B.; Zuleeg, S.; Hagendorfer, H.; Burkhardt, M.; Siegrist, H., *Environ. Sci. Technol.* **2011,** *45,* 3902-3908.

(5) Sharma, V. K.; Yngard, R. A.; Lin, Y. *Adv Colloid Interface Sci.* **2009,** 145, 83-96.

(6) Gu, F. X.; Karnik, R.; Wang, A. Z.; Alexis, F.; Levy-Nissenbaum, E.; Hong, S.; Langer, R. S.; Farokhzad, O. C. Nano Today **2007,** *2,* 14-21.

(7) AshaRani, P. V.; Low Kah Mun, G.; Hande, M. P.; Valiyaveettil, S. *Acs Nano* **2008,** *3,* 279-290.

(8) Sanpui, P.; Chattopadhyay, A.; Ghosh, S. S. *ACS Appl. Mater. Interfaces* **2011,** *3,* 218-228.

(9) Drake, P. L.; Hazelwood, K. J. *Ann. occup. Hyg.* **2005,** 49, 575-585.

(10) Wang, Y.; Biradar, A. V.; Wang, G.; Sharma, K. K.; Duncan, C. T.; Rangan, S.; Asefa, T. *Chem.—Eur. J.* ***2010,*** 16, 10735-10743.

(11) Ressler, T. B.; Kniep, L.; Kasatkin, I.; Schlogl, R. *Angew. Chem. Int. Ed*. **2005,** *44*, 4704-4707.

(12) Ranu, B. C.; Dey, R.; Chatterjee, T.; Ahammed, S. ChemSusChem **2012** *5*, 22-44.

(13) Pastoriza-Santos, I.; Sánchez-Iglesias, A.; Rodriguez Gonzalez, B.; Liz-Marzán, L. M. Small **2009,** *5*, 440-443.

(14) Huang, H. H.; Yan, F. Q.; Kek, Y. M.; Chew, C. H.; Xu, G. Q.; Ji, W.; Oh , P. S.; Tang, S. H. *Langmuir* **1997,** ***13***, 172- 175.

(15) Liu, Z.; Bando, Y. *Adv. Mater.* **2003,** *15*, 303- 305.

(16) Cioffi, N.; Torsi, L.; Ditaranto, N.; Tantillo, G.; Ghibelli, L.; Sabbatini, L.; Bleve-Zacheo, T.; D'Alessio, M.; Zambonin, P. G.; Traversa, E. *Chem. Mater*. **2005,** *17*, 5255-5262.

(17) Anyaogu, K. C.; Fedorov, A. V.; Neckers, D. C. *Langmuir* **2008,** *24*, 4340-4346.

(18) Wei, Y.; Chen, S.; Kowalczyk, B.; Huda, S.; Gray, T. P.; Grzybowski . B. A. *J. Phys. Chem. C* **2010,** *114*, 15612-15616.

(19) Kim Y. H.; Lee D. K.; Cha H. G.; Kim C. W.; Kang Y. C.; Kang Y. S. *J. Phys. Chem. B* **2006,** *110*, 24923-24928.

(20) Yoon, K. -Y.; Byeon, J. H.; Park, J. -H.; Hwang, J. *Sci. Total Environ.* **2007,** *373*, 572–575.

(21) Ruparelia, J. P.; Chatterjee, A. K.; Duttagupta, S. P.; Mukherji, S. *Acta Biomaterialia* **2008,** *4*,707-716.

(22) Raffi, M.; Mehrwan, S.; Bhatti, T. M.; Akhter, J. I.; Hameed, A.; Yawar, W.; Hasan, M. M. ul. *Annals of Microbiology* **2010,** *60*, 75-80.

(23) Esteban-Cubillo, A.; Pecharroman, C.; Aguilar, E.; Santaren, J.; Moya, J .S. *J. Mater. Sci.* **2006,** *41*, 5208-5212.

(24) Taner, M.; Sayar, N.; Yulug, I. G.; Suzer S. *J. Mater. Chem.* **2011,** *21*, 13150-13154.

(25) Valodkar, M.; Modi, S.; Pal, A.; Thakore, S. *Mater. Res. Bull.* **2011,** *46*, 384–389.

(26) Gaggelli, E.; Kozlowski, H.; Valensin, D.; Valensin , G .*Chem. Rev.* **2006,** *106* , 1995-2044.

(27) Cater, M. A.; Fontaine S. L.; Shield, K.; Deal, Y.; Mercer, Julian F. B. *Gastroenterology* **2006,** *130*,493-506.

(28) Gogoi, S. K.; Gopinath, P.; Paul, A.; Ramesh, A.; Ghosh, S. S.; Chattopadhyay, A. *Langmuir* **2006,** *22*, 9322-9328.

(29) Banerjee, M.; Mallick, S.; Paul, A.; Chattopadhyay, A.; Ghosh, S. S. *Langmuir* **2010,** *26*, 5901-5908.

(30) Du, W. -L.; Xu, Y. -L.; Xu, Z. -R.; Fan, C.-L. *Nanotechnology*, **2008,** *19*, 085707(5pp).

(31) Du, W. -L.; Niu ,S. -S.; Xu, Y. - L.; Xu, Z. -R.; Fan, C. -L. *Carbohydrate Polymers* **2009,** *75*, 385-389.

(32) Gottardi, W. Iodine and Iodine compounds in "*Disinfection, sterilization, and Preservation*" 4th ed., ed. Bloc, S.S., Lea and Febiger, Philadelphia, **1991,** pp.152-166.

(33) Gottardi, W. *Arch. Pharm. Med. Chem.* **1999,** *332*, 151-157.

(34) Sudarshan, N. R.; Hoover, D. G.; Knorr, D. *Food Biotechnol*. **1992,** *6*, 257-272.

(35) Helander, I. M.; Nurmiaho-Lassila, E. -L.; Ahvenainen, R.; Rhoades, J.; Roller, S. *Int. J. Food Microbiol*. **2001,** *71*, 235-244.

(36) Rabea, E. I.; Badawy, M. E. -T.; Stevens, C. V.; Smagghe, G.; Steurbaut, W. *Biomacromolecules* **2003,** *4*, 1457-1465.

(37) Sanpui , P.; Murugadoss, A.; Durgaprasad , P. V.; Ghosh, S. S.; Chattopadhyay, A. *Int. J. Food Microbiol.* **2008,** *124*, 142-146.

(38) Li, J.; McLandsborough, L. A. *Inter. J. Food Microbiol*. **2001,** *53*, 185-193.

(39) Wilson, W. W.; Wade, M. M.; Holman, S. C.; Champlin, F. R. *J. Microbiol. Meth*. **2001,** *43*, 153–164.

(40) Borkow, G.; Gabbay, *J. Curr. Med. Chem.* **2005,** *12*, 2163-275.

Chapter 4

Synthesis, characterization and enhanced bactericidal action of chitosan core shell copper-silver nanoparticle composite

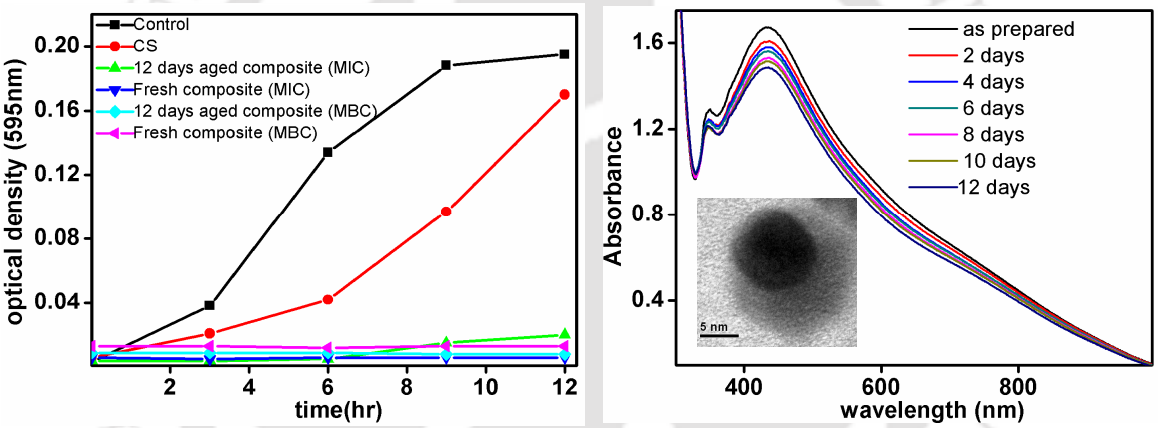

"Synthesis, characterization and enhanced bactericidal action of core-shell copper–silver nanoparticle composites. **Sadhucharan Mallick,** Siddhartha Sankar Ghosh, Arun Chattopadhyay, and Anumita Paul, ACS Appl. Mater. Interfaces, **2012/3** (manuscript to be revised and resubmitted)"

4.1: Introduction

The bactericidal properties of silver and copper are well known since ancient times. Further Ag nanoparticles (Ag NPs) and copper nanoparticles (Cu NPs) have potential bactericidal properties either individually or in composite with polymer.[1–5] In our previous studies we have prepared chitosan-Ag NP and chitosan-Cu NP composites and investigated their bactericidal activity on GFP-expressing recombinant *E. coli* and Gram-positive *B. cereus* bacteria.[1,2] The antimicrobial activity studies of chitosan-Ag NP composite in the presence of molecular iodine is described in Chapter 2 and the synthesis and enhanced bactericidal action of iodinated chitosan-Cu NP composite work described in Chapter 3 of this thesis. While chitosan (CS) is a naturally occurring biopolymer having bactericidal properties, Ag and Cu are elements with well known bactericidal properties. However, Ag and Cu are toxic to humans at doses greater than 0.1 mg/L and 1.3 mg/L in the drinking water proposed by the U.S. Environmental Protection Agency (EPA). Silver, in particular, accumulates in the human body and thus can potentially reach toxic levels from sustained environmental exposures. On the other hand Cu NPs, which are a better alternative to Ag NPs due to lower toxicity to humans, have lower stability in ambient atmospheric conditions. The presence of copper oxide on the surface of Cu NPs reduces the bactericidal activity compared to pure Cu NPs. In general oxide formation on Cu NPs can be prevented by minimizing the exposure to oxygen.

Bimetallic NPs, consisting of two different metals, offer greater advantages over their monometallic counterparts, since their optical, catalytic and biological properties can be tuned by changing the composition.[6–18] Two type of bimetallic colloids exist: alloy and core-shell. Syntheses and applications of bimetallic colloids containing either Au or Ag in combination with other noble metals have been studied extensively.[13,14] These studies show that bimetallic NPs are superior to the monometallic NPs because of their synergistic and bi functional effects. Interestingly, bimetallic core-shell NPs has been proposed as ideal surface-enhanced Raman scattering (SERS) active substrates in SERS studies. Notably, SERS has been a useful technique in biological research because it can detect small number of single molecules. Thus, core-shell NPs can further enhance

SERS signal of a molecule by electromagnetic and chemical effects in comparison to pristine NPs.[19-21] Commonly used methods of synthesis of Cu@Ag nanoparticles include: vacuum vapour deposition,[10,22] sono-chemical reduction,[23] two-step polyol reduction,[11,24] sequential ion implantation,[25] sequential ion-exchange in soda-lime glass matrix,[26, 27] electroless plating [28] and galvanic replacement reaction[9]. Langlois et al. used ultra-high vacuum technique to obtain Cu@Ag nanoparticle bimetallic nanoparticles on a substrate by sequential deposition.[22] Tsuji et al. had synthesized Cu@Ag nanoparticle using a two-step polyol reduction method under bubbling of N_2 gas.[11, 24] Anderson et al. prepared Cu coated silver nanocrystal by direct sequential implantation of Ag^+, and Cu^+ ions into silica.[25] Manikandan et. al. had prepared core-shell Cu@Ag nanocluster in soda-lime glass by sequential ion exchange and studied their optical properties when subjected to He^+ ion irradiation and vacuum annealing.[26] Sastry and co-workers had synthesized Ni@Ag nanoparticles which were stable in aqueous suspensions as well as in powdered form.[28] Their synthesized Ni NPs were coated with a silver shell in view of the extra stability and the enhanced manipulative ability afforded by the silver nanocoating.

We have recently reported CS supported Cu NPs synthesis using hydrazine hydrate as a reducing agent described in chapter 3A.[2] In our work here, Cu NPs on CS were prepared in a similar fashion and used as seed particles over which Ag^+ ions were reduced by transmetalation reaction to generate the Cu core-Ag shell NPs, denoted as Cu@Ag NPs. The CS Cu@Ag NP composite so obtained was stable for several weeks since the silver shell prevented air oxidation of the core copper metal Similar studies of bimetallic Cu@Ag NPs report improved resistance of copper to oxidation as compared to pristine Cu NPs.[29−32] Core-shell nanoparticles have been used for catalytic, optical and magnetic applications. In catalytic reactions, the association of two different metals offers superior activity, increased stability and better selectivity.[33−35] Bimetallic Cu-Ag NPs have been reported to exhibit superior catalytic activity over pure noble metal copper and silver NPs of comparable sizes.[36] In magnetic properties, core-shell nanostructures have been developed to obtain NPs with individual improved magnetic property by reducing the direct interaction between the nanoparticles. For example, bimagnetic core-shell nanoparticles of $FePt/MFe_2O_4$(M=Fe,Co) and $Fe_{58}Pt_{42}/Fe_3O_4$ are

nano-structured magnetic materials with tunable magnetic properties, achieved by varying the chemical composition and thickness of the coating materials.[37,38] Magnetic properties of the core-shell NPs are dependent on shell thickness due to the exchange coupling between core and shell.[37]

Enhanced antibacterial activity of core-shell nanostructures has also been reported.[39 – 43] Bactericidal core-shell NPs consisting of silver shell supported on organic and inorganic cores have been studied. However the bactericidal efficacy of core-shell NPs consisting of Ag shell and Cu as core has not been studied, despite the fact that Cu has well known antibacterial as well as antifungal properties.[2] Moreover, Cu is toxic to microorganisms but non-toxic to human, because sequestering of Cu ensures their proper excretion from the body.[44,45] Silver NPs on the other hand has effective bactericidal properties because both Ag ions and Ag NPs have excellent biocidal ability.[1,3– 5,46,47] Recently, several groups have reported that Cu-Ag alloy nanoparticles display superior bactericidal activity against *E. coli* as compared to pure Ag NPs.[48,49] One of the ways of reducing the effects of toxicity of Ag NPs to humans is by replacing the core of the Ag NPs by a non-toxic, yet disinfectant metal, such as copper. We report here a simple two-step, seed-mediated route to prepare core shell CS Cu@Ag NPs with enhanced bactericidal properties compared to pristine Cu NPs & Ag NPs. The resulting CS Cu@Ag NPs composite was found to be stable for several weeks and was able to significantly retard bacterial growth at very low silver concentrations.

4.2: Outline of the research work

I. We have developed a simple two-step seed-mediated route to synthesize chitosan (CS) supported core-shell nanoparticles (NPs) in aqueous solution.

II. This is the first time a composite of core-shell Cu@Ag nanoparticles in chitosan (CS Cu@Ag NPs) has been synthesized. A simple transmetallation reaction between Cu NPs in chitosan matrix and Ag^+ ions was used to prepare the CS Cu@Ag NPs composite.

III. UV-visible spectroscopy, TEM, FESEM, XRD, XPS instrument were used to characterize the CS Cu@Ag core-shell nanocomposites.

IV. Our synthesized CS Cu@Ag NPs composites were stable in solution for more than two weeks under ambient atmospheric conditions. This enhanced stability allowed us to study its antibacterial property in aqueous solution.

V. Gram-negative bacteria green fluorescent protein expression recombinant *E. coli* and Gram-positive bacteria *B. cereus* were used were used to study the details of bactericidal activities of the CS Cu@Ag NPs composite.

VI. Electron microscopic, zeta potential measurements, flow cytometric and XPS studies revealed that the Cu@Ag NPs in the composite readily attached to the bacterial cell wall through electrostatic and possible chemical interactions causing irreversible damage to the membrane and eventually leading to cell death.

4.3: Experimental section

4.3.1: Materials and methods

Copper (ll) sulphate pentahydrate ($CuSO_4.5H_2O$; Merck, India), silver nitrate ($AgNO_3$, 99.5%; Merck), chitosan of high molecular weight (75% deacetylated; Sigma-Aldrich Chemical Co.), sodium hydroxide (NaOH, 98%; Merck, India), hydrazine hydrate (80% solution, Merck, India), acetic acid (glacial, 99–100%; Merck, India) were used as received without further purification. Milli-Q grade (resistivity 18.2 $M\Omega cm^{-1}$) water was used in all experiments. Luria-Bertani (LB) broth and nutrient broth (NB) were purchased from HiMedia, Mumbai, India. Agarose for gel electrophoresis was obtained from Sigma-Aldrich Chemical Pvt. Ltd., Kolkata, India. GFP-expressing recombinant *E. coli* were grown in LB broth at $37^{\circ}C$ and at 220 rpm for 12 h; whereas *B. cereus* were grown in NB at $37^{\circ}C$ and at 220 rpm for 12 h.

4.3.2: Core-shell CS Cu@Ag nanoparticle composite preparation

Seed-mediated growth method was employed to prepare CS Cu@Ag NPs. The Cu NP seeds were synthesized by a recently established method wherein the Cu NP were synthesized by reduction of $CuSO_4$ with hydrazine hydrate in the presence of CS as stabilizer.[2] To this freshly prepared 30 ml Cu NP seed dispersion, 0.6 mL of 0.02 M $AgNO_3$–solution was injected at room temperature and stirred for 12 h. The obtained orange–reddish solution was centrifuged at 20,000 rpm and the pellet was washed with milli-Q grade water and re-dispersed in 30 mL of 0.25% aqueous acetic acid solution. The pH of the solution was adjusted to 6.3 prior to bactericidal activity studies.

4.3.3: Characterization of core-shell CS Cu@Ag NPs composite

4.3.3.1: UV-Vis spectroscopic measurements

UV-Visible spectra of the CS Cu@Ag NPs dispersion and Cu NPs seed particles, mixture of CS-Cu NPs and CS-Ag NPs were measured using a Hitachi U 2900 spectrophotometer. The bacterial growth was monitored by measuring optical density (OD) at 595 nm using a UV-visible spectrophotometer (Lambda 25; Perkin-Elmer, Fremont, CA, USA) of the sample at different times

4.3.3.2: Transmission electron microscopy (TEM) analysis

For TEM investigations, 5 μL of each sample was drop coated onto a carbon coated copper TEM grid (300 mesh) followed by air drying. The drop coated grid was then analyzed under TEM at a maximum acceleration voltage of 200 kV. High resolution transmission electron microscopic analysis was performed using the same equipment. The interactions of the CS Cu@Ag NPs composite with bacterial cells were also examined using a high resolution transmission electron microscope operating at a maximum accelerating voltage of 80 KeV. For this, CS Cu@Ag NPs composite treated on *E. coli* samples were drop coated onto the TEM grid followed by air drying and the resulting grid was then analyzed under TEM and energy-dispersive X-ray (EDX)

analysis also carried out on composite treated samples at operating accelerating voltage 200 kV.

4.3.3.3: Scanning electron microscopic analysis

Scanning electron microscopy coupled with EDX and Field emission scanning electron microscopy coupled with EDX instruments were used for the study of surface morphology and elemental analysis for CS Cu@Ag NPs composite and composite treated on *E. coli* samples. Typically, 20 µL drop of each sample was deposited on a glass slide, dried and sputter-coated with gold film using a sputter coater and analyzed under the SEM and FESEM. The FESEM-EDX analysis of CS Cu@Ag NPs composite treated on *E. coli* samples was carried out on small area of the sample for the elemental analysis of the composite.

4.3.3.4: Powder XRD studies

We performed X-ray diffraction measurements to characterize the CS Cu@Ag NPs composite. We also studied and fate of the CS Cu@Ag NPs composite during antibacterial studies using XRD measurement. Firstly, vacuum dried composites were spread on glass microslides and XRD was recorded using Philips Diffrctometer (Model 1715) with Cu Kα1 radiation (λ= 1.54060 Å), operating at 55 kV and 250 mA. In order to confirm the presence of core-shell Cu@Ag NPs on the bacterial cell walls, again bacteria treated with CS Cu@Ag NPs composite for 12 h was centrifuged at 6000 rpm and vacuum dried and stored under vacuum before analysis. The dried cell pellet spread on a glass slide and XRD was recorded.

4.3.3.5: X-ray photoelectron spectra (XPS) analysis

We have performed XPS measurements to characterize the core-shell structure of the CS Cu@Ag NPs composites. The powdered CS Cu@Ag NP composite was pressed and made into pellets and placed in an ultra high vacuum chamber at 1×10^{-10} Torr for chemical analysis. XPS spectra were recorded on a PHI 5000 Versa Probe II (ULVAC-PHI, INC, Japan) equipment employing Al Ka X-rays (hν = 1486.6 eV). Charge

neutralization was used for each measurement using a combination of low energy Ar^+ ions and electrons. The binding energy (eV) was corrected with the C1s (284.6 eV) as standard. Elemental compositions were determined from the spectra acquired at pass energy of 187.85 eV. High-resolution spectra were obtained with analyzer pass energy of 58.70 eV with a step of 0.125 eV and 50 ms time per step.

4.3.3.6: Atomic absorption spectrometry (AAS)

Quantitative analysis of the concentration of Cu and Ag present in CS Cu@Ag NPs composite was measured by using atomic absorption spectrophotometer (Model: AA240 Varian Inc) after dissolving the composite in dilute HCl solution. The supernatant solution obtained after centrifugation of the composites was also measured to determine concentration of Cu and Ag ions present in determining how much was being discarded during our synthesis.

4.3.3.7: Zeta potential (ζ)

Zeta potential *(ζ)* measurements were performed to determine the charge of CS Cu@Ag NPs composite in aqueous solution at pH 6.3. Zeta potential *(ζ)* was measured using Delsa™ Nano Submicron Particle Size and Zeta Potential Particle Analyzer.

4.3.3.8: Fourier Transform Infrared (FTIR) Spectroscopy

FT-IR spectra were recorded on a Perkin-Elmer-Spectrum One spectrometer with KBr disks in the range 4000-450 cm^{-1} for structural analysis of solid CS and solid CS Cu@Ag NPs composite. Both the CS and CS Cu@Ag NPs powders were mixed with KBr in order to make pellets for FTIR studies.

4.3.3.9: Bactericidal studies

For bactericidal activity, *B. cereus* was chosen as the Gram-positive bacteria and GFP-expressing *E. coli* as the Gram-negative bacteria. GFP-expressing *E. coli* was cultured in LB ampicillin media and *B. cereus* in NB media. Different concentrations of

CS Cu@Ag NPs composite were used to determine the minimum inhibitory concentration (MIC) and minimum bactericidal concentration (MBC) at pH 6.3. Bacteria (10^8 cfu/ml) were grown in media in the presence of different concentrations of CS Cu@Ag NPs composite for 12 h at 37^0C. The lowest concentration of composite at which there was no visual turbidity was taken as the MIC value of the composite. Further, the cultures which lacked visual turbidity were reinoculated in fresh media. The lowest concentration of the composite that killed at least 99.9% of original inoculums was taken as MBC. The experiments were performed at least in triplicate to ensure reproducibility. The bacterial growth was monitored by measuring optical density (OD) at 595 nm using a UV-Visible spectrophotometer of the sample at different times.

4.3.3.10: Flow cytometric analysis for bacterial cell viability using GFP-propidium iodide combination

GFP-expressing recombinant bacterial cells viability and disruption of membrane integrity was measured using propidium iodide (PI), which enters only permeable cells, binds DNA, and fluoresces at 620 nm when stimulated by a laser at 488 nm. In intact cells, PI remains in the medium and does not fluoresce; in compromised cells, PI enters the cell through disrupted membrane and binds to DNA exhibiting fluorescence[1, 2]. Briefly, several tubes containing 500 µL (10^8 cells/mL) of the recombinant *E. coli* cells and 250 µL of the CS Cu@Ag NPs composite (at MIC, i.e. 63.4 µg/mL consisting 3.03 µg/mL of Cu and 1.47 µg/mL of Ag) in addition to 500 µL (10^8 cells/mL) of the recombinant *E. coli* cells and 375 µL of the composite (at MBC, i.e. 92.99 µg/mL consisting 4.44 µg/mL of Cu and 2.13 µg/mL of Ag) were incubated at 25°C for various time periods (2 h, 4 h, 6 h). After incubation, 1.5 µL of 0.2 mM PI was mixed into each tube and diluted with 150 mM NaCl. Samples were analyzed by a flow cytometer. Samples were illuminated with a 15 mW argon ion laser (488 nm), and the fluorescence detected through standard filter configuration of 525±10 nm (green) and 620±10 nm (red) band pass filters. Signals were amplified in the logarithmic mode for side scattered light (SSC), forward scatter*ed* light (FSC) and fluorescence. In dot plots of fluorescence different cell populations i.e. live, compromised, dead and lysed were gated, based on the different viability stages of the cells.

4.3.3.11: DNA isolation and agarose gel electrophoresis analysis

Recombinant GFP plasmid (pGFP) isolated from control and CS Cu@Ag NPs treated *E. coli* cells by an alkaline lysis method and analyzed by agarose gel electrophoresis followed by visualization of EtBr stained DNA under UV- transilluminator.

4.4: Results and discussion

4.4.1: Synthesis and characterization of CS Cu@Ag nanoparticle composite

Synthesis of CS-Cu NPs seed particles were carried out under normal atmospheric condition in the presence of hydrazine hydrate reducing agent by our established method.[2] The reddish solid CS-Cu NPs prepared by the reduction of alkaline $CuSO_4$ in presence of CS was separated from the reaction mixture and re-dispersed in water in the presence of acetic acid. The resulting solution showed a prominent UV-Vis peak at 583 nm, indicating the formation of Cu NPs which was further confirmed by TEM (Appendix, Figure A. 4.1).[2] When $AgNO_3$-solution was added to the reddish CS-Cu NPs dispersion, the colour changed to orange-red possibly due to the formation of CS Cu@Ag NPs composite. The orange-red dispersion of CS Cu@Ag NPs composite was centrifuged and the pellet re dispersed in 30 mL of milli-Q water. The resulting orange-red solution was found to strongly absorb at 417 nm (Figure 4.1) which is attributed to the SPR band of Ag NPs. This solution was subjected to further characterizations and also employed for bactericidal studies. In this reaction silver ions were reduced to Ag (0) by the Cu (0) atoms on the surface of Cu NPs. In other words, a galvanic replacement reaction of Cu atoms by Ag atoms on the surface of the Cu NPs, led to the formation of silver shell on the copper core.[8]

The CS Cu@Ag NPs composite showed a single broad peak at 415-450 nm. When CS stabilized Cu NPs and CS stabilized Ag NPs were prepared independently and then UV-Vis spectrum recorded of a mixed solution, two distinct plasmon resonance bands were observed; one at 599 nm for Cu NPs and another at 405 nm for Ag NPs, as shown in Figure 4.1. On the other hand, it is reported that the SPR band for the alloy NPs appear

between the SPR band for pure Cu NPs (560-600 nm) and the SPR band for pure Ag NPs (390-420 nm), with the peak position of the SPR band shifting to longer wavelengths with increasing copper percentage.[48,49,50] Thus the present composite, which showed a peak at 417 nm, neither consisted of Cu-Ag alloy NPs nor consisted of a mixture of Ag NPs and Cu NPs. The band at ~ 417 nm corresponds to SPR of Ag NPs. Further there was no plasmon resonance band observed due to Cu NPs. Based on the above set of observations, it is likely that our composite contained Cu@Ag NPs with Ag as the shell.

That the SPR band for a core metal is dampened in presence of a shell metal is well documented. [25,26,27] In case of Cu@Ag NP also, several studies reported the dampening of the plasmon resonance of inner Cu core by the outer Ag shell with thickness greater than 5-7 nm.[26,27] The optical results in Figure 4.1 suggested that the NPs formed in the orange-red composite are of bimetallic core-shell structure i.e. Cu@Ag NPs, and not a mixture of Cu NPs and Ag NPs nor those of Cu-Ag alloy NPs.

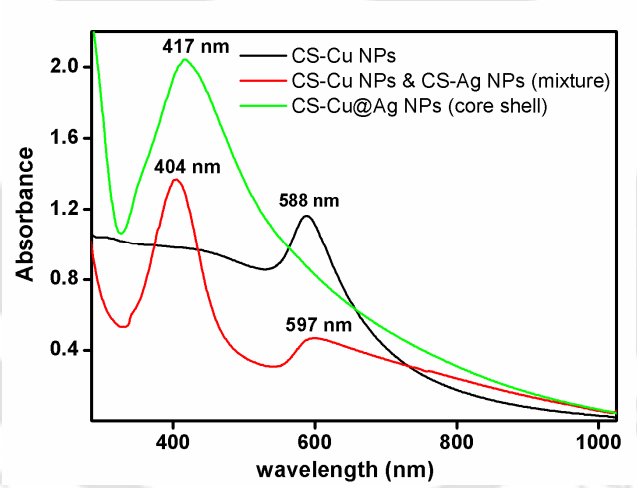

Figure 4.1: UV-Visible spectra of core shell CS Cu@Ag NPs dispersion and comparison spectra of CS-Cu NPs seed particles, mixture of CS-Cu NPs and CS-Ag NPs.

Formation of CS Cu@Ag NPs was further confirmed by TEM studies. As shown in Figure 4.2a particulates with an average size of 14.0±3.4 nm were observed. Closer inspection of the TEM image shows that most of the particles have a darker central part (core) and lighter outer part (shell).The average shell thickness is ~ 5.8 nm while the core diameter is ~ 9.5 nm. HRTEM image of a single particle (Figure 4.2b) as well as selected area electron diffraction (SAED) pattern (Figure 4.2c) of the particle clearly

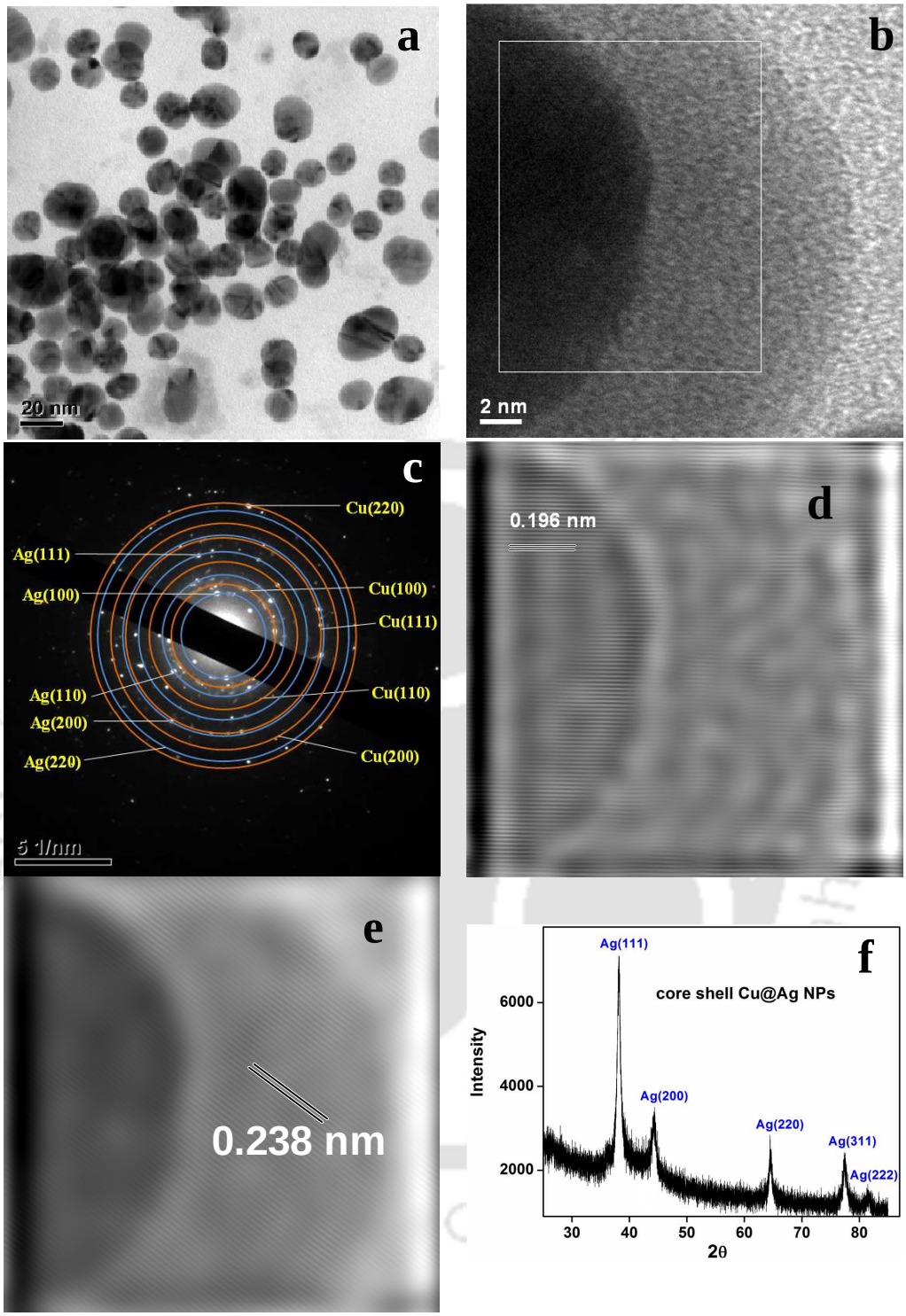

Figure 4.2.(a, b) TEM, HRTEM micrograph of CS Cu@Ag nanoparticles and (c) corresponding SAED.(d, e) Inverse Fourier transform of selected region in b showing the lattice fringes corresponding to the (111) planes of copper and (111) planes of silver. (f) Powder XRD pattern of CS Cu@Ag NPs composite.

indicated crystalline nature of the Cu@Ag NPs. In particular, the HRTEM image in Figure 4.2b showed the presence of lattice fringes which were enhanced by inverse fast Fourier Transform analysis (IFFT) and are shown in Figures 4.2d and 4.2e. A lattice fringe spacing of 0.196 nm for the core metal and 0.238 nm for the outer shell metal was clearly visible in the IFFT image of Figure 4.2d and 4.2e. The lattice spacing of 0.196 nm corresponds to Cu (111) plane[2], while that of 0.238 nm corresponds to Ag (111) plane [1,51]. These observations indicated that the dark central part is due to metallic Cu and lighter outer part is due to metallic Ag. Similar conclusions can be drawn from detailed analysis of the SAED pattern shown in Figure 4.2c, where the diffraction rings were indexed. The indices are shown in Table 4.1. Our observations in Figure 4.2 supported the presence of Cu@Ag NPs in the CS polymer. The presence of CS in the composite was confirmed by FTIR studies (refer to Appendix, Figure A. 4.2).

Table: 4.1. Lattice plane spacings (d-spacings) calculated from the SAED shown in Figure 4. 2c compared with theoretical values.

Lattice Planes	Experimental	Theoretical
Ag(100)	3.90Å	4.08Å
Ag(110)	2.96Å	2.88Å
Ag(111)	2.21Å	2.35Å
Ag(200)	1.99Å	2.04Å
Ag(220)	1.47Å	1.44Å
Cu(100)	3.67Å	3.61Å
Cu(110)	2.48Å	2.55Å
Cu(111)	2.06Å	2.08Å
Cu(200)	1.77Å	1.80Å
Cu(220)	1.36Å	1.27Å

Core-shell structure of the bimetallic Cu@Ag NPs in the chitosan composite was further investigated by powder XRD. XRD pattern of a typical sample of CS-Cu@Ag NP composite recorded after 24 h of synthesis is shown in Figure 4.2f. The diffraction peaks at 2θ = 38.16°, 44.3°, 64.6°, 77.41°, and 81.4° are due to reflections from (111), (200), (220), (331), (222) planes of metallic Ag (JCPDS-04-0783), which adopts a face-centred-cubic lattice structure. It is noteworthy that the XRD pattern in Figure 4.2f lack peaks due to the pure Cu, indicating that Cu is well shielded by the Ag shell in the CS-Cu@Ag NP composite. In most metallic core-shell NPs systems, the XRD peaks from the core metal are not observed due to the core metal being in kinematic diffraction state.[23, 26, 31] For example, Fe@Ag and Co@Ag NPs show XRD diffraction only due to the shell Ag.[51,52] In the present case too, similar phenomenon may be occurring. In short, when Ag is deposited onto the Cu NP surface, at low coverage growth is epitaxial. But as thickness of Ag shell increases, the lattice mismatch parameter between Cu and Ag generates large strain. The system releases the strain by breaking up the perfect Cu lattice into imperfect Cu lattice resulting in an incoherent interface between Cu core and Ag shell. This incoherent interface leaves the Ag shell in a dynamical diffraction state and the Cu core in a kinematic diffraction state.[31] The latter effect broadens the XRD peaks of the core Cu NPs which are not visible in contrast to the sharp XRD peaks that originate from the Ag shell. This is observed in Figure 4.2f (Appendix, Figure A. 4.3a) i.e. XRD peaks due to Ag are distinct while those due to Cu are absent. Before silver coating the diffractogram of the CS-Cu NPs sample showed distinct peaks at 2θ values of 43.42°, 50.46° and 74.17^{o} which were indexed due to diffraction from (111), (200), and (220) respectively from the planes of Cu (0) (Figure A. 4.3b). These CS-Cu NPs were used as seed particles for synthesis of core-shell CS Cu@Ag NPs composite. UV-Visible, XRD and TEM recorded on aged CS Cu@Ag NPs showed that the samples were stable in solution for more than two weeks under ambient conditions (Figure A. 4.4 (a-e)). This is to be contrasted with the lower stability of CS-Cu NPs samples (typically 12 hours) reported in our earlier studies.

Further, EDX analysis carried out during FESEM (Figure 4.3a, 4.3b) indicate the presence of both the elements Cu and Ag, consistent with the core shell structure of the CS Cu@Ag NPs composite.

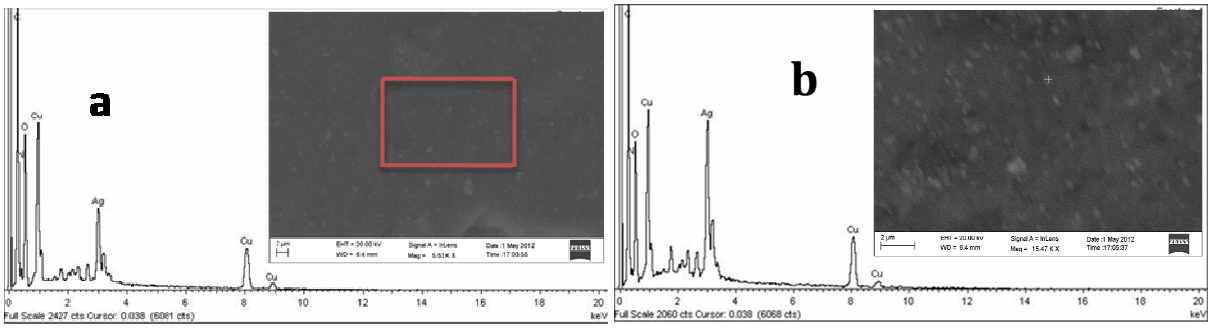

Element	Weight%	Atomic%
C K	27.52	56.56
N K	3.24	5.71
O K	13.41	20.69
Cu K	26.72	10.38
Ag L	29.11	6.66
Totals	100.00	

c

Figure 4.3: (a) EDX spectra of CS Cu@Ag nanoparticles composite, small areas used for analysis. (b) Spot EDX spectra, focus on a single Cu@Ag nanoparticle during FESEM analysis, shows presence of elemental copper & silver, inset shows corresponding FESEM image. (c) Spot EDX result, (spot size 35 nm) given in tabular form.

Chemical composition near the surface of the CS Cu@Ag NP composite was examined by XPS, where the wide energy scan revealed the presence of elemental Ag, Cu, O, N, and C in the sample (Appendix Figure A. 4.5). The corresponding high-resolution XPS spectrum for Cu and Ag element is shown in Figures 4.4a and 4.4c respectively. The binding energy for Cu $2p_{3/2}$ and Cu $2p_{1/2}$ showed two peaks at 932.4 eV and 952.2 eV associated with Cu(0) electrons. In addition, well known shake-up satellite peaks appeared at 939 eV and 942 eV in Cu 2p spectra, indicating the presence of CuOx species (Figure 4. 4a**)**.[48,53] This slight CuO formation on the surface regions of CS-Cu@Ag NPs sample indicated that at least some Cu NPs are not sufficiently covered by the Ag shell, making them prone to aerial oxidation.

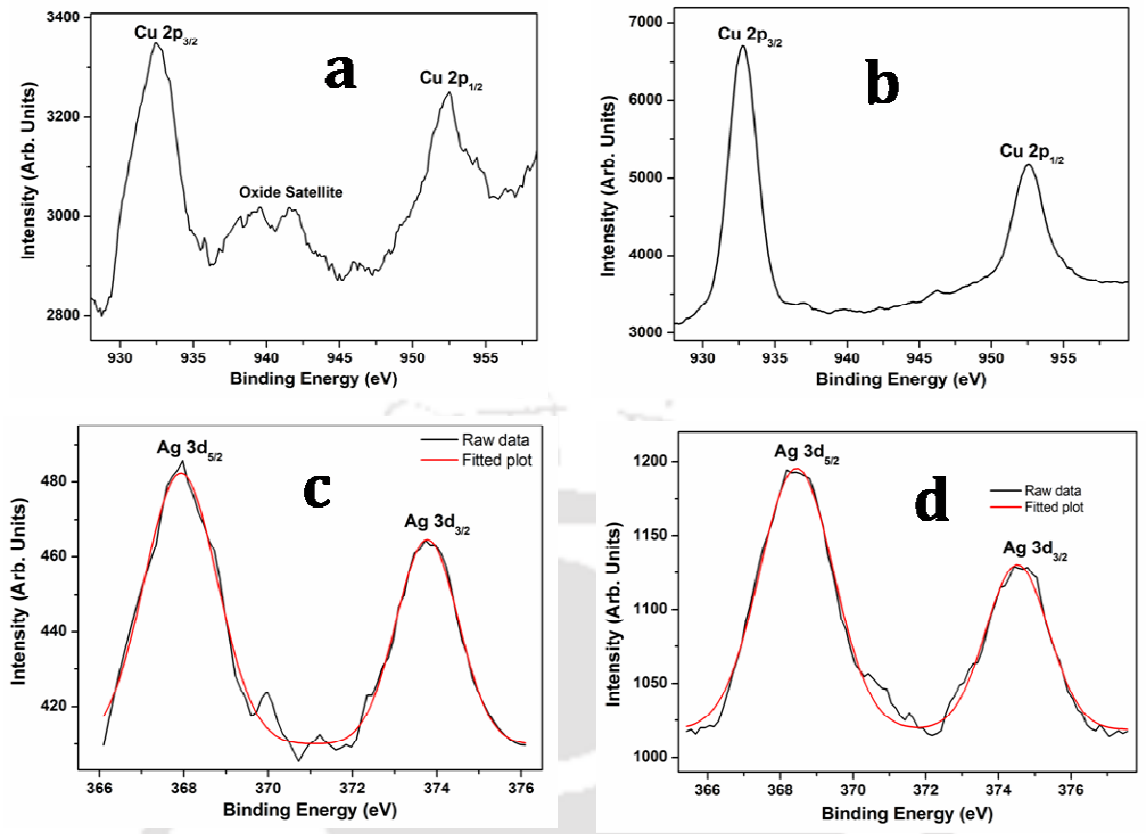

Figure 4.4: High resolution XPS spectra of Cu 2p region of the CS Cu@Ag NP composite (a) before sputtering and (b) after sputtering ~ 10 nm depth. High resolution XPS spectra of Ag 3d region of the CS Cu@Ag NP composite (c) before sputtering and (d) after sputtering ~ 10 nm depth).

In order to better understand the CS Cu@Ag NP composite structure, XPS depth profile studies were performed by bombarding a small area of the specimen surface with 3 KeV Ar^+ ions and analyzing the freshly exposed surface after ~2 minute bombardment (i.e.~10 nm depth). The high-resolution XPS spectra, before and after sputtering, for Ag 3d, is shown in Figure 4.4(c, d**).** The binding energy for Ag $3d_{5/2}$ and Ag $3d_{3/2}$ electrons in Figure 4.4(c, d) fitted by Gaussian-Lorentzian cross curves, shows two peaks at 368.3 eV and 374.3 eV, which are associated with Ag(0).[31,48,54,55] Similarly, Cu 2p signals of the sputtered sample shows two peaks at 932.4 eV and 952.2 eV corresponding to the binding energy for Cu $2p_{3/2}$ and Cu $2p_{1/2}$ (Figure 4. 4b**)**, which is similar to the reference Cu(0).[54,55] Enhancement of Cu 2p signals for a sputtered surface (Appendix, Figure A. 4.6) indicates the presence of metallic Cu in the core of the sample. Also the fact that no separate satellite peaks corresponding to CuO were observed at ~10 nm depth profiled

samples of CS Cu@Ag NP, confirmed that the oxide layer formed only on the surface of the core shell Cu@Ag NPs in the chitosan matrix. Further, as TEM results showed an average Ag shell thickness of ~ 5.8 nm, this combined with the XPS results of before and after sputtered samples (~10 nm) support the core shell structure of the CS Cu@Ag NP composite, with the core being richer in Cu(0) and the shell being richer in Ag(0). The aerial stability of the core shell NPs in the composite is probably due to the protection of the Cu core by the Ag shell.

4.4.2: Antibacterial studies of CS Cu@Ag nanoparticle composite

The bactericidal activity of the CS Cu@Ag NPs was determined on Gram-negative green fluorescent expressing *E. coli* bacteria and Gram-positive *B. cereus* bacteria by turbidity tests. In order to determine the MIC and MBC, 10^8 cfu/mL each of GFP-expressing *E. coli* and *B. cereus* was separately inoculated into Luria-Bertani (LB) medium and NB medium respectively, supplemented with various concentrations of CS Cu@Ag NPs and left to grow overnight at 37°C. Control experiments were performed with acetic acid only .The antibacterial activity of the CS Cu@Ag NPs composite (at MIC and MBC) was monitored by measuring the optical density (O.D) at 595 nm at various times (Figure 4.5). For comparison, the antibacterial activities of chitosan and Ag NPs towards the recombinant GFP-expressing *E. coli* were also measured.

The MIC of the CS Cu@Ag NPs composite against recombinant GFP-expressing *E. coli* was found to be 63.4 μg/mL, consisting of 3.03 μg/mL of Cu and 1.47 μg/mL of Ag. The corresponding MBC (92.99 μg/mL) contained 4.44 μg/mL of Cu and 2.13 μg/mL of Ag.

It may be noted that quantitative analysis of the amount of Cu and Ag metal present was determined by using AAS. The difference in the amount of Cu^{2+} and Ag^{+} ions in the initial feed solution to their amounts being discarded in supernatant solution allowed indirect estimation of the Cu^{+2} ions and Ag^{+} ions taken up by the CS Cu@Ag NPs composite. Further, the composite pellet was dissolved in HCl solution and then

subjected to AAS analysis directly. The amount of Cu and Ag content in the composite so measured by the two methods are same within the experimental error.

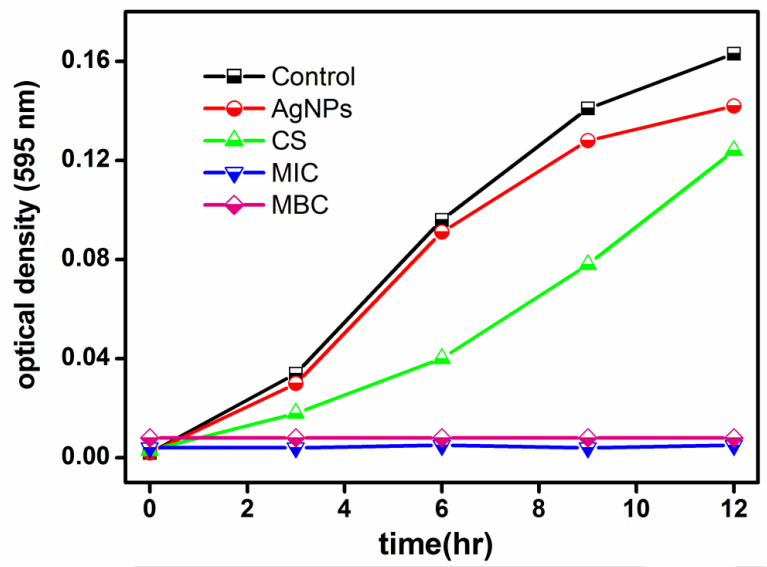

Figure 4.5: Effect of different concentration of CS Cu@Ag NPs composite and Ag NPs (~20 nm) on the growth of GFP-expressing recombinant *E. coli*. (as also indicated in the legends). **Control**: 0.02 M acetic acid only in LB media; **MIC**: CS Cu@Ag NPs composite at 63.4 µg/mL; **MBC**: CS Cu@Ag NP composite at 92.99 µg/mL; **CS**: Chitosan at 58.9 µg/mL, and **Ag NPs**: Ag NPs at 1.47 µg/mL.

The MIC of the CS Cu@Ag NPs composite against *B. cereus* was found to be 75.46 µg/mL, consisting of 3.60 µg/mL of Cu and 1.75 µg/mL of Ag. The corresponding MBC (98.74 µg/mL) contained 4.71 µg/mL of Cu and 2.28 µg/mL of Ag. Control samples with 0.02 M acetic acid only in LB media showed no growth inhibition (Figure 4.5). Also, the antibacterial activity of citrate stabilized-Ag NPs at Ag concentrations corresponding to MIC concentration of CS Cu@Ag NPs is similar to that of control (Figure 4.5). Thus, at this low concentration (1.47 µg/mL), Ag was ineffective in inhibiting bacterial growth. It must be noted that similar control studies with pristine Cu NPs are not reported as they readily oxidized in aerial conditions. And this low concentration CS-Cu NPs corresponding to MIC concentration of CS Cu@Ag NPs is not effective in bacterial growth inhibition.[2] Clearly the CS Cu@Ag NPs composite exhibited superior

antibacterial activity at this low Ag concentration. Such enhanced activity of composite materials as against the parent components are well documented in the literature and attributed due to a combination of strain and ligand effects.[56–61]

Bacterial cell viability assay of the CS Cu@Ag NP composite on GFP-expressing *E. coli* was investigated using flow cytometry. In general, flow cytometric investigations of bacterial cell viability in response to an antibacterial agent typically brings out the existence of four different cell populations, i.e. specifically living, compromised, dead and lysed. In this method, it is generally accepted that bacterial permeability to nucleic acid staining dye, such as propidium iodide (PI), is associated with the occurrence of significant damage to the membrane, indicating alteration of the cell membrane potential, which finally leads to cell death. Thus when the cell is intact, and not affected by the staining agent, only green fluorescence from the GFP of the recombinant bacteria is observed, as PI which remains in the medium, does not fluoresce. On the other hand, when the cells are compromised and membrane porosity is developed, PI is able to enter the cell and bind to DNA showing red fluorescence in addition to green fluorescence. However, when the cells are dead, the GFP leaks out of the cell and thus only red fluorescence is visible. Finally, lysed cells do not show any kind of fluorescence. Thus changes of fluorescence intensity and colour could reveal the population of different cells leading to a better understanding of the working of the antibacterial agent.

In the present study, *E. coli* treated with MIC (63.4 μg/mL) and MBC (92.99 μg/mL) of CS Cu@Ag NPs composite were incubated for different time periods, i.e. 2 h, 4 h and 6 h. It was found that the intensity of green fluorescence (GFP) and red fluorescence (PI) of the tested cells changed as a function of increasing composite concentration and incubation time. A gradual shift in the population from viable to compromised cell was observed shown in Figure 4.6 and Table 4.2. Interestingly, after 2 h of treatment at MIC dose 69.74% of the total cell was living and healthy while in MBC dose after 2 h of treatment only 0.63% cell was healthy.

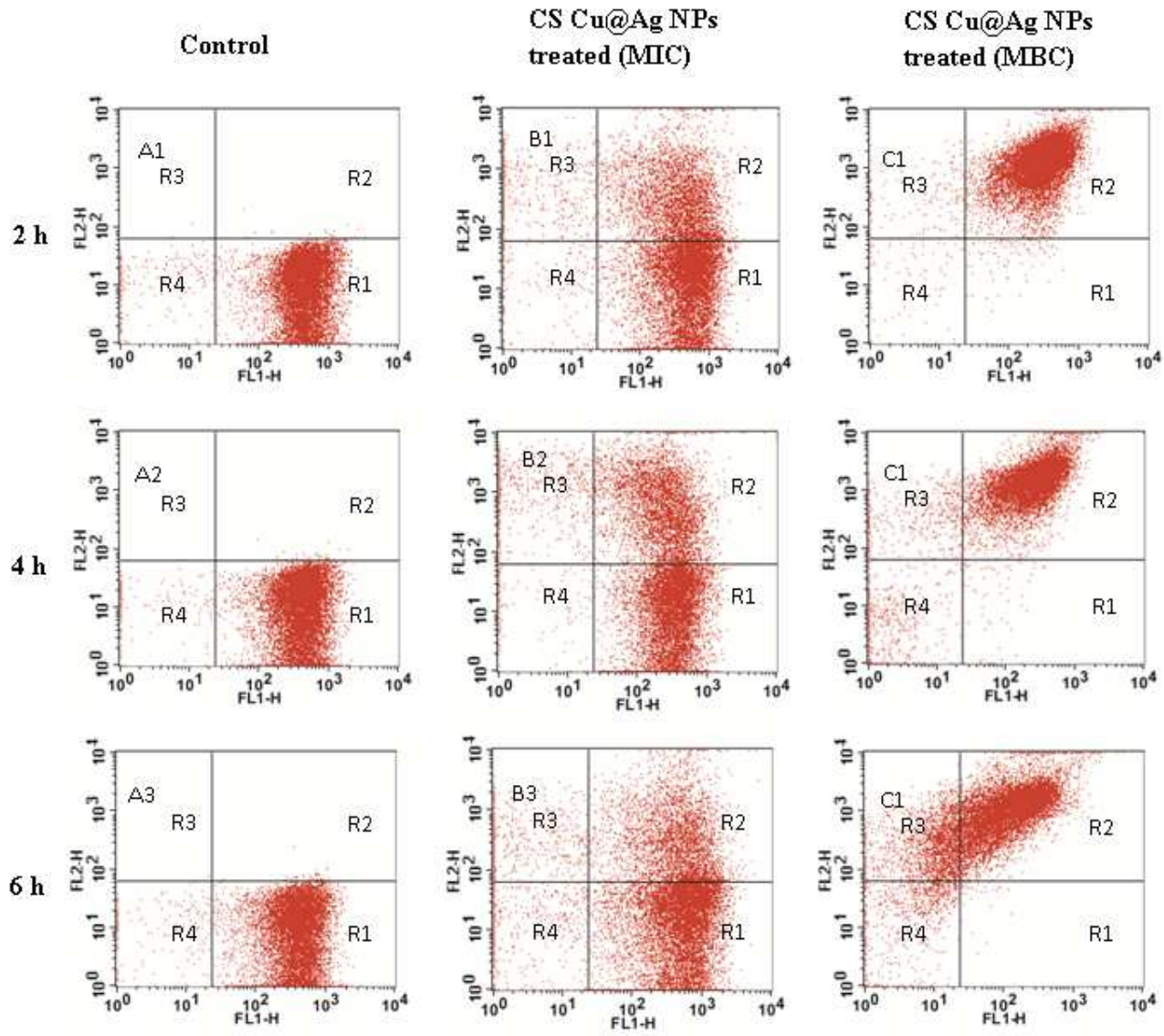

Figure 4.6. Dot plots showing populations of *E. coli* cells (GFP expressing stained with PI) at different viability stages, measured by flow cytometry at different time points and with varying concentration of the CS Cu@Ag NPs composite. Series A refers to untreated cells and series B and C refer to cells treated with MIC(63.4 µg/mL) and MBC(92.99 µg/mL) of the CS Cu@Ag NPs composite in the treated samples and 1, 2, and 3 refers to samples at 2, 4, and 6h respectively. Different viability stages are denoted as R1 (live), R2 (compromised), R3 (dead), and R4 (lysed).

However, with the progression of time the population of compromised cells gradually increased and reached ~33% of the total cell population within 6 h at MIC dose, while for MBC this population decreased to 77.48%. Parallel to this, the untreated group of bacteria (control) exhibited less number of compromised and dead cells. These results

are tabulated in Table 4.2. The results in Figure 4.6 and Table 4.2 suggested that the CS Cu@Ag NPs composite caused irreparable damage to the bacterial cell membrane, and within 2 h following treatment with either 63.4 μg/mL or 92.99 μg/mL of CS Cu@Ag NPs composite.

Table: 4.2. Percentage of *E. coli* cells at various concentration of the CS Cu@Ag NP composite and at different time points as measured by flow cytometry

		Control (%)	Treated-1(%)	Treated-11(%)
Amount of Component/Time	**CS Cu@Ag NP/ Viability stage**	0.00	63.4 μg/mL	92.99 μg/mL
2hour	Live (LR) Compromised(UR) Dead(UL) Lysed(LL)	98.10 0.18 0.02 1.70	69.74 25.46 3.61 1.19	0. 63 97.59 1.13 0.65
4hour	Live(LR) Compromised(UR) Dead(UL) Lysed(LL)	98.57 0. 38 0.01 1.04	65. 63 29.45 3.71 1.21	0.42 93.09 2.85 3.64
6hour	Live(LR) Compromised(UR) Dead(UL) lysed(LL)	98.12 0.43 0.02 1.43	59.31 33.09 4.63 2.97	0.23 77.48 16.94 5.35

Interaction of the CS Cu@Ag NPs composite with bacterial cells was further studied by TEM and FESEM. FESEM images of both the untreated and the composite treated GFP recombinant *E. coli* is shown in Figure 4.7a and 4.7b. For sample preparation, the CS Cu@Ag NP composite treated bacteria were kept in the medium with the concentration of the composite at MIC (i.e. 63.4 μg/mL) for 3 h prior to evaporation. It is interesting to observe from Figures 4.7a and 4.7b that while the untreated bacterium was healthy, and of usual surface morphology, the one being treated, had opaque cell wall densely covered with particles which could be the CS Cu@Ag NPs composite

(Figure 4.7b). TEM investigations of the CS Cu@Ag NP composite treated bacteria further confirmed the attachment of the composite to the surface of the cell wall. For example, TEM images in Figure 4.8 (a, b and c) shows dark spots of Cu@Ag NPs along with chitosan overlying on the surface of a bacterium. Further, EDX analysis carried out during TEM, (Figure 4.8d) SEM (Figure 4.8e) and FESEM (Figure 4.7a, 4.7b) indicate the presence of both the elements Cu and Ag, consistent with the core shell structure of the CS Cu@Ag NPs coating the bacterial samples. For TEM, sample preparation consisted of keeping the CS Cu@Ag NPs composite treated bacteria in the medium with composite concentration at MIC for 3 h prior to evaporation. The combined results of FESEM and TEM confirm that the CS Cu@Ag NPs composite indeed interacted with the bacterial membrane.

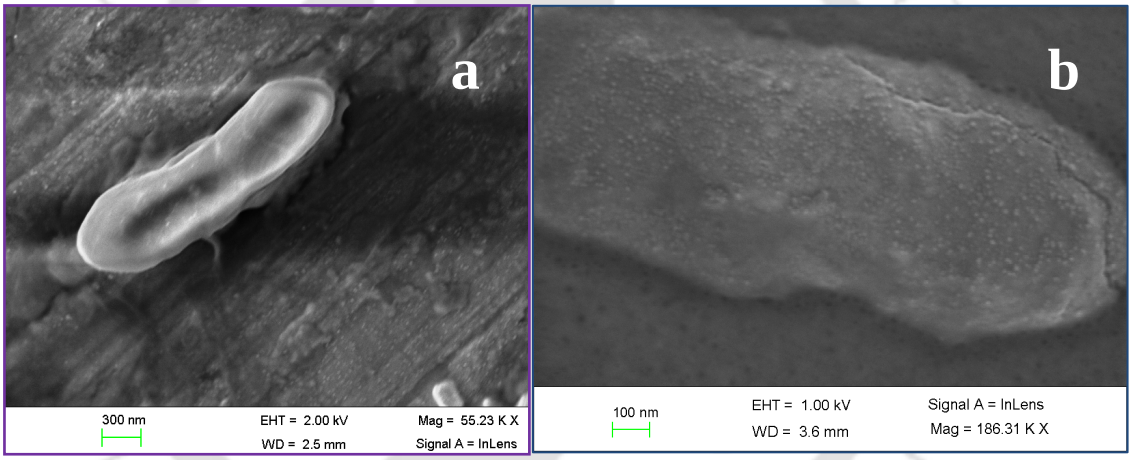

Figure 4.7: (a) Field-Emission Scanning Electron micrograph of GFP expressing recombinant *E. coli* cells and (b) *E coli* cells treated with 63.4 µg/mL CS Cu@Ag NPs composite in liquid LB medium for 3 h.

Also, the image of a bacterium damaged due to the development of pores on its cell wall (Figure 4.7b, 4.8a) supports our claim of cell death via cell wall damage. It is important to mention that the Cu@Ag NPs (in the composite) attached to the cell wall retained their individual character as the particle size distribution of as prepared sample and when attached to the bacterium were comparable (refer to Appendix, Figure A. 4.6). In other words, no agglomeration or dissolution of Cu@Ag NPs was observed when the composite got attached to the bacterial cell surface, although from the TEM and FESEM

images there appears to be several layers of the composite attached to a single bacterium. We found in our earlier studies Cu and Ag ions have minor role on the bactericidal activity and NPs play major role to kill the bacteria.[1,2] Thus here core-shell Cu@Ag NPs are likely mainly responsible for bactericidal activity of CS Cu@Ag NP composites rather than the ions.

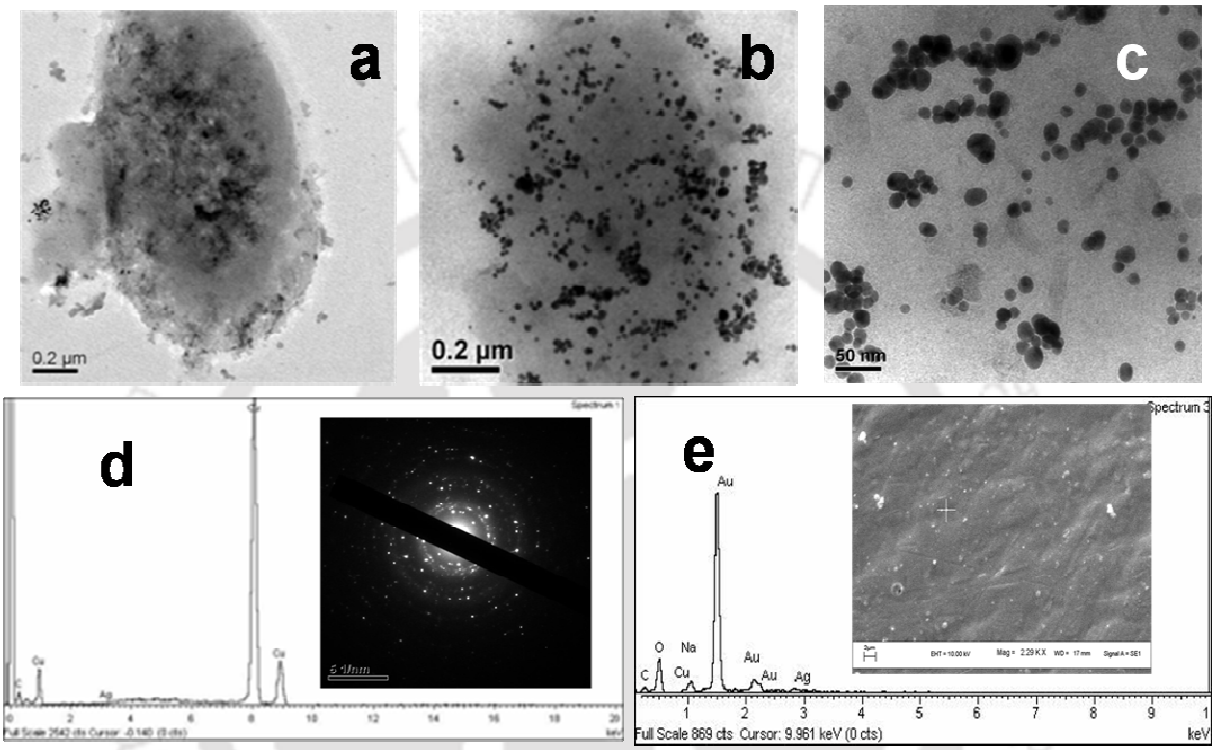

Figure 4.8: (a, b, c)TEM image of a GFP expressing recombinant *E. coli* cell treated with 63.4 µg/mL (MIC) CS Cu@Ag NPs composite in liquid LB medium for 3 h. (d) EDX spectra from TEM and corresponding SAED. (e) EDX spectra of CS Cu@Ag NPs composite from SEM (inset) shows presence of copper & silver present in a single nanoparticle. Gold peaks are due to the gold coating on CS Cu@Ag NPs composite.

Chitosan (a β-1,4 linked glucosamine) is a natural biopolymer possessing bactericidal activity against Gram-negative and Gram-positive bacteria. It interacts with bacterium cell wall through electrostatic attractions as chitosan is polycationic in nature and the bacterial cell envelop is negatively charged. Attachment of the CS Cu@Ag NPs permeabilzes the cell membrane, leading to leakage of intracellular components and cell death. This mechanism is similar to that reported earlier for iodinated CS-Ag NP composite and iodinated CS-Cu NP composite.[1,2] Zeta potential *(ζ)* measurements were

performed, under the present experimental conditions, to ascertain the charge of chitosan and CS Cu@Ag NPs in aqueous solution. The zeta potential values at pH 6.3 were as follows: chitosan: +59.57 mV and CS Cu@Ag NPs composite: +23.93 mV. Zeta potential measurements on various strains of *E. coli* in pH ranges 2 to 9 indicate that bacterial cell surface is negatively charged in this pH range.[62,63] Hence, presumably, the positive-charge of CS Cu@Ag NPs composite adheres to *E. coli* cell's negative surface charge through electrostatic interactions. Once the composite gets attached to the bacterial cell wall, Cu@Ag NPs interact with sulfur-containing proteins of bacterial cell membrane enhancing their permeability, causing leakage of proteins and other intracellular constituents, leading to the death of the bacteria.

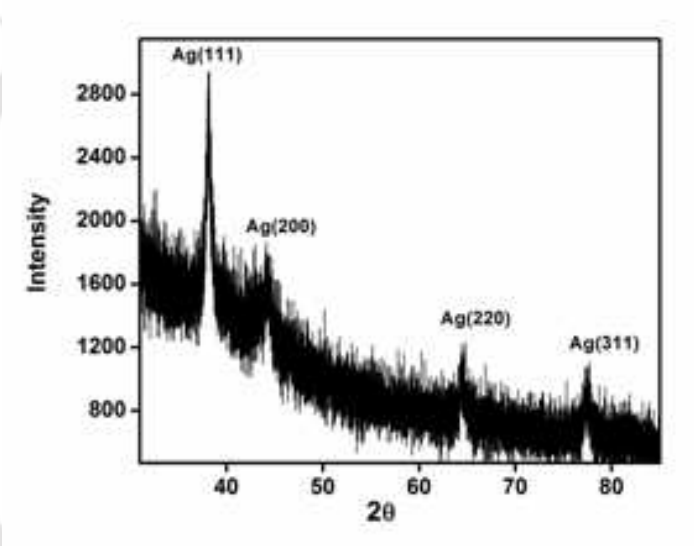

Figure 4.9: Powder XRD pattern of the centrifuged sample of *E. coli* bacteria treated with MIC of CS Cu@Ag NPs composite for 12 hours.

For a better understanding of the mechanism of bactericidal action, XRD and XPS analysis were carried out on centrifuged and vacuum-dried sample of *E. coli* treated with CS Cu@Ag NPs composite for 12 hours and 24 hours respectively. XRD (Figure 4.9) shows the presence of reflection peaks from the (111) plane of Ag.

Further, from high resolution XPS analysis, the binding energy for Ag $3d_{5/2}$ and Ag $3d_{3/2}$ electrons on this sample were found to be 367.43 eV and 373.76 eV respectively (Figure 4.10). The shift of both Ag $3d_{5/2}$ and Ag $3d_{3/2}$ (corresponding standard binding

energies for pure silver: 368.3 and 374.3 eV respectively), towards the lower binding energies is due to the interaction and electron transfer between the metallic Ag and sulphur.[64–66] Thus the XPS results support the existence of Ag-S species on the surface of *E. coli* treated CS Cu@Ag NP sample.

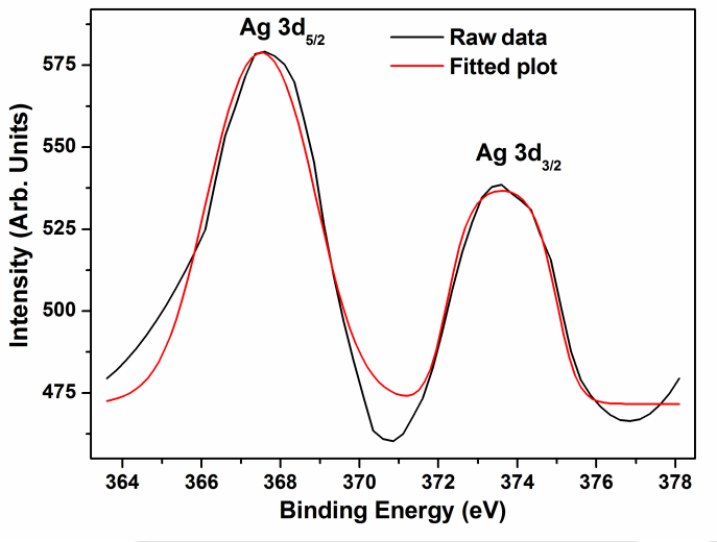

Figure 4.10: High resolution XPS spectra of Ag 3d region, of the centrifuged sample of *E. coli* treated with CS Cu@Ag NPs composite for 24 hours

Furthermore, in order to understand the interaction between DNA and CS Cu@Ag NPs, Recombinant GFP plasmid (pGFP) isolated from the control and CS Cu@Ag NPs treated samples by an alkaline lysis method at different time points were analyzed by agarose gel electrophoresis (Figure 4. 11a).[67,68] The results in Figure 4.11a showed similar migration patterns of pGFP for both control and composite treated samples, which implied that the composite had apparently no effect on DNA degradation. Gel retardation assay of isolated pGFP, incubated for 2 h with varying concentrations of CS and with varying concentration of CS Cu@Ag NP composite are reported in Figure 4.11b. The bands observed in the wells of lane 2 and lane 3, in Figure 4.11 b, confirmed the complexation of pGFP with CS, as this stopped the movement of the pGFP from the wells when compared with control sample containing free pGFP (lane 1). Likewise, the limited movement in lane 4 and 5 confirmed the electrostatic interaction and

complexation of pGFP with the CS Cu@Ag NPs composite. Partial retardation of pGFP movement in lane 4 and almost complete retardation in lane 5 is observed on increasing the concentration of CS Cu@Ag NPs composite. It is worth mentioning that the charge density and fraction of free deacetylated unit is important in determining the complexation ability of CS with polyanions, such as DNA.[69,70] In order to ascertain whether such interactions were responsible for our agarose gel electrophoresis results in Figure 4.11, we have measured the zeta potentials of CS and CS Cu@Ag NPs composite at pH 6.3. They were: CS: +59.57 mV and CS Cu@Ag NPs composite: +23.93 mV. Further, FTIR spectra of native CS and CS Cu@Ag NPs (refer to Appendix, Figure A. 4.2) show that the N-acetyl glucosamine unit peaks at 1418 cm^{-1}, 1383 cm^{-1} assigned to the CH_3 symmetrical deformation mode and at 1314 cm^{-1} due to C-N stretching vibration vanished in the composite, probably due to their interaction with the surface of the NPs. The interaction of N-acetyl glucosamine units to the surface of NPs will result in reduced charge density in the CS Cu@Ag NPs composite, as is the case here.

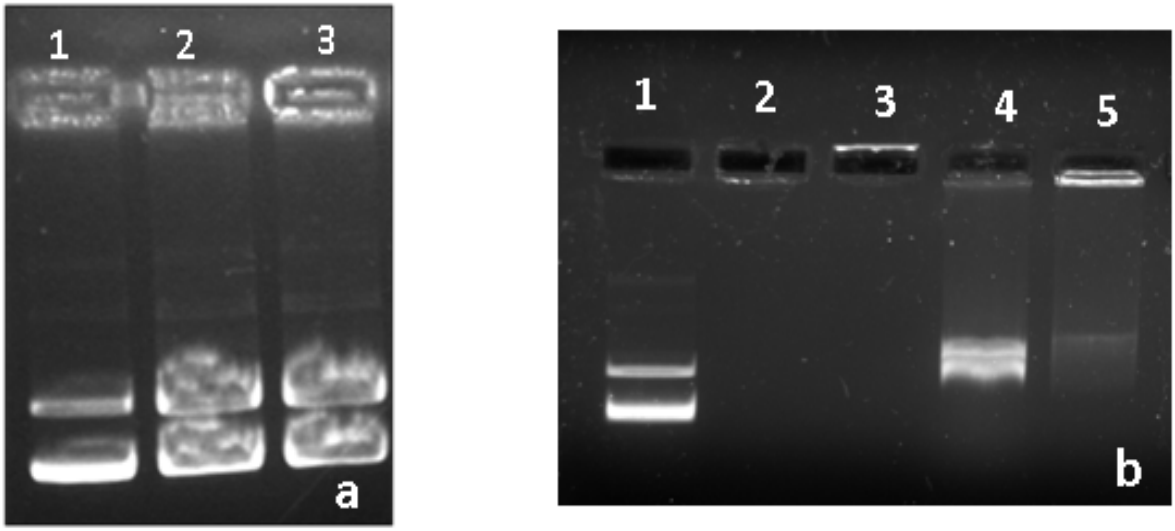

Figure 4.11: (a) Agarose gel electrophoresis of pGFP isolated from *E. coli* cells treated with 3.4 µg/mL of CS Cu@Ag NPs composite. Lane 1: control; Lane 2: 2hr treatment; Lane 2: 4hr treatment. (b) Gel retardation assay of isolated pGFP (0.5 µg in 20 µL reaction volume) incubated for 2 h with varying concentration (1.8, 3.6 µg) of CS (lanes 2, 3) and with varying concentration (1.98, 3.96 µg) of CS Cu@Ag NPs composite (lanes 4, 5). Lanes 1 corresponds to pGFP only (control).

In our agarose gel electrophoresis experiments (Figure 4.11b) the migration of plasmid DNA in CS treated samples was stopped as the charge density of CS is large. On the other hand, the reduced charge density of CS Cu@Ag NPs results in partial movement of the pGFP in lanes 4 and 5, the extent of which depends on the relative amount of the composite present.

Finally, we have recorded the XRD pattern of CS Cu@Ag NPs composite-treated *E. coli* bacteria, where the XRD sample was prepared 12 h after treatment (Figure 4.9). The observation in Figure 4.11 indicated that NPs were still present in the sample as the diffraction peaks due to (111), (200), (220) and (311) planes of silver were still present.

4.5: Conclusion

In summary, we have synthesized a CS composite of bimetallic core–shell Cu@Ag NPs at ambient conditions by reducing silver nitrate on pre-synthesized CS-Cu NPs. The presence of Ag shell around the core Cu NPs markedly reduced the tendency of Cu to oxidize at ambient conditions, increasing their stability from 12 h in CS-Cu NPs to more than two weeks in CS Cu@Ag NPs. UV-Visible, TEM, HRTEM, XRD and XPS analysis strongly support the formation of the core shell structure Cu@Ag of the NPs. The NPs in the CS Cu@Ag NPs composite were spherical with a size distribution of 14.0 ±3.4 nm. CS Cu@Ag NP composite was found to be highly active against a Gram-negative *E. coli* and Gram-positive *B. cereus* bacteria. The MIC of the CS Cu@Ag NPs composite against recombinant GFP-expressing *E. coli* was found to be 63.4μg/mL, consisting of 3.03 μg/mL of Cu and 1.47 μg/mL of Ag. Bactericidal activity of the composite was found to be superior to those of the individual components, due to synergistic effect. TEM, FESEM, XPS, zeta potential measurements and flow cytometry were used to understand the details of the antibacterial property of the CS Cu@Ag NP composite. Polycationic CS matrix interacted with the negatively charged cell surface while Cu@Ag NPs got attached to sulfur-containing proteins of bacterial cell membrane, causing cell permeability eventually leading to death of bacteria. The experiments established the importance of synthesis and synergy of antimicrobial activity of CS Cu@Ag NP composite.

References

(1) (a) Banerjee, M.; Mallick, S.; Paul, A.; Chattopadhyay, A.; Ghosh, S. S. *Langmuir* **2010,** *26*, 5901–5908. (b) Chapter 2 of current thesis

(2) (a) Mallick, S.; Sharma, S.; Banerjee, M.; Ghosh, S. S.; Chattopadhyay, A.; Paul, A. *ACS Appl. Mater. Interfaces* **2012,** *4*, 1313–1323. (b) Chapter 3A of current thesis

(3) Gogoi, S. K.; Gopinath, P.; Paul, A.; Ramesh, A.; Ghosh, S. S.; Chattopadhyay A. *Langmuir* **2006,** *22*, 9322–9328.

(4) Sanpui, P.; Murugadoss, A.; Durgaprasad, P. V.; Ghosh, S. S.; Chattopadhyay, A. *Int. J Food Microbiol.* **2008,** *124*, 142–146.

(5) Sahoo, A. K.; Sk, Md Palashuddin.; Ghosh, S. S.; Chattopadhyay, A. *Nanoscale* **2011,** *3*, 4226–33.

(6) Morriss, R. H.; Collins, L. F. *J. Chem. Phys.* **1964,** *41*, 3357–3363.

(7) Toshima, N.; Yonezawa, T. *New J. Chem.* **1998,** *22*, 1179–1201.

(8) Grouchko, M.; Kamyshny, A.; Magdassi, S. *J. Mater. Chem.* **2009,** *19*, 3057–3062.

(9) Cazayous, M.; Langlois, C.; Oikawa, T.; Ricolleau, C.; Sacuto, A. *Phys. Rev. B* **2006,** *73*, 113402.

(10) Langlois, C. T.; Oikawa, T.; Bayle-Guillemaud, P.; Ricolleau, C. *J. Nanopart. Res.* **2008,** *10*, 997–1007.

(11) Tsuji, M.; Hikino, S.; Tanabe, R.; Matsunaga, M.; Sano, Y. *CrystEngComm* **2010,** *12*, 3900–3908.

(12) Zhang, J.; Tang, Y.; Lee, K.; Ouyang, M. *Science* **2010,** *327*, 1634–1638.

(13) Rodriguez-Gonzalez, B.; Burrows, A.; Watanabe, M.; Kiely, C. J.; Liz-Marzan, L. M. *J. Mater. Chem.* **2005,** *15*, 1755–1759.

(14) Ma, Y.; Li, W.; Cho, E. C.; Li, Z.; Yu, T.; Zeng, J.; Xie, Z.; Xia, Y. *ACS Nano* **2010,** *4*, 6725–6734.

(15) Srnova-Sloufova, I.; Lednicky, F.; Gemperle, A.; Gemperlova, J. *Langmuir* **2000,** *16*, 9928–9935.

(16) Henglein, A. *J. Phys. Chem. B* **2000,** *104*, 6683–6685.

(17) Fernando, R.; Jellinek, J.; Johnston, R. L. *Chem. Rev.* **2008,** *108,* 845–910.

(18) Cortie, M. B.; McDonagh, A. M. *Chem. Rev.* **2011,** *111,* 3713–3735.

(19) Cao, L.; Diao, P.; Tong, L.; Zhu, T.; Liu, Z. *ChemPhysChem* **2005,** *6,* 913–918.

(20) Kim, K.; Lee, H. S. *J. Phys. Chem. B,* **2005,** *109,* 18929–18934.

(21) Netzer ,N. L.; Qiu, C.; Zhang, Y.; Lin, C.; Zhang, L.; Fong, H.; Jiang, C. *Chem. Commun.* **2011,** *47,* 9606–9608.

(22) Langlois, C.; Alloyeau, D.; Le Bouar, Y.; Loiseau, A.; Oikawa, T.; Mottet, C.; Ricolleau, C. *Faraday Discussions* **2008,** *138,* 375–391.

(23) Mancier, V.; Rousse-Bertrand, C.; Dille J.; Michel, J.; Fricoteaux, P. *Ultrason. Sonochem.* **2010,** *17,*690–696.

(24) Tsuji, M.; Hikino, S.; Sano, Y.; Horigome, M. *Chem. Lett.* **2009,** *38,* 518–519.

(25) Anderson, T. S.; Magruder, R. H. I.; Wittig, J. E.; Kinser, D. L.; Zuhr, R. A. *Nucl. Instrum. Methods Phys. Res., Sect. B* **2000,** *171,* 401–405.

(26) Manikandan D.; Mohan S.; Magudapathy P.; Nair K.G.M. *Nucl. Instrum. Methods Phys. Res., B* **2002,** *198,* 73–76.

(27) Manikandan, D.; Mohan, S.; Nair, K. G. M. *Physica B* **2003,** *337,* 64–68.

(28) Bala, T.; Bhame, S. D.; Joy, P. A.; Prasad, B. L. V.; Sastry, M. *J. Mater. Chem.* **2004,** *14,* 2941–2945.

(29) Xu, X.; Luo, X.; Zhuang, H.; Li, W.; Zhang, B.; *Mater. Lett.* **2003,** 57, 3987–3991.

(30) Jung, D. S.; Lee, H. M.; Kang Y. C.; Park S. B.; *J. Colloid Interface Sci.* **2011,** *364,* 574–581.

(31) Zhao, J.; Zhang, D.; Zhao, J. *J. Solid State Chem.* **2011,** *184,* 2339–2344.

(32) Zhao, J.; Zhang, D.; Song, X. *Appl. Surf. Sci.* **2012,** *258,* 7430–7434.

(33) Toshima, N.; Harada, M.; Yamazaki, Y.; Asakura, K. *J. Phys. Chem.* **1992,** *96,* 9927–9933.

(34) Toshima N. Pure *Appl. Chem.* **2000,** *72,* 317–325.

(35) Mizukoshi, Y.; Fujimoto, T.; Nagata, Y.; Oshima, R.; Maeda, Y. *J. Phys. Chem. B* **2000,** *104,* 6028–6032.

(36) Shen, S.; Zhuang, J.; Yang, Y.; Wang, X. *Nanoscale* **2011,** *3,* 272–279.

(37) Zeng, H.; Li, J.; Wang, Z. L.; Liu, J. P.; Sun, S. *Nano Lett.* **2004,** *4,* 187−190.

(38) Zeng, H.; Sun, S.; Li, J.; Wang, Z. L.; Liu, J. P. *Appl. Phys. Lett.* **2004,** *85,* 792.

(39) Rana, S.; Rawat, J.; Misra, R. D. K. *Acta Biomaterialia.* **2005,** *1,* 691–703.

(40) Chudasama, B.; Vala, A.; Andhariya, N.; Upadhyay, R. V.; Mehta, R. V. *Nano Research.* **2010,** *2,* 955–965.

(41) Kim, Y. H.; Lee, D. K.; Cha, H. G.; Kim , C. W.; Kang, Y. S. *J. Phys. Chem. C* **2007,** *111* , 3629–3635.

(42) Gong, P.; Li, H. M.; He, X. X.; Wang, K. M.; Hu, J. B.; Tan, W. H.; Zhang, S. C.; Yang, X. H. *Nanotechnology* **2007,** *18,* 28560.

(43) Banerjee, M.; Sharma, S.; Chattopadhyay, A.; Ghosh, S. S. *Nanoscale* **2011,** *3,* 5120–5125.

(44) Gaggelli, E.; Kozlowski, H.; Valensin, D.; Valensin, G. *Chem. Rev.* **2006,** *106,* 1995–2044.

(45) Cater, M. A.; Fontaine S. L.; Shield, K.; Deal, Y.; Mercer, Julian F. B. Gastroenterology ***2006,*** *130,* 493–506.

(46) Feng, Q. L.; Wu, J.; Chen, G. Q.; Cui, F. Z.; Kim, T. M.; Kim, J. O. J. Biomed. *Mater. Res.* **2000,** *52,* 662– 668.

(47) Williams, R. L.; Doherty, P. J.; Vince, D. G.; Grashoff, G. J.; Williams, D. F. *Crit. Rev. Biocompat.* **1989,** *5,* 221–243.

(48) Taner, M.; Sayar, N.; Yulug, I. G.; Suzer S. *J. Mater. Chem.* **2011,** *21,* 13150–13154.

(49) Valodkar, M.; Modi, S.; Pal, A.; Thakore, S. *Mater. Res. Bull.* **2011,** *46,* 384–389.

(50) Mott, D.; Galkowski, J.; Wang, L.; Luo, J.; Zhong, C.-J. *Langmuir* **2007,** *23,* 5740–5745.

(51) Lu, L.; Zhang, W.; Wang, D.; Xu, X.; Miao, J.; Jiang, Y. *Mater. Lett.* **2010,** *64,* 1732–1734.

(52) Torres, J.; Valles, E.; Gomez, E. *J. Nanopart. Res.* **2010,** *12,* 2189–2199.

(53) Kim, Y. H.; Lee, D. K.; Cha, H. G.; Kim, C. W.; Kang, Y. C.; Kang, Y. S. *J. Phys. Chem. B* **2006,** *110,* 24923–24928.

(54) Seah, M. P.; Gilmore, I. S.; Beamson, G. *Surf. Interface Anal.* **1998**, *26,* 642–649.

(55) Moulder, J. F.; Chastain, J. *Handbook of X Ray Photoelectron Spectroscopy: A Reference Book of Standard Spectra for Identification and Interpretation of XPS* Data. Perkin-Elmer: **1995.**

(56) Burch, R. *Acc. Chem. Res.* **1982,** *15,* 24–31.

(57) Mavrikakis, M.;Hammer, B.; Norskov, J. K. *Phys. Rev. Lett.* **1998,** *81,* 2819–2822.

(58) Kitchin, J. R.; Norskov, J. K.; Barteau, M. A.; Chen, J. G. *Phys. Rev. Lett.* **2004,** *93,* 156801 (4 pp)

(59) Kitchin, J. R.; Norskov, J. K.; Barteau, M. A.; Chen, J. G. *J. Chem. Phys.* **2004,** *120,* 10240–10246.

(60) Wang, J. X.; Inada, H.; Wu, L.; Zhu, Y.; Choi, Y.; Liu, P.; Zhou, W.-P.; Adzic, R. R. *J. Am. Chem. Soc.* **2009,** *131,* 17298–17302.

(61) Xing, Y.; Cai, Y.; Vukmirovic, M. B.; Zhou, W.-P.; Karan, H.; Wang, J. X.; Adzic, R. R., *J. Phys. Chem. Lett.* **2010,** *1,* 3238–3242.

(62) Li, J.; McLandsborough, L. A. *Inter. J. Food Microbiol.* **2001,** *53,* 185–193.

(63) Wilson, W. W.; Wade, M. M.; Holman, S. C.; Champlin, F. R. *J. Microbiol. Methods* **2001,** *43,* 153–164.

(64) *Bensebaa, F.; Yu, Z.; Deslandes, Y.; Kruus, E.; Ellis, T. H. Surf. Sci.* **1998,** *405,* L472–L476.

(65) Esplandiu, M. J.; Noeske, P. L. M. *Appl. Surf. Sci.* **2002**, *199,* 166–182.

(66) Chen, R.; Nuhfer, N. T.; Moussa, L.; Morris, H. R.; Whitmore, P. M. *Nanotechnology* **2008,** *19,* 455604 (11pp).

(67) Birnboim, H. C.; Doly. J. *Nucl. Acids Res.* **1979,** *7,* 1513-1523.

(68) Sambrook, J.; Russell, D. W. *Molecular Cloning-A Laboratory Manual,* 3rd ed.; Cold Spring Harbor Press: New York, **2001,** Vol. 1, pp 1.31-1.34.

(69) Strand, S. P.; Danielsen, S.; Christensen, B. E.; Varum, K. M. *Biomacromolecules* **2005,** *6,* 3357-3366.

(70) Maurstad, G.; Danielsen, S.; Stokke, B. T. *Biomacromolecules* **2007,** *8,* 1124-1130.

Chapter 5

Facile preparation of mixed metal nanoparticles composite as a potential antibacterial agent

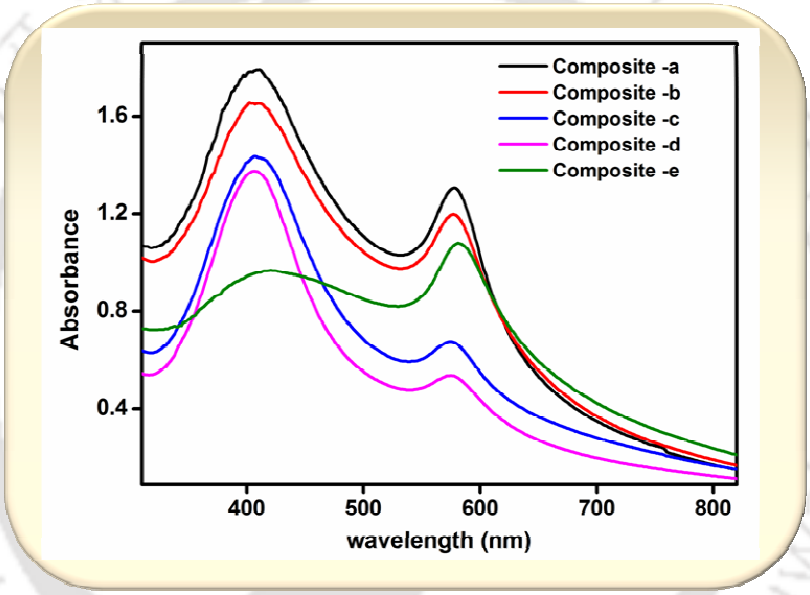

"Facile preparation of mixed Cu and Ag nanoparticle composites in chitosan: implications as a potent antibacterial agent. **Sadhucharan Mallick,** Siddhartha Sankar Ghosh, Arun Chattopadhyay, and Anumita Paul. (Manuscript to be submitted)"

5.1: Introduction

Mixed metal Nanoparticles (NPs), also called hetero metal NPs, play important role in several areas of chemistry and physics. The most common use for mixed NPs has been in the area of catalysis, where researchers have found their use both as catalyst and as catalytic supports.[1−4] It is well known that combining a transition metal element with platinum enhances catalytic activity for reactions such as oxygen reduction in fuel cells and direct oxidation of methanol.[1] Further, these studies attracted attention towards preparation of new materials having mixed metal NPs with variable composition displaying unique properties. Various research groups have explored and developed physical and chemical methods by which such materials can be prepared. Zhang et al. prepared mixed Pt-Co NPs and Pt-Ru NPs catalysts using water-in-oil reverse micro emulsion system composed of water-Triton X-100-propan-2-ol-cyclohexane.[1, 2] These Pt-Ru NPs supported on a carbon electrode possessed high dispersion and high catalytic activity for methanol oxidation at room temperature. On the other hand, Liu et al. synthesized nano sized Pt-Ru alloy particles on carbon support which showed greater electro catalytic activities for methanol oxidation.[3]

Bimetallic NPs with core-shell, hetero structure, or inter metallic and alloyed structures are being realized as more useful materials than monometallic NPs.[5-8] Bimetallic NPs (Cu, Ag) with different hetero structure i.e. alloy, core shell and heterodimer have been synthesized and their applications studied by several groups, but in situ synthesis of mixed metal NPs in a polymer matrix with emphasis on their biological applications is not reported until now. Synthesis and application of dumbbell like Cu-Ag nanostructures,[8] Cu-Ag alloy NPs [9−14] and core-shell Cu@Ag NPs[15−17] has been reported by several groups. Using RAPET (reaction under autogenic pressure at elevated temperatures) technique Gedanken et al. have developed a method for synthesis of carbon coated Cu@Ag and Ag@Cu core-shell NPs.[7] Huang et al. had synthesized dumbbell like Cu-Ag nanostructures which exhibit enhanced catalytic activity in the hydrogenation of 4-nitrophenol.[8] Phase-separated Ag-Cu composite colloids containing different mole fractions of Ag and Cu in ethanol solution were synthesized by photo reduction in the presence of benzoin and poly(N-vinyl-2-pyrrolidone by Itakura.[18] Suyal

et al. had synthesized bimetallic alloy and phase separated mixed colloids particles of Cu and Ag in thin films using sol-gel route and studied their optical properties.[19] Woo et al. had prepared mixed metal-based (Cu-Ag) conductive ink from which highly conductive tracks were formed on a transparent polyethersulphone substrates after annealing at low temperature. They prepared Cu-Ag based mixed metal conductive ink using mixture of Cu NP and Ag NP at varying volume ratios (Cu/Ag) from 2:1 to 4:1 in a mixed solvent system of methanol, 2-methoxy ethanol and ethylene glycol.[20] Y.-S Li have developed Ag-Cu colloid ink which they filled into a felt-tip pen and written on a substrate to make conducting lines using Ag-Cu composite NPs.[21] Kiran et al. prepared Ag-Cu nanoclusters (NCs) co-doped in SiO_2 matrix by the sol-gel process and studied their nonlinear optical properties and the role of the surface-plasmon resonance on optical limiting properties.[22] Grouchko, et al. synthesized well-dispersed Cu NPs by reduction of copper nitrate in aqueous solution using hydrazine monohydrate as a reducer in the presence of preformed Ag NPs as catalysts and poly-acrylic acid as a stabilizer.[23] K. Hamad-Schifferli and co-workers synthesized Au-Cu NPs and found the oxidation stability depends on composition and temperature. They found that the Cu oxidation rate depends on NP composition where increasing Au% improves stability as also exhibited improved catalytic activity for CO oxidation.[24]

The antibacterial properties of bulk Cu and Ag as well as Cu NPs and Ag NPs are well known. [25-37] Bactericidal activity studies with Cu NPs, Ag NPs and with their alloy had been reported by us and by others groups. Small size Cu NPs or Ag NPs both have high bactericidal activity because these NPs (less than 20 nm diameters) get attached to sulfur-containing proteins of bacterial cell membranes, altering the permeability of the membrane, which causes leakage of protein and other intracellular material such as amino acids, glucose, and lactate dehydrogenase, electrolytes, and finally leads to the death of bacteria.[26,29,33,34] A few reports have suggested that Ag^+ and Cu^{2+} ions are main bactericidal species, which are provided by active surfaces of NPs and their oxide present on the surfaces of these NPs.[27,32,37,38 ,39] Cu NPs and Ag NPs has been variously portrayed as antimicrobial agent owing to their biocidal activity at low concentrations and comparatively less toxic to mammalian cells .[28–36]

Recently, we prepared core-shell CS-Cu@Ag NPs with excellent antibacterial activity discussed in Chapter 4 of my thesis.[36] However; there is no report about the antibacterial properties of Cu NPs and Ag NPs working in tandem in same composite. Recently, a few groups have reported that Cu-Ag alloy NPs display superior bactericidal activity against *E. coli* as compared to pristine Ag NPs or Cu NPs;[14,15] but there is no report on the synthesis and bactericidal activity study of phase separated mixed Cu NP and Ag NP composite. We have prepared phase separated mixed metal nanoparticle (Cu NP and Ag NP) composite in presence of chitosan biopolymer and iodine and studied their antibacterial activity against *E. coli.* Zhang, L et al. synthesized Ag NCs (~2 nm) and Ag NCs-coated with TiO_2 NPs and studied bactericidal activities against *Micrococcus lylae* and found Ag NCs-coated TiO_2 material with optimal Ag loading shows enhanced photocatalytic and bactericidal activities compared to uncoated TiO_2.[40] Recently, we have reported bactericidal properties of iodinated CS-Ag NP composite and iodinated CS-Cu NPs composite and CS Cu@Ag NPs with excellent antibacterial activity as discussed in Chapter 2, 3B and 4 of this thesis.

5.2: Outline of the research work

I. A novel method of synthesizing mixed metal nanoparticles composite (Cu NPs and Ag NPs) in presence of chitosan and iodine has been developed.

II. UV-Visible spectroscopy, transmission electron microscopy, field emission scanning electron microscopy and X-ray diffraction were used to characterize the mixed metal NP composite

III. In the chapter, synergistic bactericidal action of iodinated mixed NP composite was investigated using green fluorescent protein (GFP) expressing *E. coli* bacteria.

IV. Combination of Cu NPs and Ag NPs with biodegradable and biocompatible chitosan increased antimicrobial activity through joint effects.

V. Here smaller Ag NPs and Cu NPs worked in tandem together with antibacterial components CS and iodine for better antibacterial activity. This allowed the use

of reduced amounts of Cu and Ag NPs as well as the reduced amount of the composite required for inhibitory and killing action.

5.3: Experimental section

5.3.1: Materials and methods

Copper (ll) sulphate pentahydrate ($CuSO_4.5H_2O$; Merck, India), silver nitrate ($AgNO_3$, 99.5%; Merck), chitosan of high molecular weight (75% deacetylated; Sigma-Aldrich Chemical Co.), sodium hydroxide (NaOH, 98%; Merck, India), hydrazine monohydrate (80% solution, Merck, India), acetic acid (glacial, 99–100%; Merck, India) were used as received without further purification. Milli-Q grade (resistivity 18.2 MΩ cm^{-1}) water was used in all the experiments. Iodine (I_2) was obtained from Sigma-Aldrich Chemical Pvt. Ltd., Kolkata, India. Luria-Bertani (LB) broth was purchased from HiMedia, Mumbai, India. GFP-expressing recombinant *E. coli* were grown in LB broth at 37 ^{0}C and at 220 rpm for 12 h.

5.3.2: Iodinated chitosan mixed NP composites (I_2-CS-Ag NP-Cu NP) preparation

We have prepared mixed Cu NPs and Ag NPs composite in presence of chitosan and molecular iodine abbreviated as I_2-CS-Ag NP-Cu NP composite. Several different compositions of the composite were studied using same amount of chitosan (50 mg) , 300 µL 0.02 M iodine solution and different amounts of Cu and Ag, i.e. Cu/Ag as 40:1, 20:1, 15:1, 13.33:1 and 10:1 (Table 5.1). I_2-CS-Ag NP-Cu NP composite was prepared by two step reduction process, first $AgNO_3$ solution to Ag NPs then $CuSO_4.5H_2O$ solution to Cu NPs. First Ag NPs were synthesized by adding the requisite amount of freshly prepared 20 mM $AgNO_3$ solution to 50 mg of chitosan in 50 mL Milli-Q grade water in a 100 mL round bottom flask, which was placed in an oil bath, with vigorous stirring and refluxing for 15 min at ~ 100 ^{0}C. Then 200 µL of 0.6 M NaOH solution was added to the reaction mixture and within 1 min the solution turned yellow, indicating formation of Ag NPs in the medium. The reaction was allowed to continue for another 15 min to ensure complete reduction of $AgNO_3$. Yellow colored solid appeared at the

bottom of the flask thereafter, to this CS-Ag NP dispersion, 40 mg of copper (II) sulphate pentahydrate was added and after 5 min 400 µL of 0.6 M NaOH solution was added upon which the yellow coloured solution turned brown. After about 10 min 0.4 mL of hydrazine monohydrate solution was added to the above solution with constant and vigorous stirring. The reaction was allowed to continue for an additional 30 min till a reddish coloured solid appeared at the bottom of the round bottom flask. The flask was then taken out from the oil bath and cooled to room temperature. The solution along with the precipitate was centrifuged at 5300 rpm and the precipitate was washed several time with milli-Q grade water and made into a pellet. The pellet was then re dispersed in 30 mL of 0.25% aqueous acetic acid solution and to this 300 µL of 0.02 M iodine solution in ethanol was added and mixed thoroughly. UV-Visible spectra were recorded for all I_2-CS-Ag NP-Cu NP dispersed solution. For further characterization of the I_2-CS-Ag NP-Cu NP composites, the reddish solution was centrifuged, vacuum dried and stored under vacuum before analysis. Here [Cu]/ [Ag] molar ratios of 20:1, 40:1, 15:1, 13.33:1, 10:1 respectively were used to synthesize I_2-CS-Ag NP-Cu NP composite.

Table 5.1: Elemental composition used for synthesis of I_2-CS-Ag NP-Cu NP composite.

Composites	$CuSO_4.5H_2O$	$AgNO_3$ solution (20mM)	Cu:Ag molar feed ratio
a	40 mg	600 µL	13.33:1
b	40 mg	400 µL	20:1
c	30 mg	400ul	15:1
d	20 mg	400 µL	10:1
e	40 mg	200 µL	40:1

To facilitate easy discussion, all samples are abbreviated as Cu/Ag (X:Y) for I_2-CS-Ag NP-Cu NP composite that are prepared with an X:Y copper to silver molar feed ratio.

In these all I_2-CS-Ag NP-Cu NP composites, pH was adjusted to 6.3 by the addition of dilute NaOH solution prior to antibacterial activity study. The synthesis of controlled mixed metal NPs is a complex problem because in addition to the variable composition other factors such as size distribution of the component NPs and their phase separation are also decisive in the property displayed by the composites. However, given the possible rich variation in their properties, synthesis of hetero metal NPs in polymer matrix may become a new strategy for preparation of mixed metal NPs composite, worthwhile pursuing.

5.3.3: Characterization of the I_2-CS-Ag NP-Cu NP composites

5.3.3.1: UV-Vis spectroscopic measurements

UV-Visible spectra of the I_2-CS-Ag NP-Cu NP composite dispersion was measured using a Hitachi U 2900 spectrophotometer. The UV-Vis spectra varied greatly depending on the Cu/Ag molar feed ratio. The bacterial growth was monitored by measuring optical density (OD) at 595 nm using a UV-visible spectrophotometer (Lambda 25; Perkin-Elmer, Fremont, CA, USA) of the sample at different times.

5.3.3.2: Transmission electron microscopy (TEM) analysis

For TEM investigations, 5 μL of each I_2-CS-Ag NP-Cu NP composite sample was drop coated onto a carbon coated copper TEM grid followed by air drying. The drop coated grid was then analyzed under TEM. The interactions of the composite with bacterial cells were also examined using a high resolution transmission electron microscope operating at a maximum accelerating voltage of 200 KeV. For this, mixed NPs composite treated on *E. coli* samples were drop coated onto the TEM grid followed by air drying and the resulting grid was then analyzed under TEM. EDX analysis was carried on small area of the sample using TEM operating at accelerating voltages up to 200 kV.

5.3.3.3: Field emission scanning electron microscopy (FESEM)

Interaction of the I_2-CS-Ag NP-Cu NP composite with bacterial cells was further studied by using field emission scanning electron microscopy (FESEM, Carl Zeiss, SIGMA VP) coupled with energy dispersive X-ray (EDX) analysis facility. Typically, 20 μL drop of each sample was deposited on a glass slide, dried and sputter-coated with gold film using a sputter coater and analyzed under the FESEM. The FESEM-EDX analysis of mixed NPs composite treated on *E. coli* samples was carried out on small area of the sample for the elemental analysis of the composite.

5.3.3.4: Powder XRD studies

We performed X-ray diffraction measurements to characterize the I_2-CS-Ag NP-Cu NP composites. Vacuum dried I_2-CS-Ag NP-Cu NP composites were spread on glass microslides and XRD recorded using Philips Diffrctometer (Model 1715) with Cu Kα1 radiation (λ= 1.54060 Å) operating at 55 kV and 250 mA. We also studied the fate of the I_2-CS-Ag NP-Cu NP composite during antibacterial studies using XRD measurement. Here bacteria treated with I_2-CS-Ag NP-Cu NP for 12 h was centrifuged and vacuum dried and stored under vacuum before analysis. The dried cell pellet was spread on a glass slide and XRD was recorded.

5.3.3.5: Atomic absorption spectrometry (AAS)

Quantitative analysis of the concentration of copper and silver present in I_2-CS-Ag NP-Cu NP composite was performed with the help of atomic absorption spectrophotometer (Model: AA240 Varian Inc) after dissolving the composite in dilute HCl solution. The supernatant solution obtained after centrifugation of the composites was also measured to determine concentration of Cu and Ag ions present in the supernatant solution.

5.3.3.6: Bactericidal studies

Bactericidal activity studies were carried out on Gram negative GFP-expressing *E. coli* bacteria. GFP-expressing *E. coli* was cultured in LB ampicillin media. Different concentrations of I_2-CS-Ag NP-Cu NP composite were used to determine the minimum inhibitory concentration (MIC) and minimum bactericidal concentration (MBC)**.** We determined the MIC and MBC for all of the composites a, b, c, d, e (Table 5.1). GFP-expressing *E. coli* (10^8cfu/ml) were grown in LB media in the presence of different concentrations of I_2-CS-Ag NP-Cu NP for 12 h at 37°C. The lowest concentration of composite at which there was no visual turbidity was taken as the MIC value of the composite. Further, the cultures which lacked visual turbidity were reinoculated in fresh media. The lowest concentration of the composite that killed at least 99.9% of original inoculums was taken as MBC. The experiments were performed in at least triplicate to ensure reproducibility. The bacterial growth was monitored by measuring optical density (OD) at 595 nm using a UV-Visible spectrophotometer (Lambda-25; Perkin-Elmer, Fremont, CA, USA) of the sample at different times.

5.4: Results and discussion

5.4.1: Synthesis and characterization of I_2-CS-Ag NP-Cu NP composites

I_2-CS-Ag NP-Cu NP composites were prepared under normal atmospheric condition in the presence of chitosan, iodine and hydrazine hydrate as a reducing agent. First $AgNO_3$ solution was reduced to Ag NPs using chitosan as a reducing and stabilizing agent, following which $CuSO_4.5H_2O$ solution was reduced to Cu NPs using hydrazine hydrate as the reducing agent. When the yellow coloured CS-Ag NPs dispersion turned reddish it indicated completion of the reaction with the formation of I_2-CS-Ag NP-Cu NP composite. The I_2-CS-Ag NP-Cu NP composites were more stable when [Cu]/ [Ag] molar feed ratios 13.33:1, 20:1. SPR bands corresponding to both Cu NPs and Ag NPs broadened slowly in ~ 6-7 days (Appendix, Figure A. 5.1a, b). I_2-CS-Ag NP-Cu NP composite was less stable when either less of amount of Cu or Ag was used in the preparation of the composite (Refer to Appendix, Figure A. 5.1 c, d).

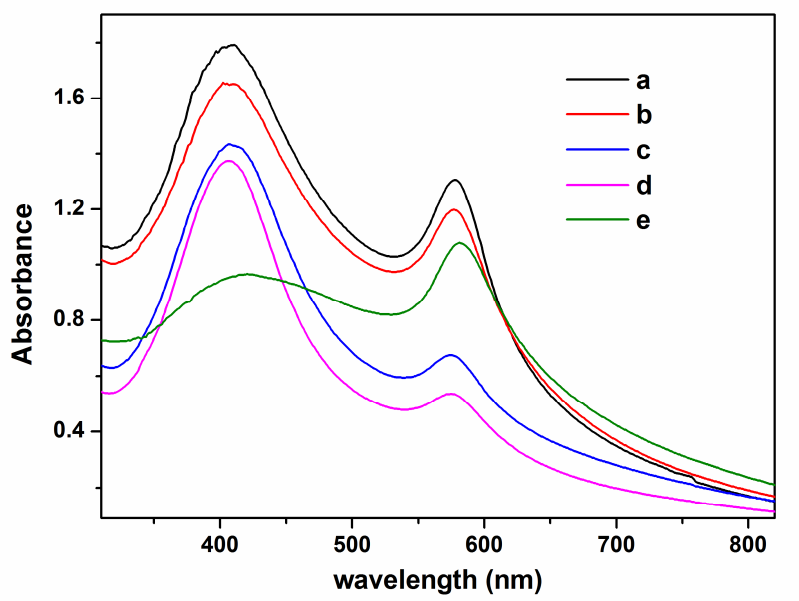

Figure 5.1: UV-Visible spectrum of freshly prepared I_2-CS-Ag NP-Cu NP composite with different molar feed ratio of Cu to Ag (a)13.33:1, (b) 20:1, (c) 15:1, (d) 10:1, (e) 40:1.

The UV-Vis spectrum consisted of a two sharp peaks at 415 nm and 585 nm, indicative of the formation of Ag NP and Cu NPs. The exact peak positions varied depending on the Cu/ Ag molar feed ratio. The two sharp peaks, one due to Ag NPs showed a peak maximum which varied from 400 nm to 415, and the other due to Cu NPs showed a peak maximum which varied from 575 to 590 nm, on changing the molar fractions of Ag and Cu. These UV-Vis results are consistent with the presence of phase separated colloids of Ag and Cu NPs in the composite.

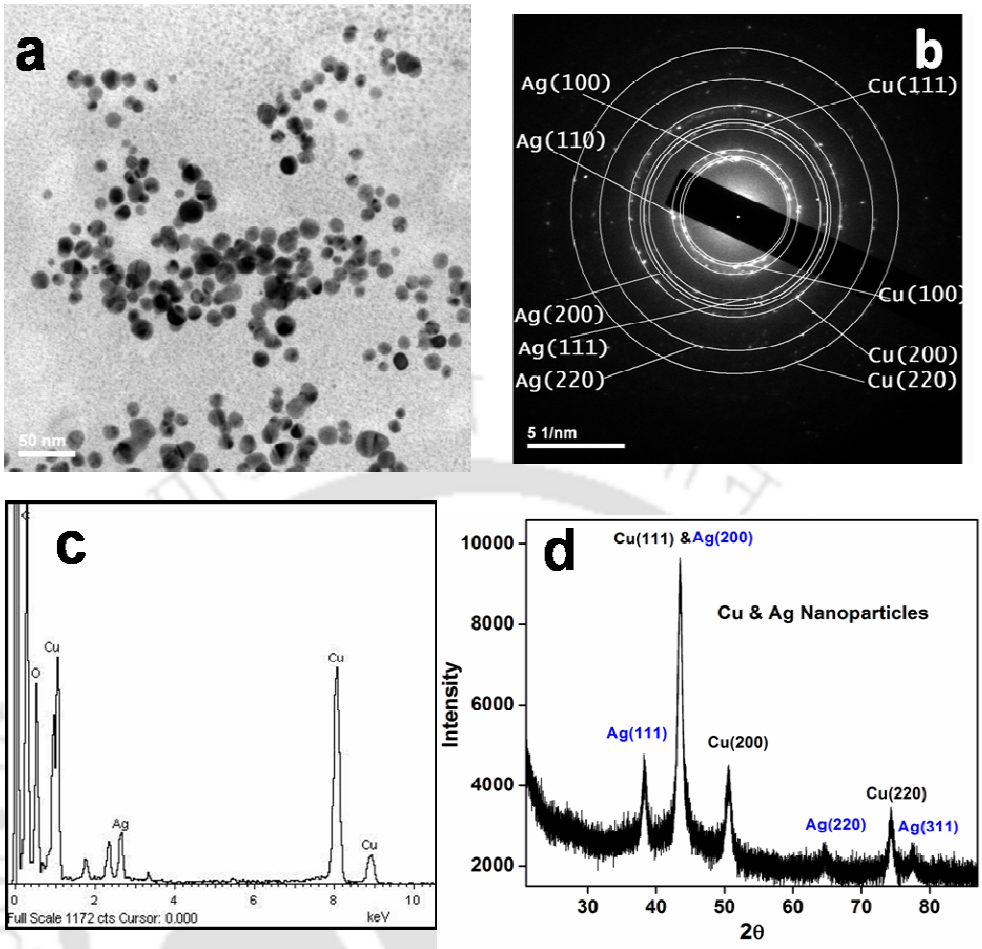

Figure 5.2: (a) TEM micrograph of I_2-CS-Ag NP-Cu NP composite for Cu/ Ag molar feed ratio 13.33:1. **(b)** SAED pattern with the diffraction rings indexed of selected region **(c)** EDX profile of I_2-CS-Ag NP-Cu NP composite showing the presence of copper and silver. **(d)** Powder XRD pattern of freshly prepared I_2-CS-Ag NP-Cu NP composite.

As the particles are phase separated, their respective plasmon bands are unaffected by the presence of the other metal, thus their optical absorption spectrum is a simple addition of the spectrum of Ag NP and Cu NP.[19] The SPR bands corresponding to both Ag NP and Cu NP are clearly seen in the mixed metal NPs composite; indicating that these Cu, Ag did not form alloys and that they retained their individual identities. In the case of an alloy formation – which is not the case herein-, a single SPR band is observed between the position of the surface-plasmon band of Ag and Cu NPs, as reported for the Au–Cu and Au–Ag systems. [11-13]

Further analysed by TEM and XRD were carried out for composites with compositions listed in Table 5.1. TEM analysis confirmed the presence of metal NPs in all the cases; Figure 5.2a and Figure 5.3a being the representative TEM images for Cu/ Ag molar feed ratio of 13.33:1 and 20: 1 respectively. Selected area electron diffraction (SAED) patterns of I_2-CS-Ag NP-Cu NP composite with Cu/ Ag molar feed ratio of 13.33:1 is shown in Figure 5.2B. The resulting diffraction rings were indexed and corresponding lattice planes tabulated in Table 5.2, which confirmed the presence of Cu NPs and Ag NPs in the face-centered cubic lattice structure in the composite. SAED results are also consistent with EDX results shown in figures 5.2C. The EDX analysis was also carried out on small area of the sample, indicating the presence of the elements Cu and Ag and I (Appendix Figure A. 5.2).

Interestingly, X-ray diffraction (XRD) pattern of the I_2-CS-Ag NP-Cu NP composite-a was recorded a day after the synthesis, which indicated the presence of two sets of diffraction peaks which were assigned to the fcc crystal structure of Cu and Ag (Figure 5.2d). The diffraction peaks at 2θ values of 43.34°, 50.46°, 74.14° were due to diffraction from (111), (200), and (220) planes of face-centered-cubic (fcc) crystal planes of Cu(0). This diffraction pattern matched with the standard powder diffraction data file for copper (fcc, JCPDS file No. 04–0836). The diffraction peaks at 2θ values of 38.16°, 44.3°, 64.6°, 77.41° and 81.4° are due to reflections from (111), (200), (220), (331), (222) planes of metallic Ag (0) (fcc, JCPDS-04-0783). No other crystalline phases were observed in the XRD patterns. Appearance of the diffraction pattern is equivalent to simple addition of the corresponding XRD patterns of Cu (0) and Ag (0), which also supported the presence of mixed Cu NPs and Ag NPs .[19] XRD patterns of the NPs composite negate possibility of alloy or core shell formation. XRD studies of the I_2-CS-Ag NP-Cu NP composite-e (Cu/Ag molar ratio=40:1) also give similar diffraction pattern (Appendix, Figure A. 5.3). The presence of CS in the composite was confirmed by FTIR studies (refer to Appendix, Figure A. 5.4).

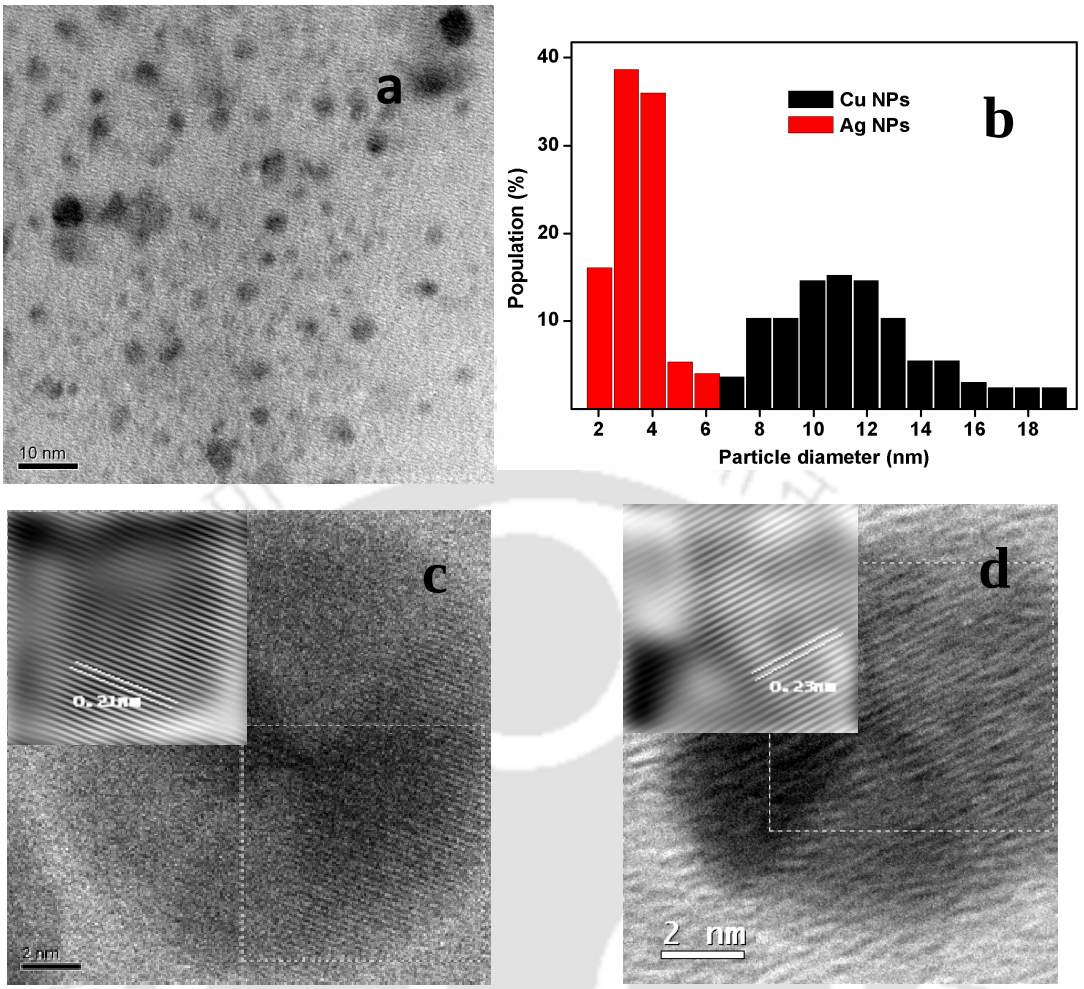

Figure 5.3:**(a)**TEM image of freshly prepared I_2-CS-Ag NP-Cu NP composite, Cu/ Ag molar feed ratios 20:1 **(b)** Size histograms of Cu NPs and Ag NPs in I_2-CS-Ag NP-Cu NP composite average Ag NPs size 3.4 ± 0.9 nm and Cu NPs size 11.4± 3.0 nm **(c)** HRTEM image of a particle showing the lattice fringes corresponding to the (111) planes of copper, inset shows the inverse Fourier transform of selected region showing the lattice fringes corresponding to the (111) planes of copper. (d) HRTEM micrographs of Ag NP in I_2-CS-Ag NP-Cu NP composite. Inset shows inverse Fourier transform of selected region indicating lattice fringes spacing of 0.23nm corresponding to Ag (111) planes.

Depending on the feed ratio of Cu/Ag (Table 5.1) the size distribution of the resulting Ag NPs and Cu NPs in the composite varied; for example a comparison can be made between Figure 5.2a and 5.3a. However, in all cases, it was found that the Ag NPs generated were considerably smaller than the corresponding Cu NPs. Figure 5.3b shows the size distribution histogram plot, obtained from the TEM image in Figure 5.3a, which is a bimodal distribution in the sizes of the NPs. Ag NPs represented by the red

histogram distribution is found to have an average size of 3.4±0.9 nm in diameter, while Cu NPs represented by the black histogram distribution is found to have an average size of 11.4±3.0 nm in diameter. Both these NPs were found to co-exist in the composite as shown in Figure 5.3a. High resolution TEM (HRTEM) images on individual NPs confirmed the presence of individual Cu NPs (Figure 5.3 c) and Ag NPs (Figure 5.3 d). Both Cu NP and Ag NP were present as fcc crystal structure, with lattice spacing of 0.21 nm and 0.23 nm due to (111) planes of Cu(0) and Ag(0) respectively, which are clearly visible in the IFFT images shown as insets in Figures 5.3b and 5.3c respectively.

Table 5.2: Lattice plane spacings (d-spacings) obtained from the SAED pattern shown in Figure 5.2d compared with the theoretical values.

Lattice Planes	Experimental	Theoretical
Ag(100)	4.04Å	4.08Å
Ag(110)	2.92Å	2.88Å
Ag(111)	2.35Å	2.35Å
Ag(200)	2.09Å	2.04Å
Ag(220)	1.44Å	1.44Å
Cu(100)	3.79Å	3.61Å
Cu(111)	2.14Å	2.08Å
Cu(200)	1.81Å	1.80Å
Cu(220)	1.24Å	1.27Å

5.4.2: Antibacterial activity assessment

Gram negative GFP-expressing *E. coli* bacteria were chose as a model system to study the bactericidal activity of the I_2-CS-Ag NP-Cu NP composite. Minimum inhibitory concentration (MIC) and minimum bactericidal concentration (MBC) were determined for each of the composites a, b, c, d, e (Table 5.1). A compilation of their MIC and MBC

values along with the amount of Cu, Ag, CS and I_2 is given in Table 5.3. In addition, time dependent bactericidal activity and mechanism were studied with composite b (Cu/Ag molar ratio = 20:1) as it has sufficient stability and displays bactericidal activity at low concentration of Cu and Ag. Time dependent antibacterial activity of I_2-CS-Ag NP-Cu NP composite b (at MIC and MBC) was monitored against GFP expressing *E. coli* by measuring optical density (OD) at 595 nm at various time points (Figure 5.4).

Table 5.3: Antibacterial efficacy of the of the I_2-CS-Ag NP-Cu NP composites against GFP-expressing *E. coli* bacteria.

Composite details		Composite (µg/mL)	Cu (µg/mL)	Ag (µg/mL)	CS (µg/mL)	I_2 (µg/mL)
Composite a	MIC	51.28	8.00	0.95	42.20	0.13
(Cu: Ag 13.33:1)	MBC	75.47	11.27	1.40	62.10	0.19
Composite b	MIC	63.50	9.98	0.74	52.64	0.16
(Cu :Ag 20:1)	MBC	93.02	14.61	1.08	73.43	0.22
Composite c	MIC	81.12	9.73	0.98	70.20	0.21
(Cu :Ag 15:1)	MBC	107.58	12.90	1.31	93.08	0.28
Composite e	MIC	98.76	15.6	0.44	82.27	0.25
(Cu :Ag 40:1)	MBC	132.13	20.86	0.60	110.07	0.33

The MIC of the I_2-CS-Ag NP-Cu NP composite was found to be 63.50 µg/mL, which consisted of 9.98 µg/mL of Cu NPs and 0.74 µg/mL of Ag NPs. The corresponding MBC (93.02 µg/mL) contained 14.61 µg/mL Cu NP and 1.06 µg/mL of Ag NPs. Control samples with 0.02 M acetic acid and 6 µL ethanol in LB media showed no growth inhibition. From the results of growth curve in Figure 5.4 it is evident that individual components at their respective individual concentrations (in the composite) either did not exhibit antibacterial properties (0.16µg/mL of iodine) or exhibited limited bactericidal

properties [52.64 µg/mL of CS; 53.40 µg/mL of CS-Ag NP composite (CS: Ag =1:0.17); 63.20 µg/mL of iodinated CS-Cu NP composite (CS:Cu:I=1:0.20:0.003)]. Interestingly, a physical mixture of I-CS-Cu NPs and CS-Ag NPs (1:1 volume ratio) which consisted CS 52.0 µg/mL, Ag 0.73 µg/mL , Cu 5.0 µg/mL , I_2 0.08 µg/mL exhibited limited bactericidal properties.

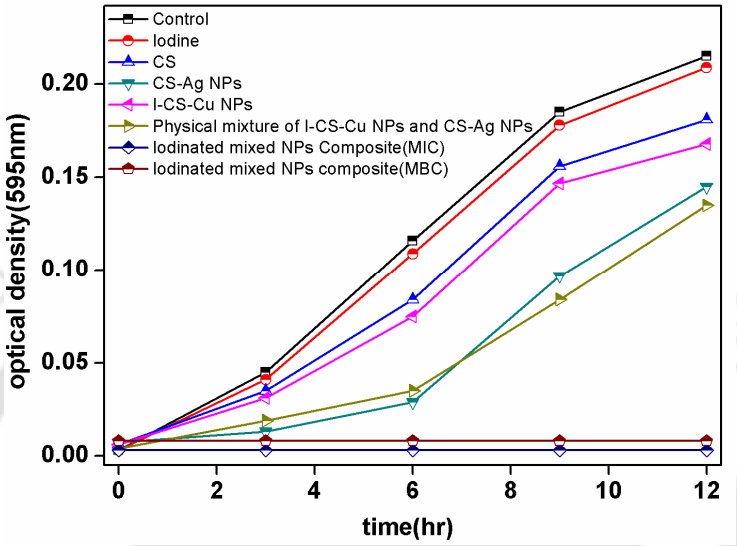

Figure 5.4: Growth curve of GFP recombinant *E. coli* in the presence of the following **Control:** 0.02 M acetic acid and 6 µL ethanol in LB media; **Iodine:** Iodine at 0.16 µg/mL. **CS:** Chitosan at 52.64 µg/mL, **CS–Ag NPs :** CS-Ag NP composite at 53.40 µg/mL **I-CS-Cu NPs:** iodinated CS-Cu NP composite at 63.20 µg/mL; **Physical mixture of I-CS-Cu NPs and CS-Ag NPs** (1:1 volume ratio) **:** Amounts of components in mixed solution CS 52.0 µg/mL, Ag 0.73 µg/mL ,Cu 5.0 µg/mL , I_2 0.08 µg/mL **I_2-CS-Ag NP-Cu NP composite-b (MIC) :** mixed Cu and Ag NPs composites at 63.50 µg/mL; and **I_2-CS-Ag NP-Cu NP composite-b (MBC):** mixed Cu and Ag NPs composites at 93.02 µg/mL.

From the results of figure 5.4 we conclude that mixed NP composite exhibited higher antibacterial activity compared to individual components at their individual concentrations (in the composite). Presumably, in the composite smaller Ag NPs and Cu NPs worked in tandem with CS and iodine for more effective antibacterial activity. Details of the MIC and MBC results for other compositions are tabulated in Table 5.3.

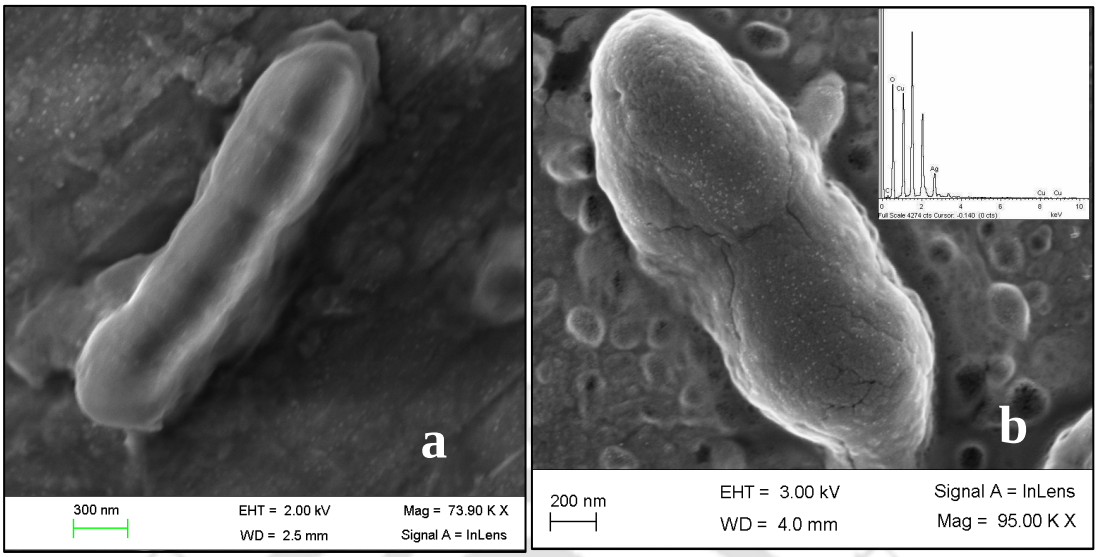

Figure 5.5: (a) Field emission scanning electron micrograph of GFP expressing recombinant *E. coli* cells and (b) *E. coli* cells treated with I_2-CS-Ag NP-Cu NP composite (63.50 µg/mL) in liquid LB medium for 4 h, in inset shows FESEM-EDX profiles, clearly indicates presence of elemental Cu and Ag corresponding sample.

Interaction of the iodinated mixed NP composite with *E. coli* was investigated by TEM and FESEM. FESEM images of both the untreated and the composite treated GFP recombinant *E. coli* are shown in Figure 5.5 (a, b). *E. coli* cells were incubated with 63.50 µg/mL of iodinated mixed NPs composite (MIC dose) in the LB medium for 4 h prior to the evaporation step required for sample preparation. While the control bacteria showed the usual surface morphology (Figures 5.5a) the treated bacteria (with composite) were found to be distinctly different with the bacterial cells covered with a layer of the composite (Figures 5.5b). In this regard, it is noteworthy that the positively charged chitosan readily attached to the negatively charged bacterial cell wall in the chitosan stabilized composites described in chapters 2, 3B and 4. Further, FESEM -EDX result (Figure 5.5b, inset) proved presence of both the elements Cu and Ag in same sample, and corresponding TEM images in Figure 5.6 a and b and showed that dark spots of particle were superimposed on the image of an *E. coli* bacterium. Small metal NPs with diameter of 13.5± 3.5 nm for Cu NPs and diameter of 4.2 ±1.0 nm for Ag NPs were clearly discernible (Appendix, Figure A. 5.5). That the two size distributions were very similar to the size distribution of the two metal NPs in the original composite (see section

5.4.1) augers well with our conclusion that the Ag and Cu NPs got attached to the bacterial cell wall, causing irreparable damage possibly by developing pores on the surface of the cell walls (Figure 5.6: a, b and Appendix, Figure A. 5.5a). Similar results were observed for chitosan stabilized Cu NPs (~15 nm) in chapter 3B and chitosan stabilized Ag NPs (~10 nm) in chapter 2 where the metal NPs were found to interact with the bacterial cell wall, inducing pore formation leading to death of the bacteria. To confirm the composition of the NPs in bacteria treated sample, EDX spectra were also taken during TEM analysis. A representative EDX profiles, taken from the sample is shown in Figure 5.6c. This spectrum confirms the presence of Cu and Ag and iodine in the composite.

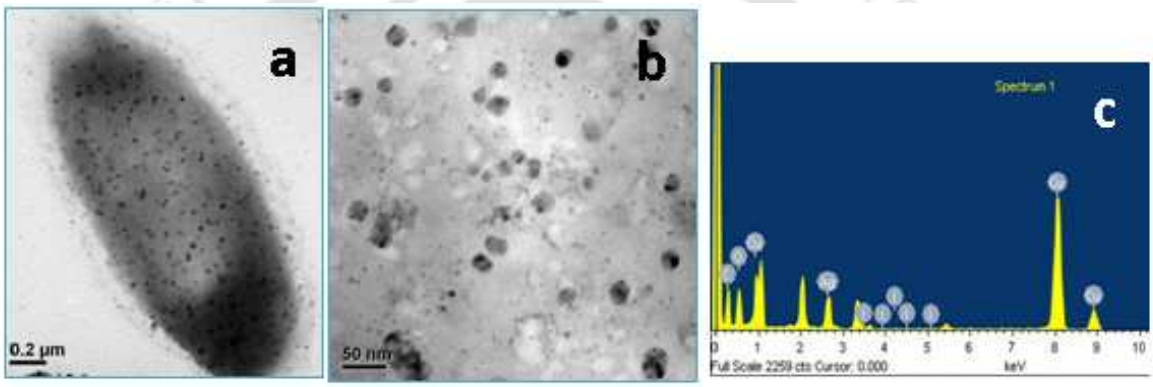

Figure 5.6: (a) Transmission electron micrograph of GFP expressing recombinant *E. coli* cells treated with 63.50 µg/mL (MIC) I_2-CS-Ag NP-Cu NP composite in liquid LB medium for 4 h. TEM micrograph clearly showing both Cu NPs (12± 3.0 nm) and Ag NPs (3.5 ± 1nm) are interacting with *E. coli* cells. In TEM-EDX profiles also shows presence of elemental Cu and Ag and iodine of composite treated samples.

We have also recorded the XRD pattern of I_2-CS-Ag NP-Cu NP composite-treated *E. coli* bacteria, where the sample was prepared 12 h after treatment. The observation in Figure 5.7 indicated that the Cu NPs and Ag NPs both present in the sample as the diffraction peaks due to (111), (200), (220) and (311) planes of Ag(0) and (111), (200), and (220) planes of Cu(0) were noted. Further, it is important to note that even after 12 hours of treatment by MIC of composite, when bacterial cell inhibition had effectively taken place, Cu NPs and Ag NPs were still present in the LB medium. This indirectly shows that the bactericidal role is being played out by the Ag and Cu NPs in the

composite, rather than the corresponding metal ions, a theme we have found consistently true in all composites studied and which have been discussed in all the earlier chapters of this thesis.

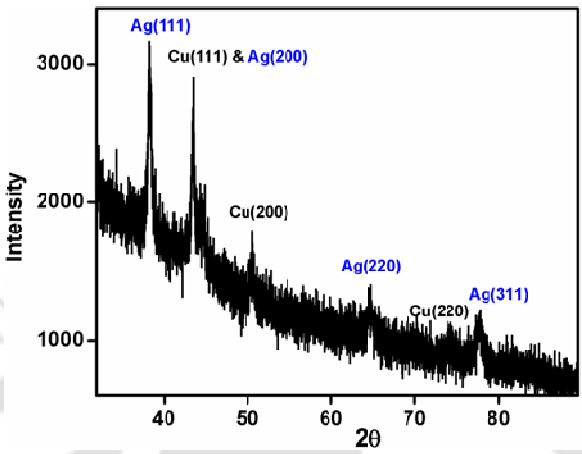

Figure 5.7: XRD of the centrifuged sample of *E. coli* bacteria treated with I_2-CS-Ag NP-Cu NP composite at Cu/Ag molar ratio 20:1 for 12 hours.

Finally in essence, the four component system i.e. chitosan, Cu NPs, Ag NPs and iodine work together for superior antibacterial activity in comparison to the individual components in the I_2-CS-Ag NP-Cu NP composite. Further, it is plausible that positively charged CS gets attached to the negatively charged bacterial cell wall; Ag and Cu NPs present in the composite create pores on the cell walls, whereas molecular iodine upon dissociation on the surfaces of Ag and Cu, in conjunction with Ag NPs induces ROS generation, thereby creating the synergy of the four-component system.

5.5: Conclusion

In summary, we have developed a novel synthetic method for the preparation of bimetallic phase separated mixed NP (Cu, Ag) composite in CS matrix. The composite material was characterized by various spectroscopic and microscopic techniques and also showed good efficacy as a bactericidal agent. Ag NPs were found to be suitably combined with Cu NPs (although as separate entities) as the composite was found to be stable for 6-7 days under ambient conditions, and which also exhibited good bactericidal

activity. TEM and FESEM experiments were carried out to elucidate the possible mechanism for the killing action of the material, and it was found that the bactericidal action is mainly via contact killing. Combining Ag NPs and Cu NPs and with natural biopolymers CS and molecular iodine enhanced bactericidal efficiency as CS got attached to the bacterial cell wall while the Cu NPs and Ag NPs in the composite turned the cell wall porous and molecular iodine upon dissociation on the metallic surfaces lead to enhancement antimicrobial activity, leading to death of bacteria at very low doses of each component.

References:

(1) Zhang, X.; Chan, K.-Y. *J. Mater. Chem.* **2002,** *12,* 1203-1206.

(2) Zhang, X.; Chan, K.-Y. Chem. Mater., **2003,** *15,* 451–459.

(3) Liu, Z.; Lee, J. Y.; Han, M.; Chen, W.; Gan, L. M. *J. Mater. Chem.* **2002**, *12,* 2453-2458.

(4) Zeng, J. H.; Lee, J. Y. *Materials Chemistry and Physics* **2007,** *104,* 336-341.

(5) Lim, B.; Kobayashi, H.; Yu, T.; Wang, J. G.; Kim, M. J.; Li, Z. Y.; Rycenga, M.; Xia, Y. *J. Am. Chem. Soc.* ***2010,*** *132,* 2506-2507.

(6) Harpeness, R.; Gedanken, A. *Langmuir* **2004,** *20,* 3431-3434.

(7) Butovsky, E.; Perelshtein, I.; Gedanken, A. *J. Mater. Chem.* **2012,** *22,* 15025-15030.

(8) Huang, X. Q.; Li, Y. J.; Zhou, H. L.; Zhong, X.; Duan, X. F.; Huang, Y. *Chem. Eur. J.* ***2012*** *,18,* 9505-9510.

(9) Li, G. P.; Luo, Y. J. *Inorg. Chem.* **2008,** 47, 360-364.

(10) Rapallo, A.; Rossi, G.; Ferrando, R.; Fortunelli, A.; Curley, B. C.; Lloyd, L. D.; Tarbuck, G. M.; Johnston, R. L . *J. Chem. Phys.* **2005,** *122,* 194308.

(11) Chowdhury, S.; Bhethanabotla, V. R.; Sen, R. *Appl. Phys. Lett.* **2009,** *95,* 131115.

(12) Tabrizi, N. S.; Xu, Q.; van der Pers, N. M.; Schmidt-Ott, A. *J. Nanopart. Res.* **2010,** *12,* 247-259.

(13) Smetana, A. B.; Klabunde, K. J.; Sorensen, C. M.; Ponce, A. A.; Mwale, B. *J. Phys. Chem. B* **2006,** *110,* 2155-2158.

(14) Valodkar, M.; Modi, S.; Pal, A.; Thakore S. *Mater. Res. Bull.* **2011,** *46,* 384–389.

(15) Taner, M.; Sayar, N.; Yulug, I. G.; Suzer S. *J. Mater. Chem.* **2011**, *21,* 13150-13154.

(16) Cazayous, M.; Langlois, C.; Oikawa, T.; Ricolleau, C.; and Sacuto, A. *Phys. Rev. B* 2006, *73,* 113402.

(17) Grouchko, M.; Kamyshny, A.; Magdassi, S. *J. Mater. Chem.* **2009**, *19,* 3057-3062.

(18) Itakura, T.; Torigoe, K.; Esumi, K. *Langmuir* **1995,** *11,* 4129-4134.

(19) Suyal, G. *Thin Solid Films* **2003,** *426,* 53-61.

(20) Woo K.; Kim, D.; Kim, J. S.; Lim, S.; Moon, J. *Langmuir* **2009,** 25, 429-433.

(21) Li, Y.-S.; Lu, Y.-C.; Chou, K.-S.; Liu, F.-J. *Mater. Res. Bull.* **2010,** *45,* 1837-1843.

(22) Kiran, P. P.; Bhaktha, B. N. S.; Rao, D. N.; De, G. *J. Appl. Phys.* **2004,** *96,* 6717-6723

(23) Grouchko, M.; Kamyshny, A.; Ben-Ami, K.; Magdassi, S. *J. Nanopart. Res.* **2009,** *11,* 713-716.

(24) Xu, Z.; Lai, E.; Shao-Horn, Y.; Hamad-Schifferli, K. *Chem. Commun.* **2012**, *48,* 5626-5628**.**

(25) McLean, R. J. C.; Hussain, A. A.; Sayer, M.; Vincent, P. J.; Hughes, D. J.; Smith, T. J. N. *Can. J. Microbiol.* **1993,** 39, 895-899.

(26) Sondi, I.; Salopek-Sondi, B. *J. Colloid Interface Sci.* **2004,** 275, (1), 177-182.

(27) Jose Ruben, M.; Jose Luis, E.; Alejandra, C.; Katherine, H.; Juan, B. K.; Jose Tapia, R. r.; Miguel Jose, Y. *Nanotechnology* **2005,** 16, 2346.

(28) Pal, S.; Tak, Y. K.; Song, J. M. *Appl. Environ. Microbiol.* **2007,** 73, 1712-1720.

(29) Gogoi, S. K.; Gopinath, P.; Paul, A.; Ramesh, A.; Ghosh, S. S.; Chattopadhyay, A. *Langmuir* **2006,** *22,* 9322-9328.

(30) Sanpui, P.; Murugadoss, A.; Prasad, P. V. D.; Ghosh, S. S.; Chattopadhyay, A. *Int. J Food Microbiol.* **2008,** *124,* 142-146.

(31) Ruparelia, J. P.; Chatterjee, A. K.; Duttagupta, S. P.; Mukherji, S *Acta Biomaterialia* **2008,** *4,* 707-716.

(32) Yoon, K. -Y.; Byeon, J. H.; Park, J. -H.; Hwang, J. *Sci. Total Environ.* **2007,** *373,* 572–575.

(33) Wei, Y.; Chen, S.; Kowalczyk, B.; Huda, S.; Gray, T. P.; Grzybowski , B. A. *J. Phys. Chem. C* **2010,** *114,* 15612-15616.

(34) Banerjee, M.; Mallick, S.; Paul, A.; Chattopadhyay, A.; Ghosh, S. S. *Langmuir* **2010**, *26,* 5901–5908.

(35) Mallick, S.; Sharma, S.; Banerjee, M.; Ghosh, S. S.; Chattopadhyay, A.; Paul, A., *ACS Appl. Mater. Interfaces* **2012,** *4,* 1313–1323.

(36) Mallick, S.; Ghosh, S. S.; Chattopadhyay, A.; Paul, A. *ACS Appl. Mater. Interfaces* Manuscript ID: am-2012-02402n (Synthesis, characterization and enhanced bactericidal action of core shell copper- silver nanoparticle composites)

(37) Feng, Q. L.; Wu, J.; Chen, G. Q.; Kim, T. N.; Kim, J. O. *J. Biomed. Mater. Res.* 2000, 52, 662–668.

(38) Borkow, G.; Gabbay, *J. Curr. Med. Chem.* 2005, *12*, 2163– 275.

(39) Cioffi, N.; Ditaranto, N.; Torsi, L.; Picca, R. A.; De Giglio, E.; Sabbatini, L.; Novello, L.; Tantillo, G.; Bleve-Zacheo, T.; Zambonin, P. G. *Anal Bioanal Chem.* **2005,** *382,* 1912-1918.

(40) Zhang, L.; Yu, J. C.; Yip, H. Y.; Li, Q.; Kwong, K. W.; Xu, A.-W.; Wong, P. K., *Langmuir* **2003,** *19,* 10372-10380.

Overview of the thesis and future prospects

In the thesis, we describe a few significant results in the area of synthesis and characterization of metal NP composites for therapeutic applications, and specifically their anti-bacterial properties. The present findings provided evidence for chitosan based NP composite materials acting as bactericidal agents. These studies represent a novel paradigm in antibacterial therapeutics, owing to the fact that they can be used against certain bacterial pathogens which have evolved mechanisms to evade the action of most commercially available antibiotics. We have synthesized iodinated CS-Ag NP composite, CS-Cu NP composite, iodinated CS-Cu NP composite, CS Cu@Ag NPs composite, I_2-CS-Ag NP-Cu NP composite and investigated their bactericidal potency against Gram positive *B. cereus* and Gram negative GFP-expressing *E. coli* bacteria. Attempts were also made to elucidate and understand the molecular mechanism of their bactericidal action. Our findings indicated the potential use of these nanocomposites in various biomedical and therapeutic applications.

Other than antimicrobial activity, iodinated CS-Ag NP composite and iodinated CS-Cu NP composite can also be active in mammalian cells. Our group has reported chitosan nanocarrier-based delivery of Ag NPs to mammalian cells for induction of apoptosis at low concentrations of Ag NPs.[1] The cytotoxic efficacy of the iodinated CS-Ag NP composite and iodinated CS-Cu NP composite systems can also be examined for use of these composite materials in cancer therapy. Further, CS Cu@Ag NPs composites were stable in solution for more than two weeks under ambient atmospheric conditions and exhibited bactericidal activity using lower concentration of Cu and Ag. These CS Cu@Ag core-shell NPs can be further tested in mammalian cells for therapeutic applications.

Because of growing environmental concerns with regard to Ag NPs, Cu NPs has received more attention in organic synthesis owing to their more environmentally benign character, easy availability and low cost. Cu NPs are attractive catalysts for chemical reactions including the reduction of CO_2 to methane or methanol, carbon-carbon bond formation reactions and carbon-heteroatom bond formation reactions. The CS-Cu NP

composite and iodinated CS-Cu NP composite can serve as active catalysts in organic synthesis. In catalytic reactions, the association of two different metals offers superior activity compare to monometallic NPs. Bimetallic Cu-Ag NPs exhibit superior catalytic activity over pure noble metal Cu NPs and Ag NPs of comparable sizes.[2] Newly prepared bimetallic CS Cu@Ag NPs composite can also be used as catalyst in various organic reactions. Core-shell Cu@Ag NPs are resistant to corrosion and oxidation. Hence CS Cu@Ag NP dispersions can possibly be used as inject ink for conductive and decorative patterns on metallic surfaces.

I_2-CS-Ag NP-Cu NP composites were synthesized using CS as a stabilizer. Mixed NP composites achieved oxidation stability through presence of Ag and iodine. Mixed NP composite had higher antibacterial activity compared to individually used Cu NPs and Ag NPs or their core- shell structure. Apparently smaller quantities of Ag NPs and Cu NPs worked together along with antibacterial components CS and iodine yielding overall antibacterial activity of the composite. Iodinated mixed NP (in chitosan) dispersions can also be used as colloid ink for writing on substrates such as conducting lines. Mixed NPs could be used as highly active SERS substrates as larger extinction coefficient of Ag NPs will help to significantly enhance the SERS signals, when an appropriate SERS active molecule is immobilized on the NPs surface.

The CS-metal NP composite materials and iodinated CS-metal NP composite materials can be used to prepare antibacterial food packaging materials and food storage equipment. They can also be used as ingredient for preparation of antibacterial paints and coating for household materials. Iodine doped CS-Ag NP composite, CS-Cu NP composite, iodinated CS-Cu NP composite, CS Cu@Ag NPs composite, CS supported iodinated mixed NP composites may replace at least some traditional antibiotics or medicine to destroy pathogenic bacteria in the gastrointestinal tracts. Scaffolds can also be made from these iodinated CS-metal NPs composite materials for wound dressing application. Finally, we do hope that through the efforts of last five years of mine, a small contribution has been made for the development of latest of science and technology, which would be applicable for the betterment of humanity.

References:

(1) Sanpui, P.; Chattopadhyay, A.; Ghosh, S. S. *ACS Appl. Mater. Interfaces* **2011,** *3,* 218-228.

(2) Shen, S.; Zhuang, J.; Yang, Y.; Wang, X. *Nanoscale* **2011,** *3*, 272–279.

Appendix

Chapter 2

Bactericidal activity of the iodinated composite in the presence of NaCl

The bactericidal activity of the iodinated chitosan-Ag NP composite in the absence of Ag^+ was determined by taking five centrifuge tubes containing water, $AgNO_3$ (10^{-4}M), NaCl, NaCl added to $AgNO_3$ (10^{-4}M), iodinated composite (MIC) and NaCl added to MIC of composite respectively. These samples were stirred in a vortex shaker, centrifuged and then the supernatant was added to five fresh LB ampicillin media containing bacterial cell suspension.

Role of Ag^+ ions in the bactericidal activity of the iodinated composite

The results showed no bacterial growth after treatment with iodinated composite alone (MIC) or iodinated composite added with NaCl. If Ag^+ would have been the major contributor to the bactericidal activity of the composite, little or no activity would be found when NaCl was present. This was not the case here. On the other hand when NaCl was added to $AgNO_3$, almost no inhibition to bacterial growth was observed (Figure A1.1).This shows that Ag ions, if at all, present in the iodinated composite have little or no effect on the bactericidal potency of the composite.

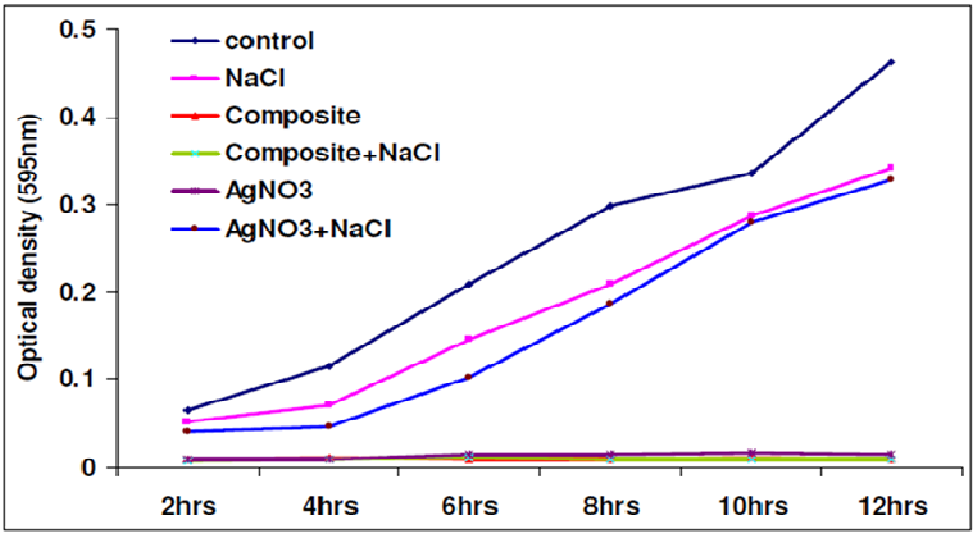

Figure A. 2.1: Effect of bactericidal potency of iodinated composite and $AgNO_3$, in Presence and absence of NaCl

Effect of iodinated chitosan-Ag NP composite on DNA

The reactive oxygen species produced inside the bacterial cells along with the chitosan, Ag NP and iodine can have direct effect on both DNA and protein. Supercoiled circular DNA allows the detection of structural alteration such as strand break or damaged bases easily by separating the supercoiled form (form I), nicked relaxed form (form II) and linear form (form III) by agarose gel electrophoresis. It was interesting to observe that there was no change in band pattern of plasmid DNA from GFP-expressing recombinant E. coli (Dh5α) treated with Ag NP or iodine separately. Surprisingly, when exposed to the iodinated composite, plasmid DNA showed no band at all times of observations since the mixing of DNA with the iodinated composite. The reason may be due to attachment of DNA to the composite by electrostatic interactions, because of which migration of the DNA was not possible. Binding of chitosan with DNA and inhibition of mRNA synthesis have been reported to be occurring through chitosan penetration toward the nuclei of the microorganisms and interference with the synthesis of mRNA and proteins.[1] However, chitosan would not, normally be able to reach a cytoplasmic target, unless it is able to circumvent the plasma membrane.

Chapter 3A

Synthesis of the CS-Cu NP composite in absence of hydrazine hydrate

50 mg of chitosan and 40 mg of copper (II) sulphate pentahydrate were added to 50 mL Milli-Q grade water in a 100 mL round bottom flask placed in an oil bath with vigorous stirring and refluxed for 20 min at ~ 100^0C resulting in a light blue colored solution. To this 0.6 mL of 0.6 M NaOH was added upon which the color of the solution turned brown. The reaction was allowed to continue for an additional 1 h which remained brown. The solution along with the precipitate was centrifuged at 5300 rpm and the precipitate was washed with milli-Q grade water and made into a pellet. The pellet was redispersed in 20 mL of 0.25% aqueous acetic acid solution. UV-visible spectra of the brown dispersion were measured using a Hitachi U 2900 spectrophotometer. The solution absorbs at 738 nm (Figure A. 3A.1a) while Cu NPs absorb at around 591nm.

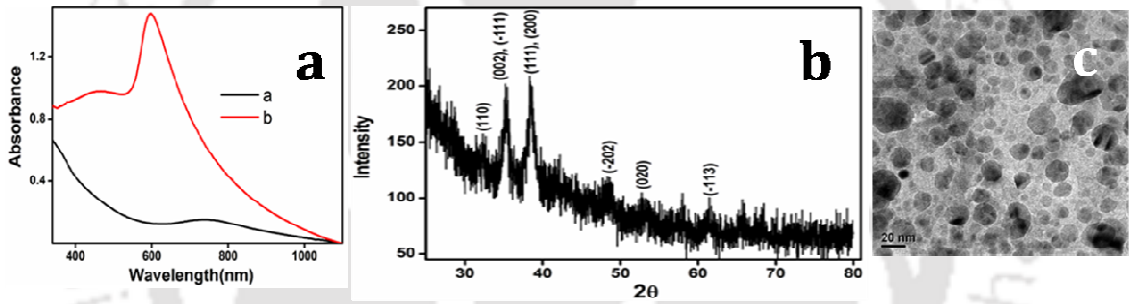

Figure A. 3A.1: (a) UV-Vis spectra of composite prepared (a) in absence of hydrazine hydrate (b) in presence of hydrazine hydrate. **(b)** XRD pattern and **(c)** TEM image of the solution corresponding to curve 'a' in the UV-visible spectra (A).

Further characterization was done by powder XRD and TEM (Figure A. 3A.1 b, c). The peaks at 2θ values of 32.4°, 35.4°, 38.6°, 48.5°, 53.2° and 61.5° in Figure A. 3A.1b correspond to the crystal planes of (1 1 0), (0 0 2), (−1 1 1), (1 1 1), (2 0 0), (−2 0 2), (0 2 0), (−1 1 3), respectively for crystalline cupric oxide. Both planes (0 0 2)/(−1 1 1), and (1 1 1)/(2 0 0) are too close to be identifiable. The XRD pattern of the composite matched with the standard powder diffraction data file for cupric oxide (monoclinic, JCPDS file No. 05–0661). The presence of cuprous oxide (Cu_2O) and Cu NPs was not detected in the diffraction. TEM images in Figure A. 3A.1C show that particles between 5-20 nm are formed. We conclude that in absence of hydrazine hydrate, instead of Cu

NPs, cupric oxide (CuO) monoclinic phase NPs are formed in the composite. Hence chitosan is unable to reduce $CuSO_4$ solution to Cu NPs.

Time evolution of CS-Cu NP and iodinated CS-Cu NP composites

Freshly prepared CS-Cu NP composite and iodinated CS-Cu NP composites showed prominent Plasmon resonance peaks in the UV-Visible spectrum, as shown in Figure A. 3A.2a and Figure A. 3A.2b respectively, confirming the formation of Cu NPs in these composites. However, while the non-iodinated composite sample (Figure A. 3A.2a) spectra rapidly broadened within one or two days, the iodinated composite sample broadened slowly (Figure A. 3A.2b) in ~ 5-6 days, showing that the presence of iodine increased the stability of the formed Cu NP in the chitosan matrix. As discussed in Chapter 3A presence of iodine also affects the size and shape of Cu NP formed in the fresh composite sample, i.e. the shapes were spherical and sizes were smaller in presence of iodine as opposed to polygonal (and larger sizes) in absence of iodine.

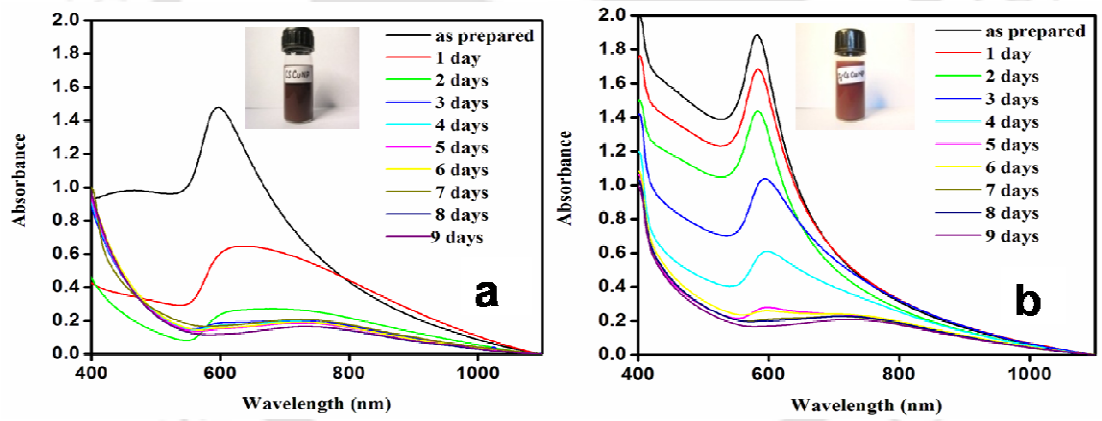

Figure A. 3A.2: UV-Vis spectra of **(a)** CS-Cu NPs solution, **(b)** iodinated CS - Cu NPs solution aged to different times as indicated. The insets show photographs of 12 hour old samples of the corresponding composites.

The reason for broadening in both the composite samples appears to be due to oxidation and agglomeration of the Cu NPs and is discussed in Chapter 3A. In absence of iodine, all of the Cu NPs agglomerated to give highly fused polygonal Cu NPs of hundreds of nm sizes as evidenced from TEM images of 10 day old sample of CS-Cu NP in Figure A2.3b. That the agglomerated structures are still due to Cu is confirmed by XRD studies in Figure A. 3A.3a. In the presence of iodine, however oxidation was prevented and

aggregation of Cu NP was limited to few Cu NP and most of them remain well separated in the chitosan matrix as discussed in Chapter 3A (Figure A. 3A.3 b). However, iodine slowly reacts with the Cu NPs to form CuI as evidenced from TEM and XRD studies and is discussed in Chapter3A. Chitosan remains chemically unaltered in presence of Cu NPs as well as in presence of molecular iodine as evidenced from FTIR measurements (Figure A. 3A.4). This is consistent with the fact that the interaction of Cu NP with the chitosan is electrostatic in nature as is true to other metal nanoparticles loaded onto the polymer matrix. The solution of CS-Cu NP composite was kept for 10 days, after that solution was centrifuged at 5300 rpm and the pellet was washed with milli-Q grade water and kept under vacuum before XRD analysis.

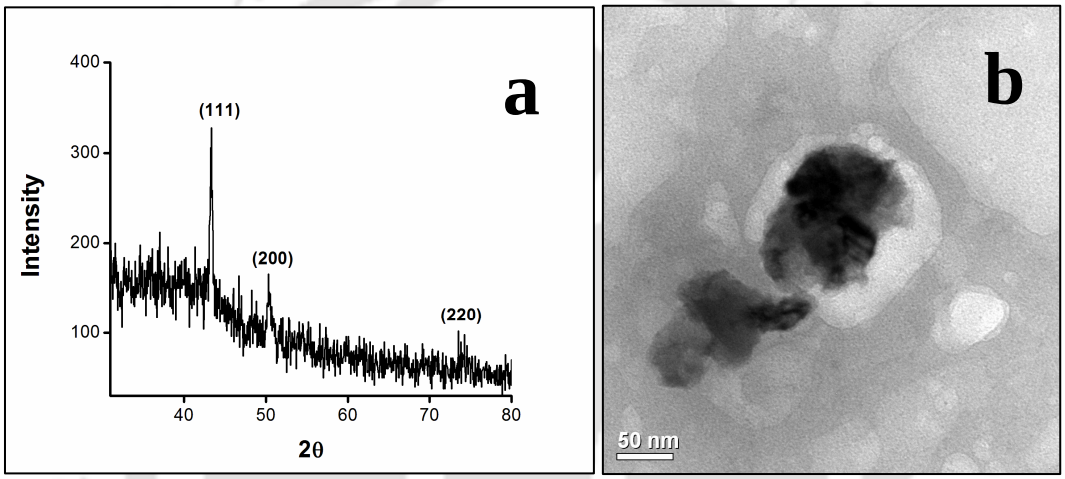

Figure A. 3A.3: **(a)** XRD pattern of 10 day old CS-Cu NP composite. **(b)** TEM image of CS-Cu NP composite of 10 day old sample.

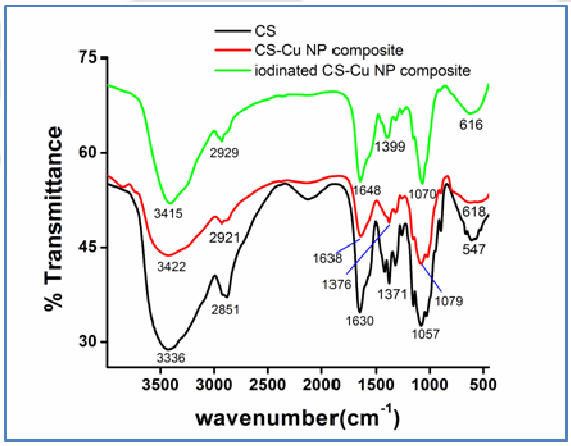

Figure A. 3A.4: FTIR spectra of CS, CS-Cu NP composite and iodinated CS-Cu NP composite.

Chapter 3B

Growth curve of GFP recombinant *E. coli* for various samples

To understand better the role of components in the bactericidal properties of the I-CS-Cu NPs (MIC) sample, we have carried out growth curve studies of various samples at various concentrations and this is shown in Figure A. 3B.1**.** The results indicated that the composite (iodine-CS-Cu NP) at concentrations greater than or equal to that of MIC was effective in inhibiting the growth or killing bacteria. On the other hand, individual components or the composite in the absence of iodine were either ineffective or were of limited efficacy in annihilating the bacterial population.

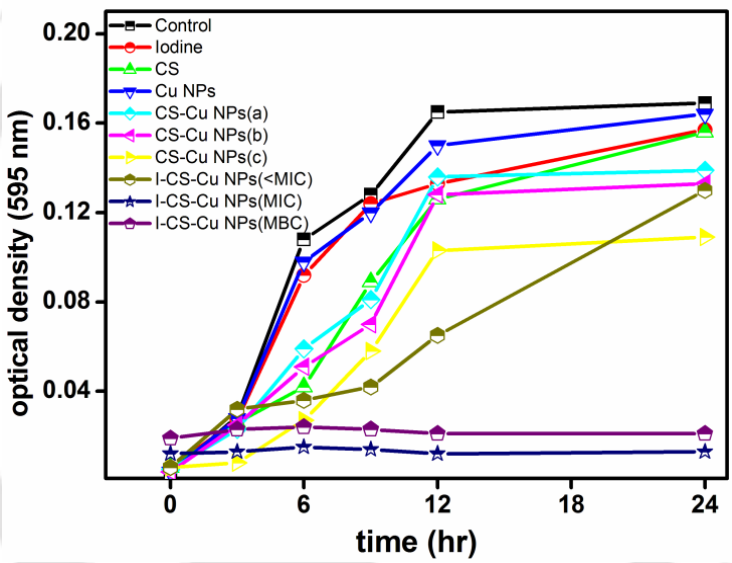

Figure A. 3B.1*: Growth* curve of GFP recombinant *E. coli* in the presence of the following (as also indicated in the legends). **Control**: 0.02 M acetic acid and 6 µl ethanol only in LB media; **I-CS - Cu NPs (<MIC)** : iodinated CS-Cu NP composite at 95.24 µg/mL; **I-CS - Cu NPs (MIC)**: iodinated CS-Cu NP composite at 130.84 µg/mL; **I-CS - Cu NPs (MBC)**: iodinated CS-Cu NP composite at 239.4 µg/mL; **CS - Cu NPs (a)**: CS - Cu NPs at composite 92.89 µg/mL ; **CS - Cu NPs (b)**: CS - Cu NPs composite at 127.62 µg/mL; and **CS - Cu NPs (c)**: CS - Cu NPs composite at 235.5 µg/mL, **CS**: Chitosan at 106.07 µg/mL, **Iodine**: Iodine at 3.22 µg/mL. **Cu NPs**: Cu NPs at 21.55 µg/mL.

Dilution experiments:

We have also performed dilution experiments (Table A.3B.1) on GFP expressing recombinant *E. coli* bacteria using MBC dose (239.4µg/mL) of I-CS-Cu NPs composites

which contained 39.43µg/mL of Cu NPs. An LB broth containing 10^8cfu/mL of the bacteria was diluted serially in sterile LB broth. Each diluted *E. coli* sample was supplemented with same amount of I-CS-Cu NPs composite (239.4 µg/mL) and incubated at 37°C. After 12 h from each tube, 100 µL of the mixture was spread on LB agar plate and incubated for 24 h at 37°C. Then the number of colonies was counted. The counts on three plates corresponding to a particular sample were averaged and reported in Table1. Only few colonies were found when concentration of *E .coli* was 10^8 cfu/mL and 10^7 cfu/mL. At all other dilutions there was no colony growth in LB agar plate. This result corroborated with earlier result which we obtained by the turbidity test.

Table A.3B.1. Dilution experiments on *E. coli* using MBC dose of I-CS-Cu NPs composite

E .coli (cfu/mL)	10^8	10^7	10^6	10^5	10^4	10^3	10^2	10	10^{-1}
Number of colonies	56	11	0	0	0	0	0	0	0

Role of Cu ions in the bactericidal activity of the iodinated CS-Cu NP composite:

AAS studies indicate that the concentration of Cu^{2+} ions released from the iodinated CS-Cu NP composite varies from 17.8 ppm in 75 minutes to 46 ppm in ~ 5 days (Figure A.3B.2a). Growth curve analysis in presence of different concentration of Cu ions which leached from iodinated CS-Cu NP composite, CS-Cu NP composite, Cu NPs after 2 h of treatment on *E. coli* as measured from AAS study and that of a control experiment without copper ions and it was found that there was no retardation of bacterial growth due to Cu ions (Figure A.3B.2b). This indicates that Cu ions that release from the composite did not contribute largely to the bactericidal activity of the composite. These shows that Cu ions released from iodinated CS-Cu NP composite have little or no effect on the bactericidal potency of the composite.

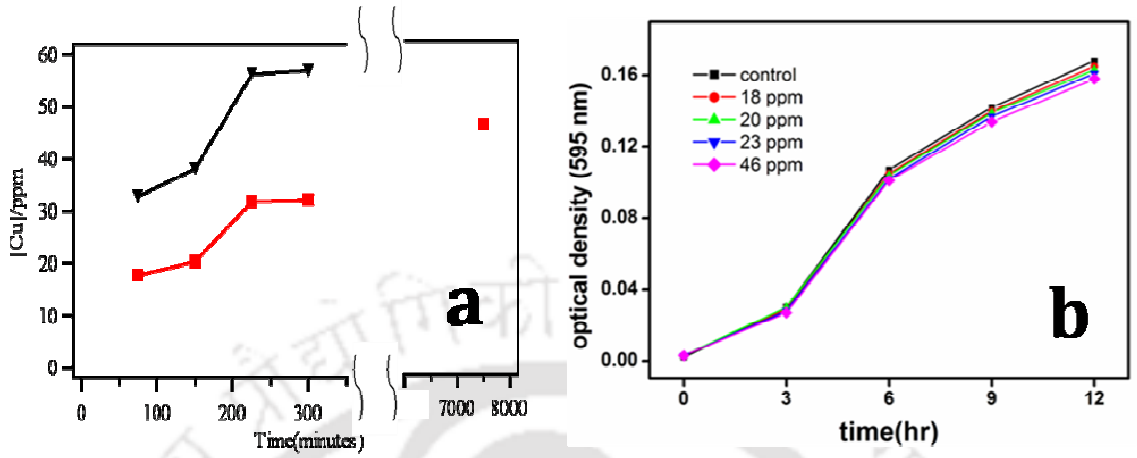

Figure A.3B.2:(a) AAS of freshly prepared iodinated CS-Cu NP showing the time dependent release of Cu^{2+} ions in aqueous solution at MIC dose 130.84µg/mL (■)and MBC dose 239.4 µg/mL of the composite (▼). **(b)** Growth of *E. coli* in presence of different concentration of Cu ions and that of a control experiment without Cu ions.

Time-dependent fluorescence microscopic monitoring of growth of GFP recombinant *E. coli*

Figure A.3B. 3 shows images of cell population among untreated bacteria (control, A-1, 2, 3, 4) and bacteria treated with iodinated CS-Cu NP in MIC (B-1, 2, 3, 4) dose and MBC (C-1, 2, 3, 4) respectively at different time intervals (3, 6, 9 and 12 h). As are apparent in the images, even at 3 h there was considerable difference in bacterial cell population in control (higher) in comparison to MIC. At 6 h and 12 h, the bacterial population showed continuous growth in control whereas in iodinated CS-Cu NP treated sample considerable loss of population had occurred.

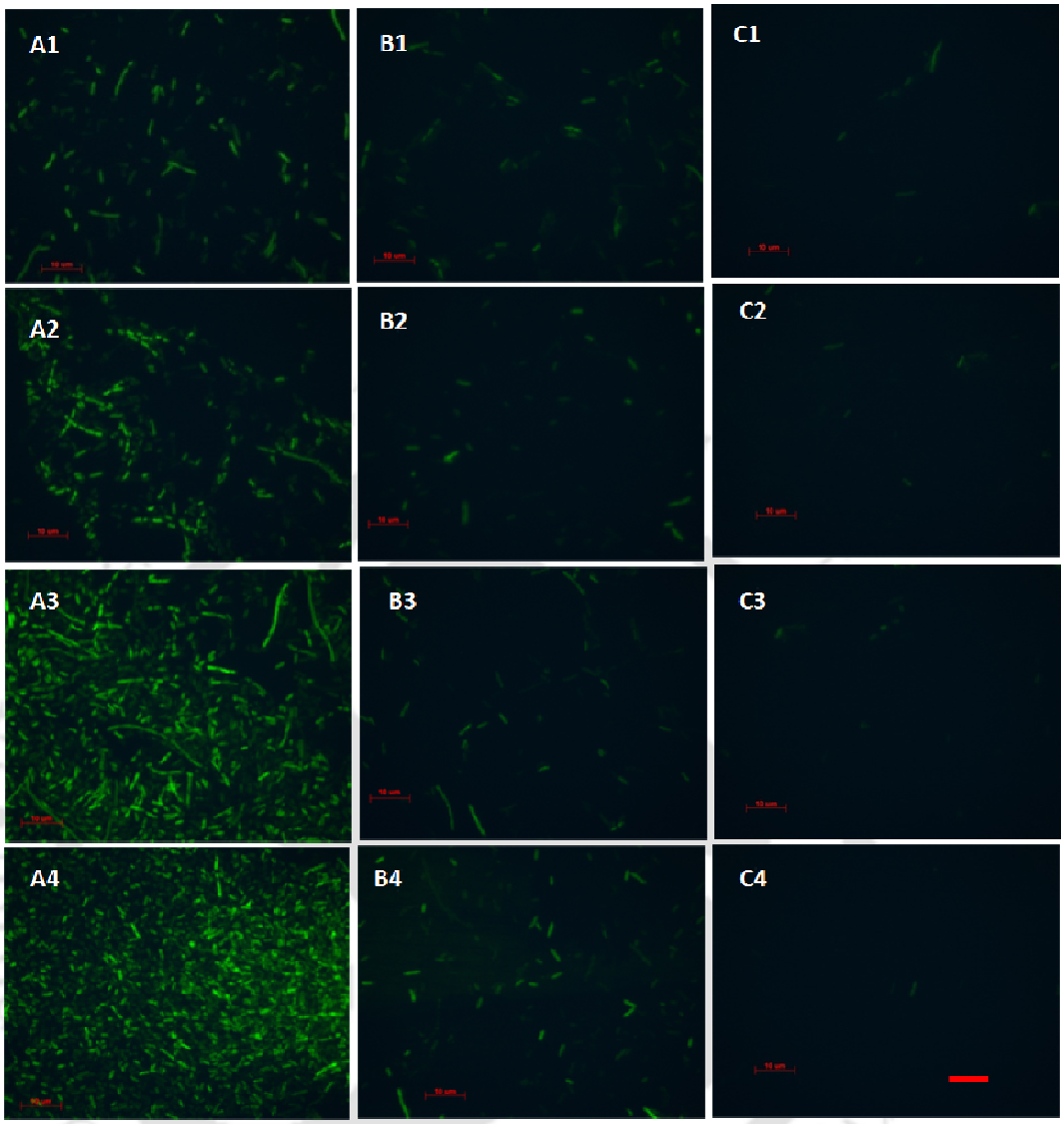

Figure A.3B. 3*:*Time-dependent fluorescence micrographs of GFP recombinant *E. coli* Series **A**, **B** and **C** refer to the control, treated with MIC (130.84 µg/mL) and MBC (239.4 µg/mL) of the iodinated CS -Cu NP composite, respectively while series **1**, **2**, **3**, and **4** refer to the samples at 3, 6, 9 and 12 h time points, respectively. Scale bars are 10 µm.

Interaction of composite with cell wall

TEM images (Figure A. 3B.4a) clearly showed dark spots attached on the cell wall when bacteria were treated with iodinated CS-Cu NP composite. Further selected area electron diffraction (SAED) confirmed that the dark spots were due to Cu NPs (Figure A. 3B.4b)

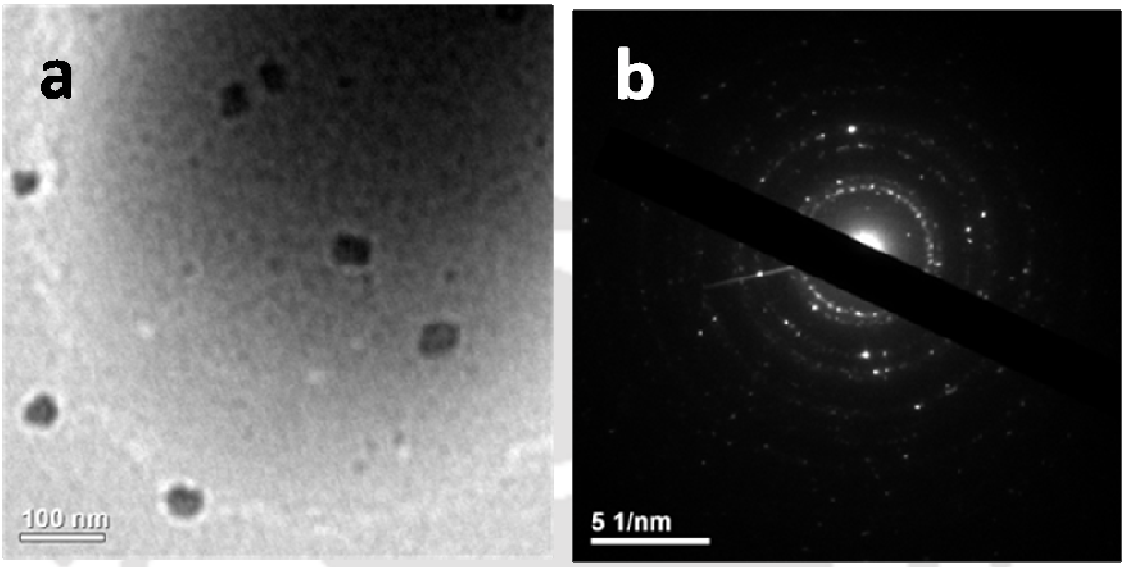

Figure A. 3B.4*:* (a) TEM image of iodinated CS-Cu NP composite attached on *E. coli* bacteria, and **(b)** corresponding SAED.

Fate of the composite during antibacterial studies:

In order to delineate the role of Cu NP as well as Cu^{2+} ions of the composite in inhibiting the growth of *E. coli*, we have centrifuged a bacterial growth culture treated with MIC of iodinated CS-Cu NP after 4 hours and measured its XRD as shown in Figure A. 3B.5. XRD showed that even after 4 hours when most of the cell inhibition has effectively taken place, Cu NPs are still present in the medium. There is no trace of CuO or Cu_2O is visible in the sample. In addition, there are trace amounts of CuI.

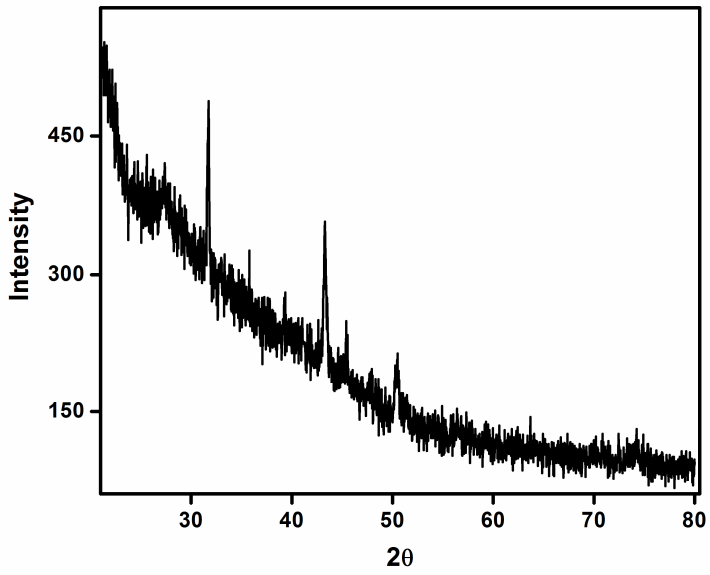

Figure A. 3B. 5*:* XRD of the centrifuged sample of *E. coli* bacteria treated with MIC of iodinated CS-Cu NP composite for 4 hours.

Effect of iodinated CS-Cu NP composite on the Bacterial DNA

Chitosan, Cu NP and iodine can have direct effect on both DNA and protein. Supercoiled circular DNA allows the easy detection of structural alteration such as strand break or damaged bases by separating the supercoiled form (form I), nicked relaxed form (form II) and linear form (form III) by agarose gel electrophoresis. Results (Figure A. 3B.6) showed that plasmid DNA, when exposed to iodinated CS-Cu NP composite, showed no band at all time points. The reason could be due to attachment of DNA to the chitosan present in the composite by electrostatic interactions and subsequent complex formation, because of which migration of the DNA during gel electrophoresis was not possible. Binding of chitosan with DNA and inhibition of mRNA synthesis have been reported to be occurring through chitosan penetration toward the nuclei of the microorganisms and interference with the synthesis of mRNA and proteins,[1] which could well have been the case here, as also revealed by other experiments.

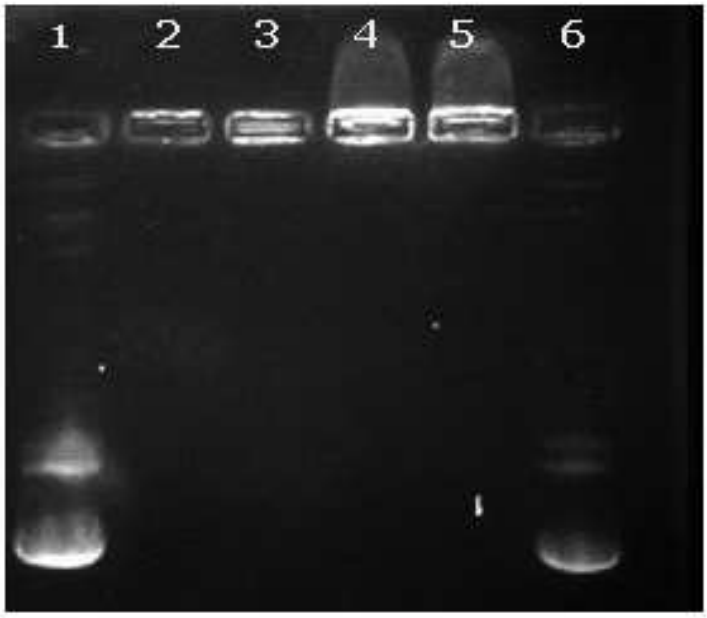

Figure A. 3B.6*:* Agarose gel electrophoresis of plasmid DNA treated with iodinated CS-Cu NP composite. Key: lanes 1 and 6 were due to control DNA; lanes 2 and 3 were due to DNA incubated with the composite at130.84µg/mL for 2 h and 4 h respectively; lanes 4 and 5 were due to DNA incubated with the composite at 186.91µg/mL for 2 h and 4 h respectively.

Chapter 4

Transmission electron microscopy (TEM) analysis of CS-Cu NPs seed particles

We had synthesized of Cu NPs seed particles in the presence of CS under normal atmospheric conditions. The reddish solid produced from the reaction of alkaline CuSO4 and hydrazine (in the presence of CS) was separated from the reaction mixture and then redispersed in water in the presence of acetic acid. TEM image of these CS-Cu NPs used are shown in Figure A. 4.1.

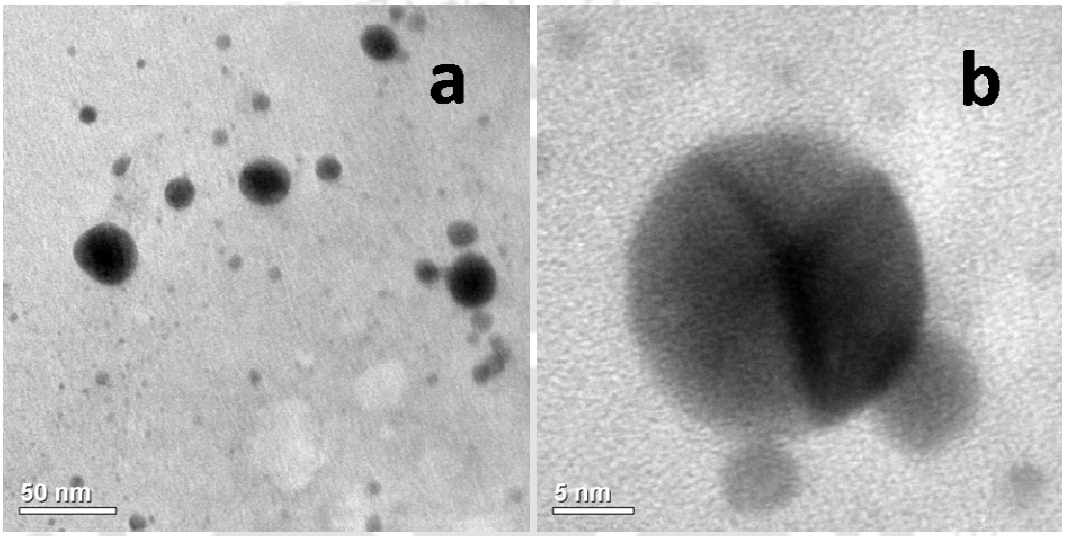

Figure A. 4.1: TEM image of freshly prepared Cu NP seed particles, HRTEM image of Cu NP seed particles.

Fourier transforms infrared spectroscopy (FTIR)

FTIR spectra of CS and CS Cu@Ag NP are shown in Figure A. 4.2. In FTIR spectrum of CS, the broad peak at 3434 cm^{-1} is characteristic of N−H stretching and OH stretching vibrations, while the peak at 1644 cm^{-1} is attributed to carbonyl (-C=O) stretching band of the $CONH_2$ group. In native CS the characteristic peaks at 1418 cm^{-1}, 1383 cm^{-1} are assigned to the CH_3 symmetrical deformation mode and 1314 cm^{-1} is C-N stretching vibration in N-acetyl glucosamine unit. A shift from 3434 cm^{-1} to 3428 cm^{-1} and 1644 cm^{-1} to 1639 cm^{-1} and band broadening indicates that amino (-NH_2) and hydroxyl (-OH) groups are involved to stabilized Cu@Ag nanoparticles. The peak of 1080 cm^{-1} in native CS was shifted to 1067 cm^{-1} in CS stabilized Cu@Ag NPs. This peak is related with the symmetric stretching vibration of C-O-C. The interaction between CS

matrix and metal nanoparticle (Cu@Ag) should lead to the shift of the peak in CS stabilized Cu@Ag NPs.

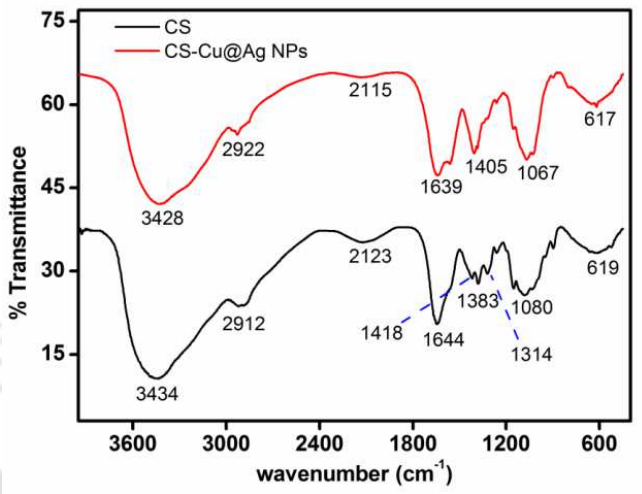

Figure A. 4.2: FTIR spectra of CS, and CS Cu@Ag NPs composite.

X-ray diffraction studies:

The X-ray diffraction (XRD) pattern of freshly prepared CS Cu@Ag NPs composite (Figure A. 4.3a) showed distinct diffraction peaks assigned face-centered-cubic (FCC) crystal planes of Ag (0); this confirms the formation of metallic shell (Ag) in the CS-Cu@Ag NPs composite. The diffraction pattern of the composite was in agreement with the metallic Ag (JCPDS-04-0783), except that the 2θ values were shifted to slightly higher values indicating a slight decrease in the spacing of the corresponding lattice planes of Ag core–shell Cu@Ag metal NPs. The X-ray diffraction (XRD) pattern of CS-Cu NPs seed (Figure A. 4.3b) showed distinct diffraction peaks assigned face-centered-cubic (FCC) crystal planes of Cu (0). These CS-Cu NPs used as a seed particle for synthesis of core-shell CS-Cu@Ag NPs composite.

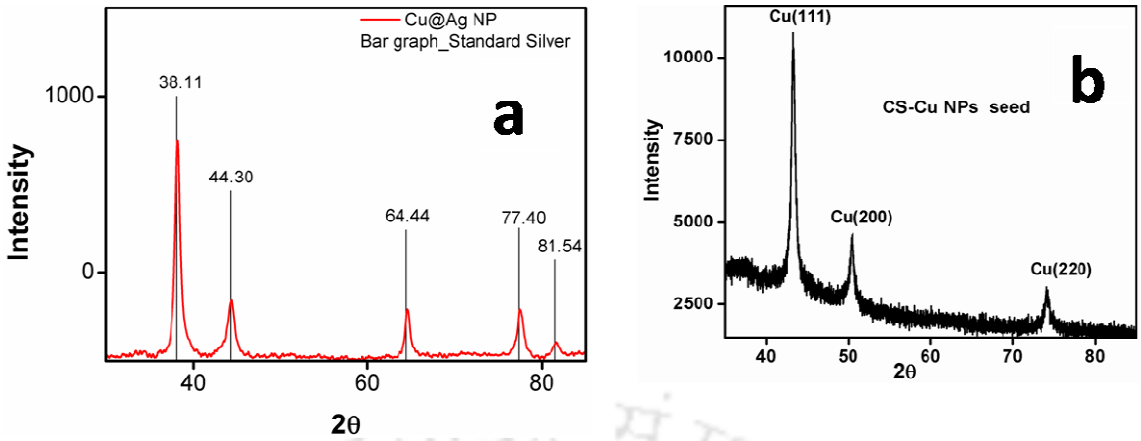

Figure A. 4.3: (a) XRD pattern of freshly prepared CS Cu@Ag NPs composite and its comparison with standard planes of pure Ag (JCPDS-04-0783).The slight shift in the observed peaks is due the dynamical diffraction state of the Ag shell. **(b)** XRD pattern of CS Cu NPs which used as seed particles.

Fate of CS Cu@Ag NPs composite in longer period of time:

Freshly synthesized CS Cu@Ag NPs composite showed Plasmon resonance peaks at 417 nm, as shown in Figure A. 4.4a affirming the formation of Ag shell in CS Cu@Ag NPs composites. The CS Cu@Ag NPs sample absorbance decreases slowly (Figure A. 4.4a) in 15 days. This shows that CS-Cu@Ag NPs were stable for at least 15 days in aqueous solution under ambient conditions. X-ray diffraction (XRD) pattern of 15 days old sample also showed distinct diffraction peaks which are fcc crystal planes of Ag (0) (Figure A. 4.4b). It may be noted that for XRD, the solution of CS Cu@Ag NP composite was kept for 15 days, after which it was centrifuged at 20,000 rpm and the pellet washed with milli-Q grade water, vacuum dried and kept under vacuum before analysis.

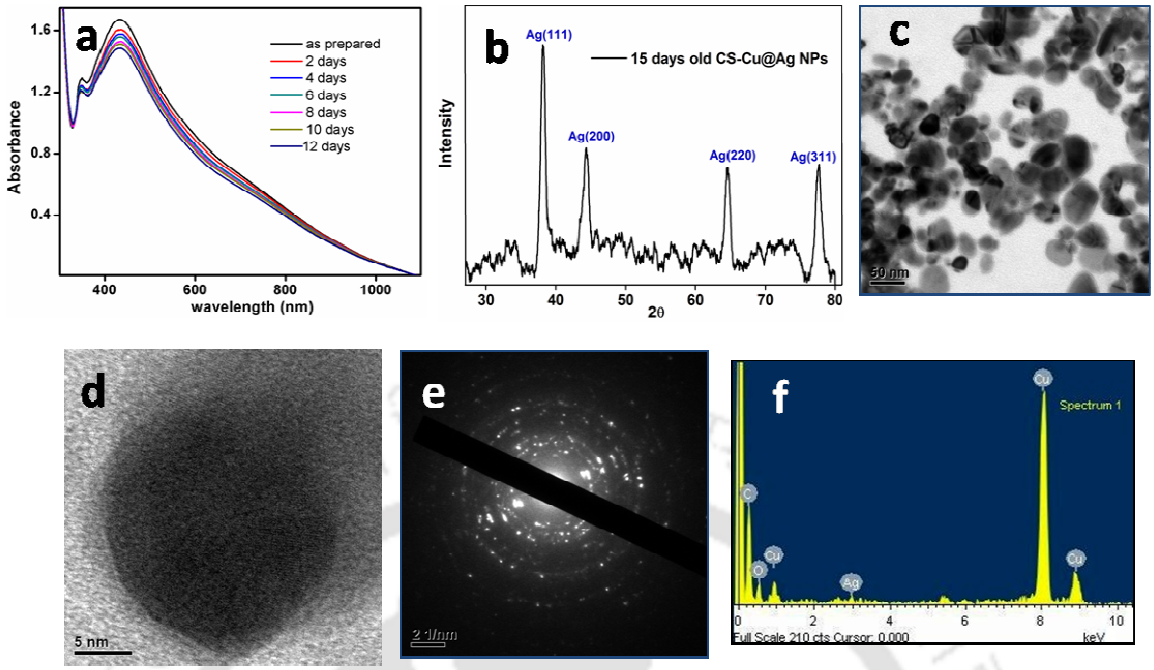

Figure A. 4.4: (a) UV-Vis spectra of CS Cu@Ag NPs solution aged to different times as indicated. **(b)** XRD pattern of 15 days old CS-Cu@Ag NPs composite. **(c, d,)** TEM, HRTEM micrograph of 20 days old CS Cu@Ag nanoparticles **(e)** Selected area diffraction (SAED) pattern of core-shell Cu@Ag NPs. **(f)** TEM-EDX result of CS Cu@Ag NPs composite shows presence of elemental copper and silver.

XPS analysis of CS-Cu@Ag NPs composite:

The chemical states of elements in CS Cu@Ag NPs composites were checked by XPS. Figure A. 4.5 shows the representative survey of XP spectra of of CS Cu@Ag NPs composite samples before sputtered and after sputtered.

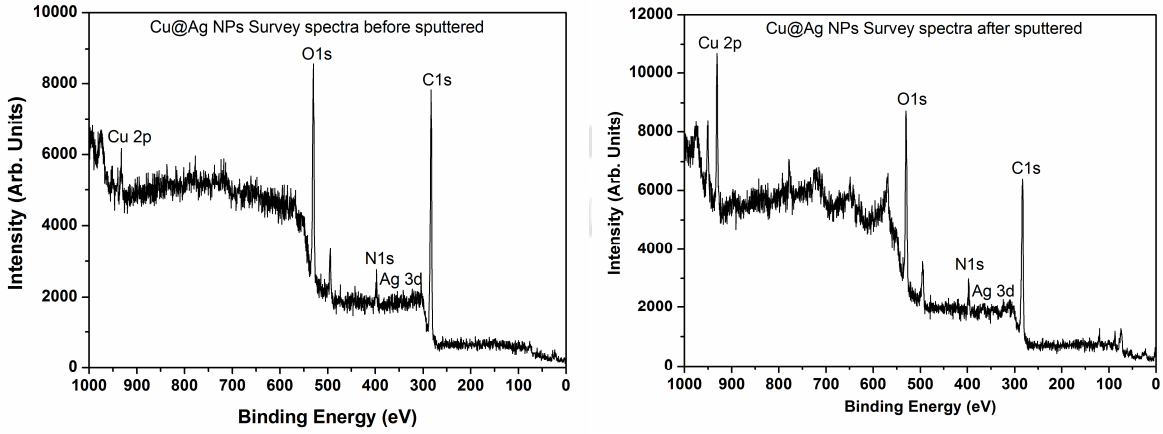

Figure A. 4.5: Wide-scan XPS survey spectra of CS Cu@Ag NPs composite samples before sputtered and after sputtered.

Interaction of CS Cu@Ag NPs composite with cell wall

TEM images showed the presence of dark spots in the freshly prepared CS Cu@Ag NPs composite samples and in CS Cu@Ag NPs composite samples attached to *E. coli* cell wall. The size distribution of the Cu@Ag NPs in the above two cases are shown below (Figure A. 4.5). It can be seen that the size distribution of the NPs does not change upon attachment of the composite to the bacterial cell membrane (Figure A. 4.5a, 4.54b).

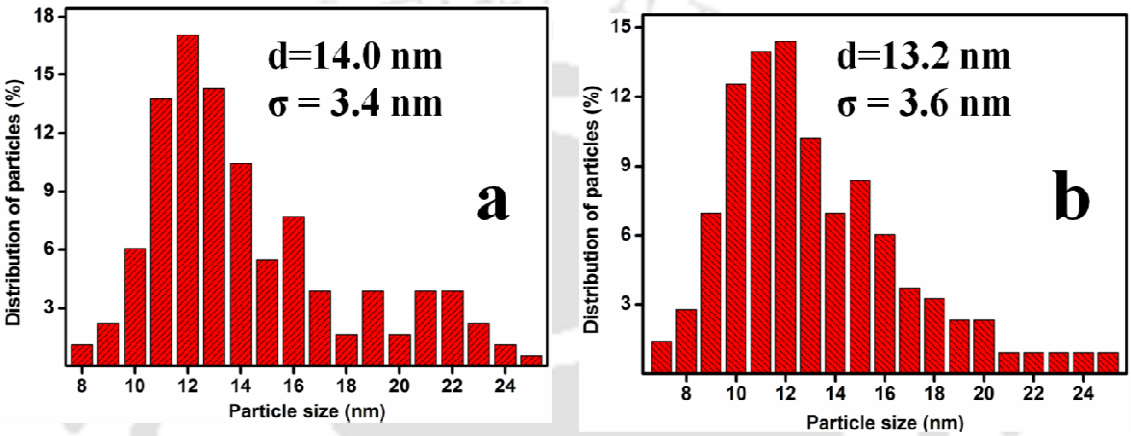

Figure A. 4.6: (a) CS Cu@Ag NPs size distribution from TEM images before bacteria treatment and average size is 14.0±3.4 nm **(b)** CS Cu@Ag NPs size distribution from TEM images when particles attached on *E. coli* bacteria and average size is 13.2 ± 3.6 nm.

Chapter 5

Time evolution of iodinated mixed NPs composite at various molar ratio of Cu to Ag

Freshly prepared I_2-CS-Ag NP-Cu NP composite showed two sharp peaks around 415 nm and 585 nm confirming the formation of Ag NP and Cu NPs. These peak positions varied between 410-420 nm and 575-595 depending on molar feed ratio of Cu to Ag as shown in Figure 5.1 and Figures A. 5.1(a-d). Spectra in Figure A. 5.1(a-d) also show the time evolution of the UV visible spectrum indicative of the stability of the NPs is the respective composite.

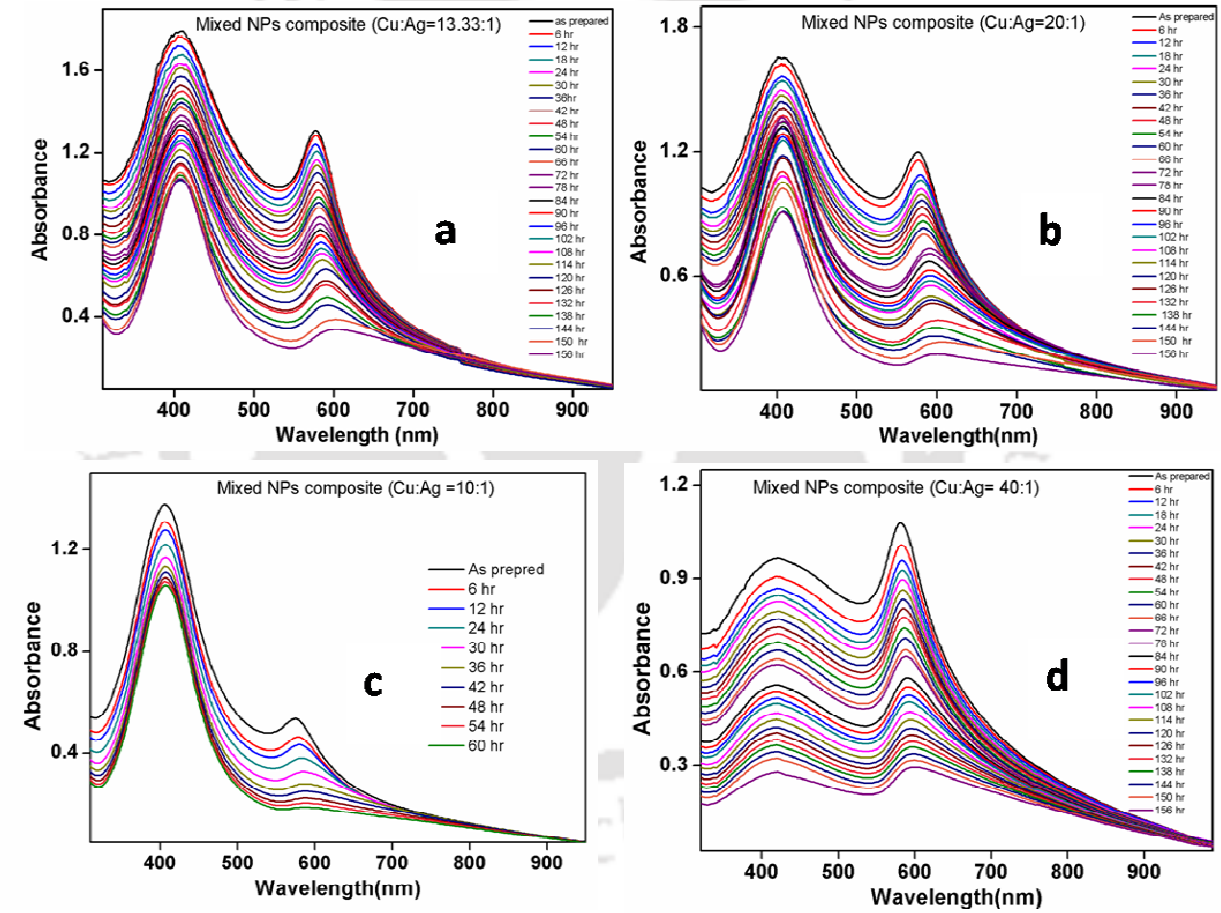

Figure A. 5.1: UV-Vis spectra of I_2-CS-Ag NP-Cu NP composite, **(a)** Cu/Ag molar feed ratios 13.3:1(**b)** Cu/ Ag molar feed ratios 20:1 **(c)** Cu/Ag molar feed ratios 10:1 **(d)** Cu/ Ag molar feed ratios 40:1 aged to different times as indicated.

It was found that the I_2-CS-Ag NP-Cu NP composites are more stable when Cu/ Ag molar feed ratios were 13.33:1 and 20:1 where the SPR bands corresponding to both Cu NPs and Ag NPs broadened slowly in ~ 6-7 days (Figure A. 5.1a and b).

However time evolution of UV-visible spectrum for I_2-CS-Ag NP-Cu NP composite with Cu/ Ag molar feed ratios 10:1 (20 mg of copper (II) sulphate pentahydrate and 400 µL of 20 mM $AgNO_3$ in 50 mg CS and 300µl 0.02 M iodine) showed that the Cu NPs SPR peaks rapidly (within 48 hrs) broadened whereas the Ag NPs SPR peaks remained almost same in the same time scale. The reason for broadening of Cu NPs SPR peaks appears due to oxidation and agglomeration of the Cu NPs. In the composites when Cu/ Ag molar feed ratio is 40:1, the UV-visible spectrum showed that the Cu NPs SPR peaks broadened slowly but that the Ag NPs SPR peaks broadened and decreased in intensity fast so that by 24 hours the spectral characteristics had changed significantly. These results in Figure A. 5.1 demonstrate that the stability of iodinated mixed NPs composites depend on the Cu/ Ag molar feed ratios.

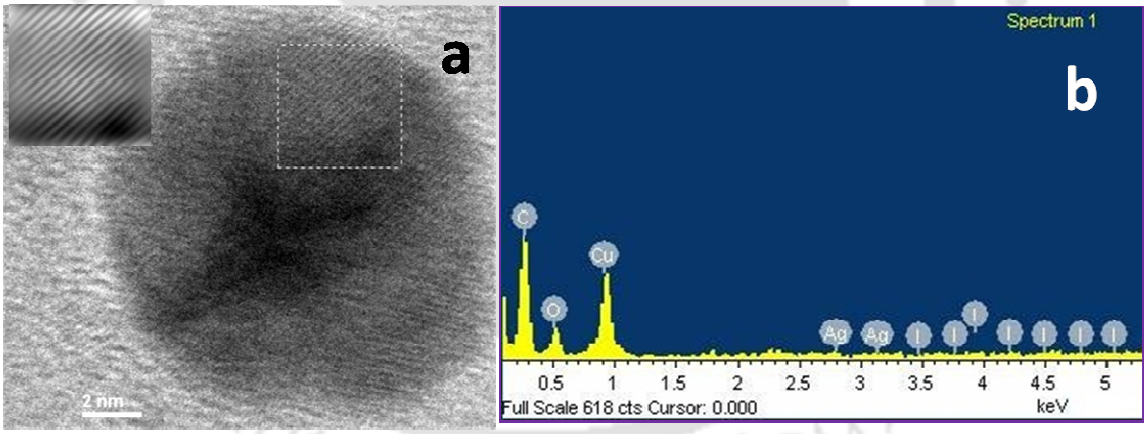

Figure A. 5.2: TEM image of freshly prepared I_2-CS-Ag NP-Cu NP composite, Cu/Ag molar feed ratios 13.33:1, EDX spectrum of the composite, showing presence of copper, silver, and iodine.

X-ray diffraction (XRD) pattern of the I_2-CS-Ag NP-Cu NP composite (Cu/ Ag molar feed ratios 40:1) was recorded after one day of synthesis indicated the diffraction peaks at 2θ values of 43.34°, 50.46°, 74.14° which were indexed as due to diffraction from (111), (200), and (220) planes of Cu(0). The diffraction peaks at 2θ = 38.16°, 44.3° are

due to reflections from (111), (200), planes of metallic Ag (0) no other crystalline phases observed in the diffraction patterns. XRD patterns of iodinated mixed NPs composite indicates the presence of individual Cu NPs and Ag NPs, nullify possibility of alloy or core shell formation.

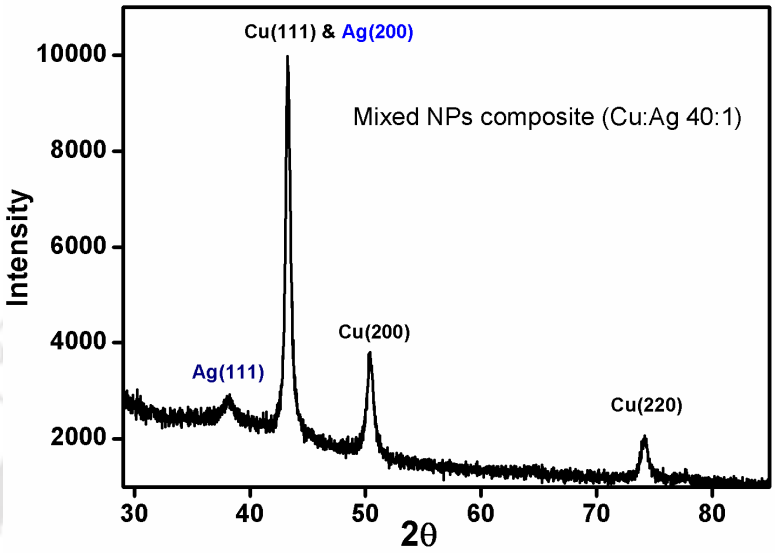

Figure A. 5.3: XRD pattern of freshly prepared I_2-CS-Ag NP-Cu NP composite (Cu/ Ag molar feed ratios 40:1).

Fourier transforms infrared spectroscopy (FTIR)

Chitosan remains chemically unaltered in presence of NPs of Cu and Ag, as well as in presence of molecular iodine as evidenced from FTIR measurements (Figure A. 5.4). This is consistent with the fact that the interaction of Cu NPs and Ag NPs with the chitosan is electrostatic in nature as was true to for other metal nanoparticles loaded onto the polymer matrix as discussed in appendix (page iv) of this thesis.

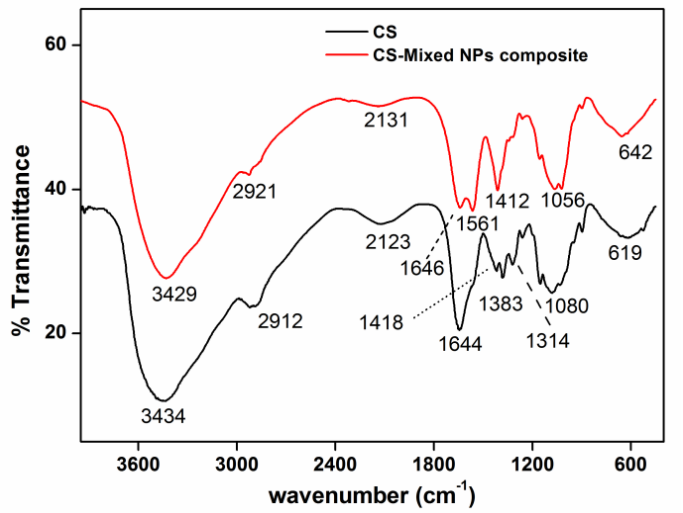

Figure A. 5.4: FTIR spectra of CS and I_2-CS-Ag NP-Cu NP composite

TEM images showed the presence of dark spots on *E. coli* cell wall; indicate the presence of Cu NPs and Ag NPs in the I_2-CS-Ag NP-Cu NP composite samples, and particles size distribution histogram obtained by TEM image analysis (Figure A. 5.5). Iodinated mixed NP composite (Cu NP, Ag NP) which attach on bacterial cell surface, consist of 4.2 ±1.0 nm sizes Ag NPs and 13.5± 3.5nm Cu NPs.

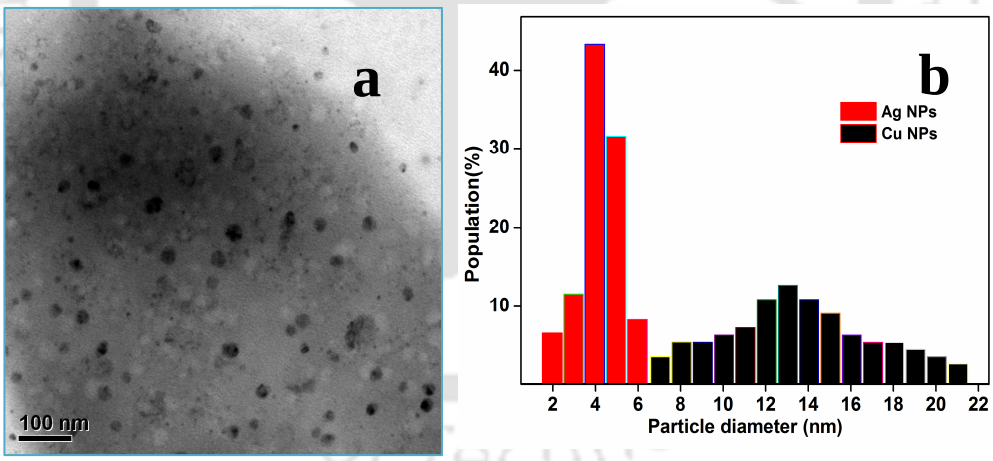

Figure A. 5.5: (a) TEM image of I_2-CS-Ag NP-Cu NP composite attached on *E. coli* bacteria. (b) Cu NPs and Ag NPs Size distribution in the I_2-CS-Ag NP-Cu NP composite when particles attached on *E. coli* bacteria and average Ag NPs size 4.2 ±1.0 nm and Cu NPs size 13.5± 3.5 nm.

Publications

(1) Heightened reactive oxygen species generation in the antimicrobial activity of a three component iodinated chitosan-Ag nanoparticle composite. Madhuchanda Banerjee, Sadhucharan Mallick, Anumita Paul, Arun Chattopadhyay, and Siddhartha Sankar Ghosh. *Langmuir* **2010,** *26(8),* 5901–5908.

(2) Iodine-Stabilized Cu Nanoparticle Chitosan Composite for Antibacterial applications. Sadhucharan Mallick, Shilpa Sharma, Madhuchanda Banerjee, Siddhartha Sankar Ghosh, Arun Chattopadhyay, and Anumita Paul. *ACS Appl. Mater. Interfaces, **2012,** 4(3),* 1313–1323.

(3) Synthesis, characterization and enhanced bactericidal action of core-shell copper – silver nanoparticle composites. Sadhucharan Mallick, Siddhartha Sankar Ghosh, Arun Chattopadhyay, and Anumita Paul**.** *ACS Appl. Mater. Interfaces, **2012/3*** (manuscript under revision)

(4) Facile preparation of mixed Cu and Ag nanoparticle composites: implication as a potent antibacterial agent. Sadhucharan Mallick, Siddhartha Sankar Ghosh, Arun Chattopadhyay, and Anumita Paul. (Manuscript to be submitted)

Presentations

(1) Poster presented entitled “Antimicrobial Iodine doped Silver Nanoparticle-Chitosan Composite” in 12th CRSI National and 4th CRSI-RSC Symposium in Chemistry 4-7 February 2010. IICT Hyderabad, India.
(Received Best Poster Award).

(2) Poster presented entitled “Role of iodine in the antimicrobial activity of silver nanoparticle chitosan as well as copper nanoparticle chitosan composite” in 2nd International Conference on Advanced Nanomaterials and Nanotechnology, (ICANN-2011) December 8 - 10, 2011, IIT Guwahati, India.

(3) Poster presented entitled “Role of iodine in the antimicrobial activity of silver nanoparticle chitosan as well as copper nanoparticle chitosan composite” in International symposium on Advances in Chemical Sciences - 2012, January 30, 2012. IIT Guwahati, India.

(4) Oral presentation entitled “Synthesis and Antibacterial properties of Iodine doped CS-Ag NP and CS-Cu NP Composites” in Conference on Photochemistry and Luminescence March 9-10, 2012, IIT Guwahati, India.

(5) Oral presentation entitled “Synthesis of metal nanoprticle-chitosan composites materials and their application in biological systems”at "Young Scientists' Colloquium 2012" organised by Materials Research Society of India (MRSI) Kolkata Chapter on 8th August 2012 at Central Glass and Ceramic Research Institute (CGCRI), Kolkata.

(6) Poster presented entitled “Synthesis, characterization and enhanced antibacterial activity of core shell Cu@Ag nanoparticles composite” in Frontiers in Chemical Sciences (FICS) -2012, during December 02-03, 2012 IIT Guwahati, India. **(Received Best Poster Award)**.

(7) Poster presented entitled “Synthesis, Characterization and Antimicrobial properties of Iodinated Copper Nanoparticle Chitosan Composites” in Processing and Fabrication of Advanced Materials. *PFAM* XXI. December 10-13, 2012. IIT Guwahati, India.